NASA Contractor Report 3136

Analysis of the Measured Effects of the Principal Exhaust Effluents From Solid Rocket Motors

R. Dawbarn, M. Kinslow, and D. J. Watson

CONTRACT PO H-19386B
JANUARY 1980

NASA

NASA Contractor Report 3136

Analysis of the Measured Effects of the Principal Exhaust Effluents From Solid Rocket Motors

R. Dawbarn, M. Kinslow, and D. J. Watson
Arnold Engineering Development Center
Arnold Air Force Station, Tennessee

Prepared for
Marshall Space Flight Center
under Contract PO H-19386B

NASA
National Aeronautics
and Space Administration

**Scientific and Technical
Information Office**

1980

CONTENTS

ILLUSTRATIONS

Figure

1.0 INTRODUCTION

1.1 BACKGROUND

There are many reasons for considering solid rocket motors as strap-on boosters for orbital payloads. Besides the operational advantages of storability and elimination of last-minute, on-pad fueling, there is the cost effectiveness of using the existing technology available from the development of such large vehicles as the Titan series.

One of the most widely used solid rocket propellants uses ammonium perchlorate as the oxidizer with a powdered aluminum filler which acts in part as a fuel and partially as a stabilizer to control the burning rate. The exhaust products from this type of fuel contain significant amounts of hydrogen chloride (HCl), aluminum oxide (Al_2O_3), and water (H_2O). In order to assess the impact of these products on the atmosphere it is necessary to know not only their quantity but also their distribution in the ground cloud which develops at the launch site after a rocket firing. A particular problem is to determine the form of the hydrogen chloride. It is possible for this compound to exist as a gas, to be dissolved in water droplets and become an acid aerosol, or to be absorbed on the aluminum oxide particles. As is quite obvious, its initial condition in the launch exhaust cloud will greatly affect its subsequent dispersion and thus its downwind concentration.

The experiments reported herein were designed and conducted in an attempt to define the state of the HCl when rocket motors are fired under various relative humidity conditions. The program consisted of three phases:

1. Building a small variable load rocket motor so that a controlled quantity of exhaust products could be produced in the environmental chamber.
2. Evaluating instruments used to detect and measure HCl concentrations in the exhaust cloud and if possible developing instrumentation which might be used to determine whether the HCl existed in the gaseous state or as an acid aerosol.

3. Monitoring a series of test firings of a 6.4-percent scale model of the space shuttle which would be conducted at the Marshall Space Flight Center (MSFC).

1.2 EVALUATION OF SCALING PROBLEM

Conducting such tests in an environmental chamber offers some obvious and distinct advantages over collecting data from actual rocket firings in the free atmosphere. These advantages include the ability to define the initial conditions of the environment, the relative ease of installing and operating monitoring instruments, and the ability to repeat test runs in order to evaluate modifications in instrumentation.

It is equally obvious, however, that there are severe limitations imposed by the scaling required to reduce a 10^6-lb rocket motor producing a ground cloud of approximately 10^{10} ft^3 volume to a size sufficiently small to fit into any environmental chamber. The initial conditions in the ground cloud at its stabilization height are an important input to the dispersion model. Thus an appropriate mixing ratio of exhaust products to ambient air of this cloud was chosen as the scaling parameter. If a small rocket motor can produce exhaust species which are reasonably similar to those from the large motors, then one might expect to reproduce those processes involving HCl, water vapor, and Al_2O_3 particulates which will occur in the free atmosphere as the ground cloud is formed. It is recognized that depletion of species will occur due to wall effects, and thus the absolute values of species concentrations measured in the chamber are not meaningful in defining contaminant levels in full-scale ground clouds. However, the rate of decay of species concentrations in a closed chamber can provide information on the physical processes causing the decay (i.e., whether a specie is diffusing to the walls in the gaseous state or falling out because of gravitational settling). In addition to the information which can be gathered concerning the physical and chemical processes, tests in an environmental chamber can provide a simulated exhaust cloud for evaluating various types of instrumentation which might be considered for atmospheric sampling at full-scale rocket launches.

Assuming that under typical conditions a ground cloud forms at 1,000 m, then the calculation conducted at JPL (Ref. 1) indicates that the cloud will contain approximately 2×10^8 gm of material from the solid rocket motors. This will include 4.4×10^7 gm of HCl and 5.0×10^7 gm of Al_2O_3. Extrapolation from observations of a Delta-Thor

launch (Ref. 2) shows an expected cloud volume of 2.8×10^8 m^3 as reasonable for a shuttle launch. Using the constraint imposed by the proposed test chamber volume of 1.13×10^2 m^3 leads to a definition of a rocket motor burning $\approx$ 80 gm of fuel.

Such a drastic scaling of the rocket motor naturally leads to a concern over the exhaust species that will be produced. The gaseous species such as HCl, H_2O, CO, CO_2, and H_2 are obviously formed regardless of engine size. Questions may be raised concerning the relative efficiency of the afterburning of the CO and H_2 with such a small engine. However, the CO_2 and the additional H_2O produced in this manner are not considered significant for the purpose of these tests. As was noted previously, the absolute quantities of the exhaust species will be compromised by chamber wall effects, and thus any inefficiencies in the combustion process leading to a slight deficiency in the quantity of any of the gaseous species will not be of any concern.

The specie most affected by the scaling of the rocket motor is the aluminum oxide. Several mechanisms for the formation of the aluminum oxide particles have been proposed (Refs. 3, 4, and 5), and it would appear that in the complex burning-quenching process of the gases passing from the combustion chamber, through the nozzle, and expanding in the rocket plume, more than one mechanism will apply. This leads not only to the variety of sizes and types of Al_2O_3 particles observed, but also to the differences in crystalline structure. A more detailed discussion of the possible mechanisms and types of aluminum oxide particles produced is presented in Section 8.1.

Several attempts have been made to correlate the aluminum oxide particle size distribution with some characteristic of the parent rocket. Sehgal (Ref. 6) found a correlation between the average particle size and the combustion chamber pressure and reports a logarithmic relationship such that over a pressure range from 75 to 1,000 psia,

$$\log P = 1.8 + 0.25\, D_{30}$$

where P = combustion chamber pressure and D_{30} is the mean mass diameter. Crowe et al. (Ref. 7), repeating this type of experiment, also see a particle size dependence for pressures up to 300 psia, with somewhat indeterminate results above this pressure. However, later

work by Dobbins et al. (Ref. 8), using the same facilities as Sehgal, report data that show no correlation between average particle size and combustion chamber pressure. Also, work by Eisel et al. (Ref. 9) indicates that there is no correlation between particle sizes and combustion chamber pressure. Thus, it would seem that if there is a pressure correlation then it is sufficiently masked by other effects or limitations of particle collection and measurement techniques as to be undefinable at this time.

A second parameter which has been considered is the nozzle throat diameter. It has been suggested that the average particle size should increase as the throat diameter increases. Radke et al. (Ref. 10) present a limited amount of data from a variety of rocket motors. Based on these data, Worster et al. (Ref. 11) have presented a distribution function of particle radii,

$$f(r) = \frac{A^4}{6} r^3 e^{-Ar}$$

where A is a function of engine throat diameter, D^*, and is presented in Fig. 1.

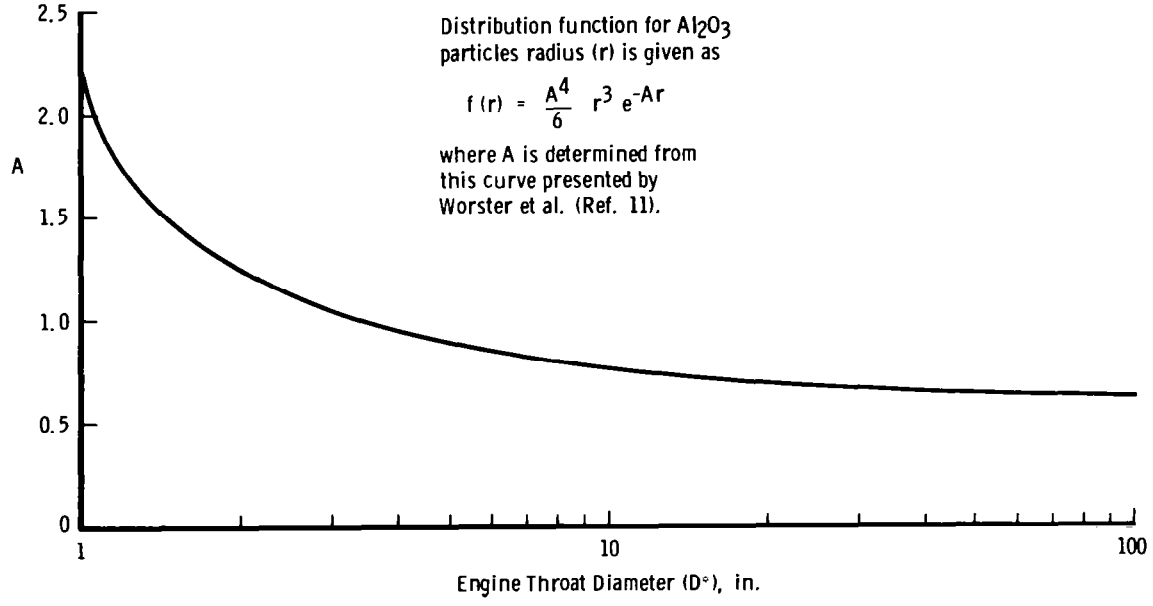

Figure 1. Radius distribution parameter.

Any attempt to correlate the particle sizes from various rocket motors should include a careful consideration of the source of the raw data and the possible bias which may be included in the particle production, collection, and analysis. For example, the bulk of the particle size data for small engines has been obtained from experiments which were concerned with the effects of particle size on combustion stability and thrust. In these studies the test chambers in which the rocket motors are fired and the particles are collected are back-filled with nitrogen or argon to quench all burning outside of the combustion chamber. As will be noted in more detail in Section 8.0, such quenching can have a significant effect on particle size. In addition, the particle samples from small motors are usually collected in tanks or chambers, whereas those collected from large engines are collected in the open atmosphere and downwind at distances varying from several yards to several miles. In the open atmospheric tests the particles pass through a very effective size filtration system as the high velocity particles encounter the ambient atmosphere. Selective fallout rates, coupled with possible condensation of atmospheric moisture on some particles and their subsequent rainout, leave serious questions as to how well data from a variety of large engine firings under random atmospheric conditions can be compared.

Aluminum oxide particles recovered from the spray cooling water used in test facilities at AEDC indicate that there is little difference in the particle size range from engines with throat diameters up to 3 in. However, once again the particles have been subjected to a collection system which obviously will affect the sample. It has been noted, however, in a series of fuel-burning tests that even free-burning fuel under appropriate humidity conditions can produce Al_2O_3 particles greater than 60 μ in diameter. This matches the largest size particles collected from rocket motors with 12-in.-diam throats. In view of the above comments it is felt that there is not yet sufficient evidence to establish a particle size versus throat diameter correlation. Thus, while it is expected that the distribution of particle sizes will be dependent on the size of the solid rocket motor, the evidence available indicates that the same range of particles can be produced by small or large rocket motors. The small rocket motor built for these tests therefore can be expected to provide a range of Al_2O_3 particle sizes sufficiently representative of those produced by the shuttle engines to permit a study of their influence in the Al_2O_3-H_2O-HCl system.

2.0 APPARATUS

2. 1 ROCKET MOTOR

The schematic of the rocket motor developed for these tests is shown in Fig. 2. The outer casing consists of a heavy-wall steel tube internally threaded at each end to accept both the tungsten nozzle and the top screw cap. Two ports were drilled into this casing; one was fitted with a rupture disk, and the other was used for attaching a pressure transducer. The combustion chamber consists of a 1.5-in. length of 2-in. -diam schedule 40 stainless steel pipe with holes drilled to match the blowout port and the pressure tap. This insert was keyed to keep these holes aligned. The fuel cartridges consist of 6-in. lengths of 2-in. -diam schedule 40 stainless steel pipe with a welded end plate. This end plate was tapped to accept a length of 1/4-in. threaded rod which was used to locate a spacer block. This block was positioned so that regardless of the length of the fuel load the front face of the fuel was always flush with the top edge of the cartridge. The fuel was cast in 2-in. -diam sticks approximately 12 in. long. These were sliced into the appropriate lengths ($\approx$ 1, 2, and 3 in.) required for the tests and were cemented into the fuel cartridges with an epoxy cement. The starting fuse consisted of a short length of nichrome wire which was inserted into the center of the front face of the fuel. The electrical leads from the nichrome were brought out of the rocket through the nozzle throat.

The fuel cartridge was positioned in the rocket casing with a top seal cap which carried an O-ring. The complete assembly was locked in place with the screw cap.

2.2 OPERATION OF THE ROCKET MOTOR

Several minor problems were experienced with the rocket motor during the first firings. The pressure traces from early firings are shown in Fig. 3. After such a pressure history it was noted that the nozzle was almost completely plugged. On several firings the pressure disk ruptured, and on these occasions it was found that the nozzle was completely closed. Several lubricants were used on the nozzle, including a silicone vacuum grease and STP® oil additive. While this lubrication seemed to help keep the nozzle cleaner, it did not solve the pressure spiking problem. The cause was finally traced to two factors. One was occasionally setting the fuse too deep

into the fuel load, and the other was voids cast into one of the fuel sticks. All fuel was subsequently X-rayed before loading, and sections of fuel with voids were used for open burn studies. After these precautions were followed, all motors fired in the environmental tests burned smoothly, and their pressure profiles and burn times were highly repeatable. Typical data from several tests are presented in Fig. 4.

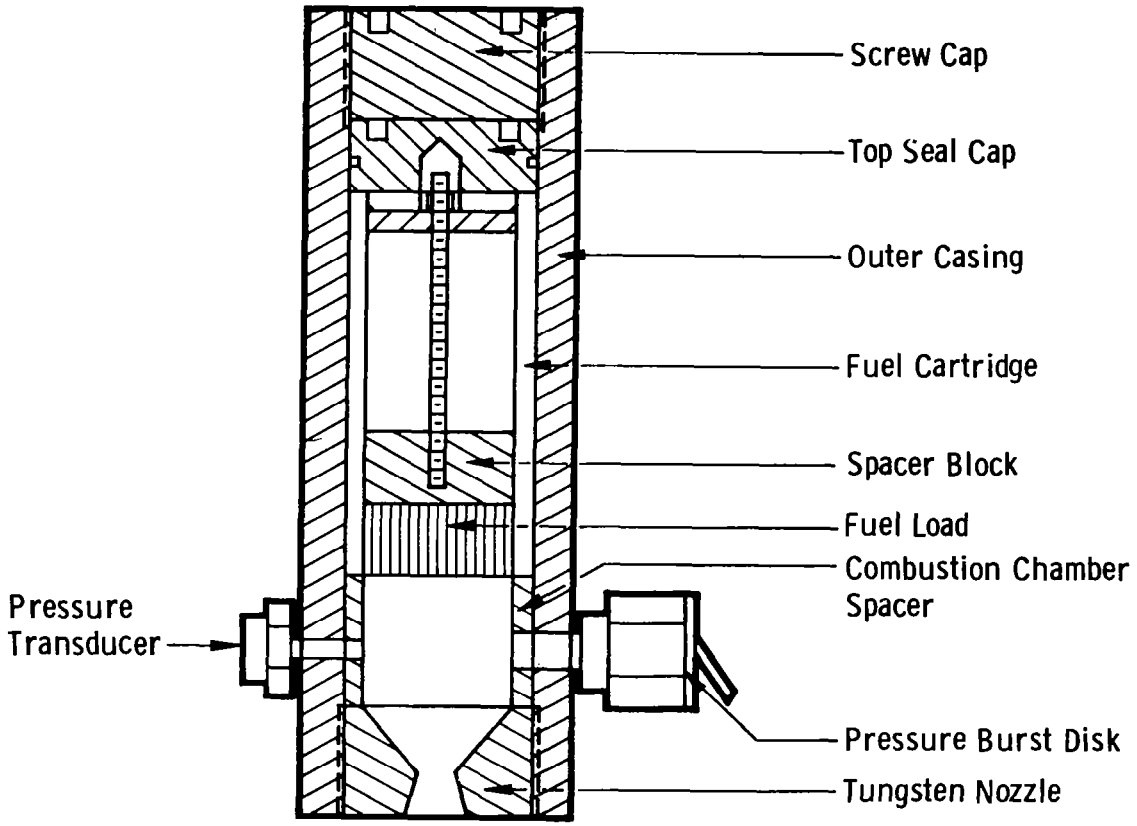

Figure 2. Variable load rocket motor.

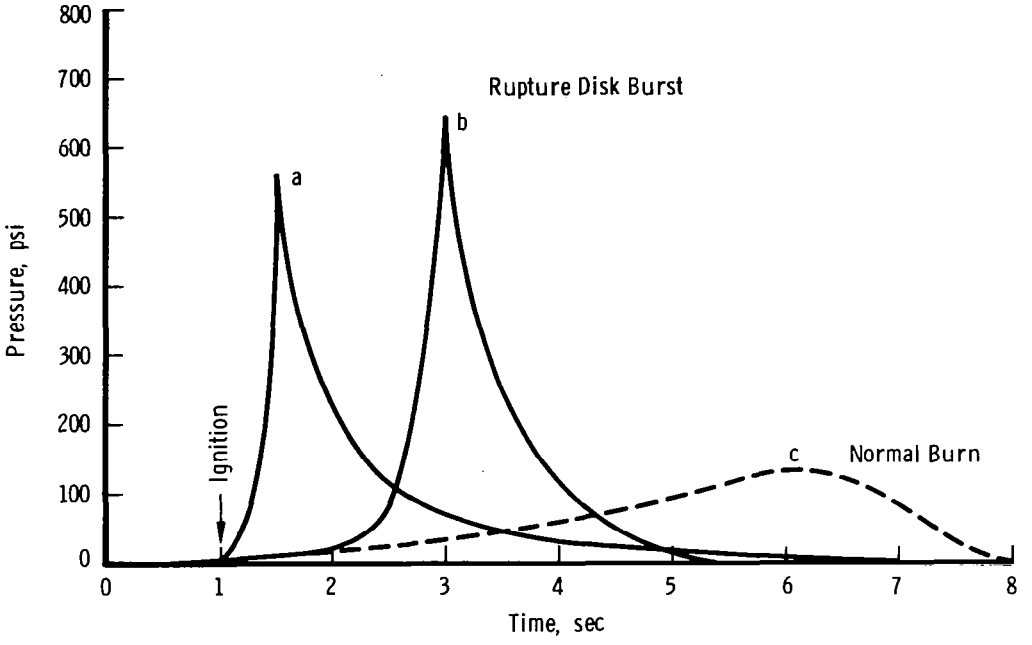

Figure 3. Pressure profile with throat plugged.

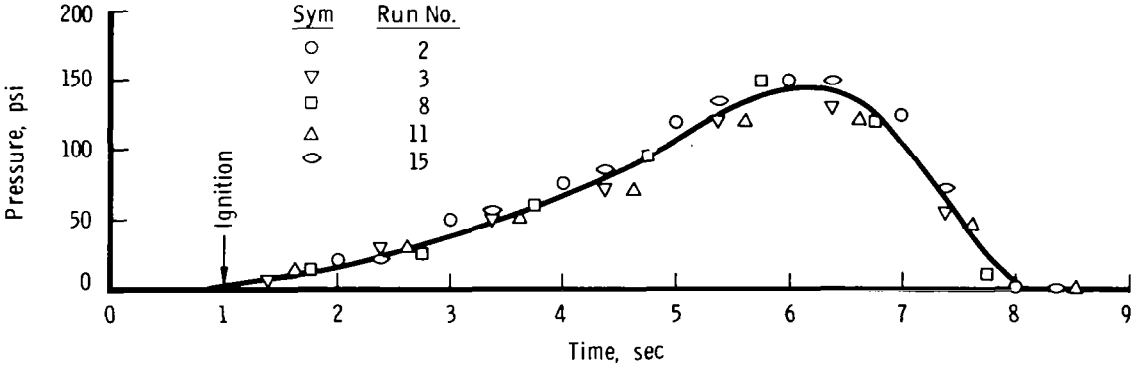

Figure 4. Pressure profile during rocket burn.

2.3 ROCKET SUPPORT STAND

A 1/100-scale model of the proposed Kennedy Space Center launch complex was constructed from steel plate. The flame trench was fitted with a glass side wall so that high-speed motion pictures could be made of the exhaust gases leaving the rocket nozzle. A side view of this assembly with a rocket motor burn is shown in Fig. 5. The flame trench was fitted with a spray bar and a pressurized water system, so that on selected firings cooling water could be added to the exhaust gases. The rate at which the water was sprayed into the flame trench was controlled by adjusting the pressure in the spray system. The total quantity of water was determined by operation of the solenoid valve. Typical spray rates were 6 gm/sec with a total of 50 gm of water sprayed into the exhaust flame. Figure 6 presents a top view of the launch stand during a rocket motor burn.

3.0 INSTRUMENTATION

3.1 INSTRUMENTATION TO DETECT AND MEASURE HCl

The following instruments were used to detect and measure the concentrations of hydrogen chloride in these tests:

1. Bubblers
2. Chemiluminescent detector (Geomet)
3. Coulometer
4. Modified Condensation Nuclei Counter (General Electric)
5. Millipore filters
6. Copper-coated glass disks
7. pH papers

Several of these instruments had been used in previous attempts to obtain measurements of HCl concentrations downwind of actual launches of solid rockets at both the Kennedy Space Flight Center and Vandenberg Air Force Base. However, due to the problems involved in trying to predict the path of the ground cloud and thereby prelocate the instruments, minimal data had been obtained. In such field tests it soon becomes very apparent that one must either deploy an extensive grid of measuring devices or have the instrumentation highly mobile and capable of following the cloud. Thus, in these environmental chamber tests one of the peripheral objectives was to evaluate several inexpensive HCl detectors which might reasonably be deployed over a large area as well as to check the operation of the more sophisticated detectors, which could be flown through a ground cloud.

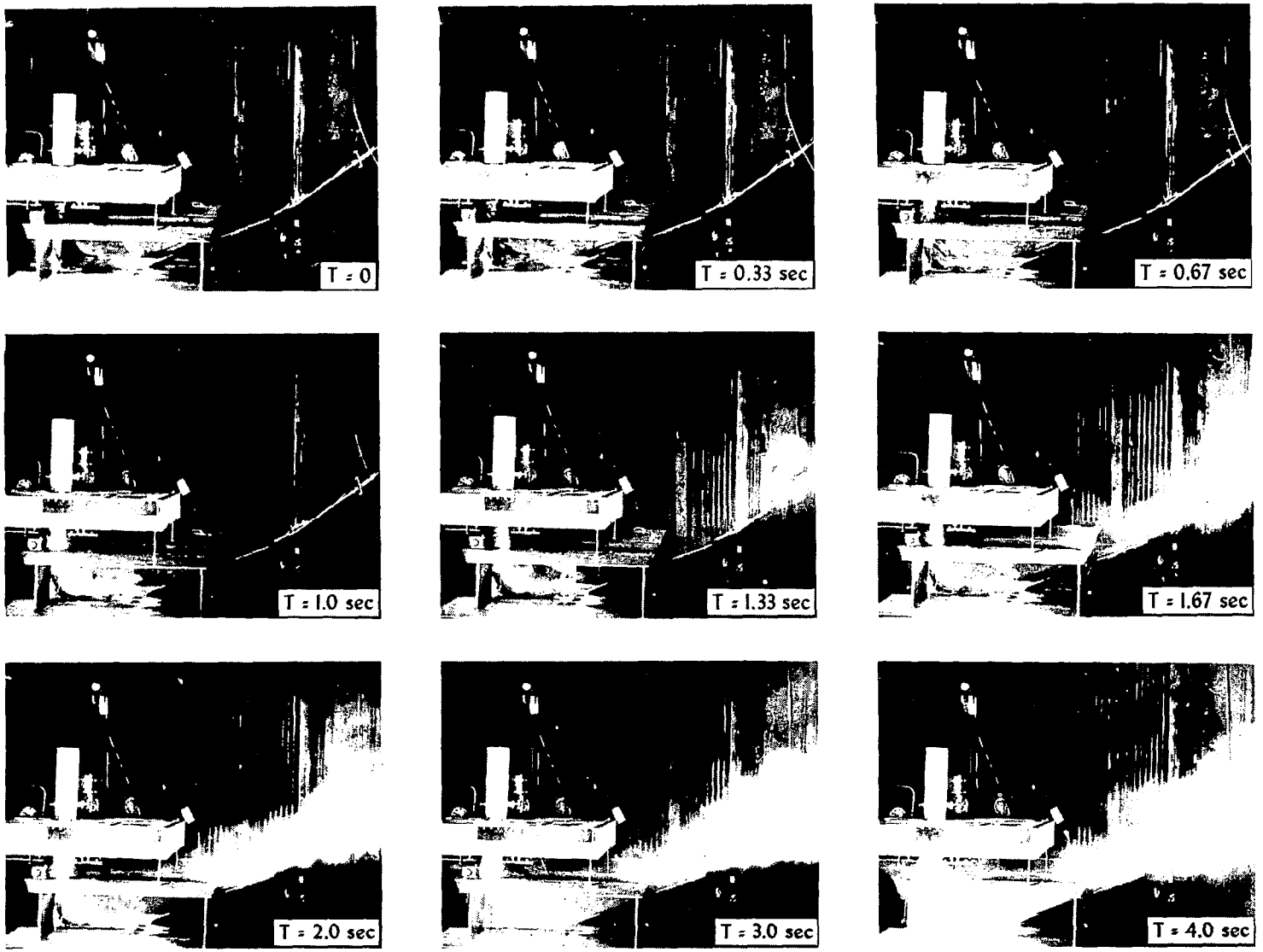

Figure 5. Side view of motor firing.

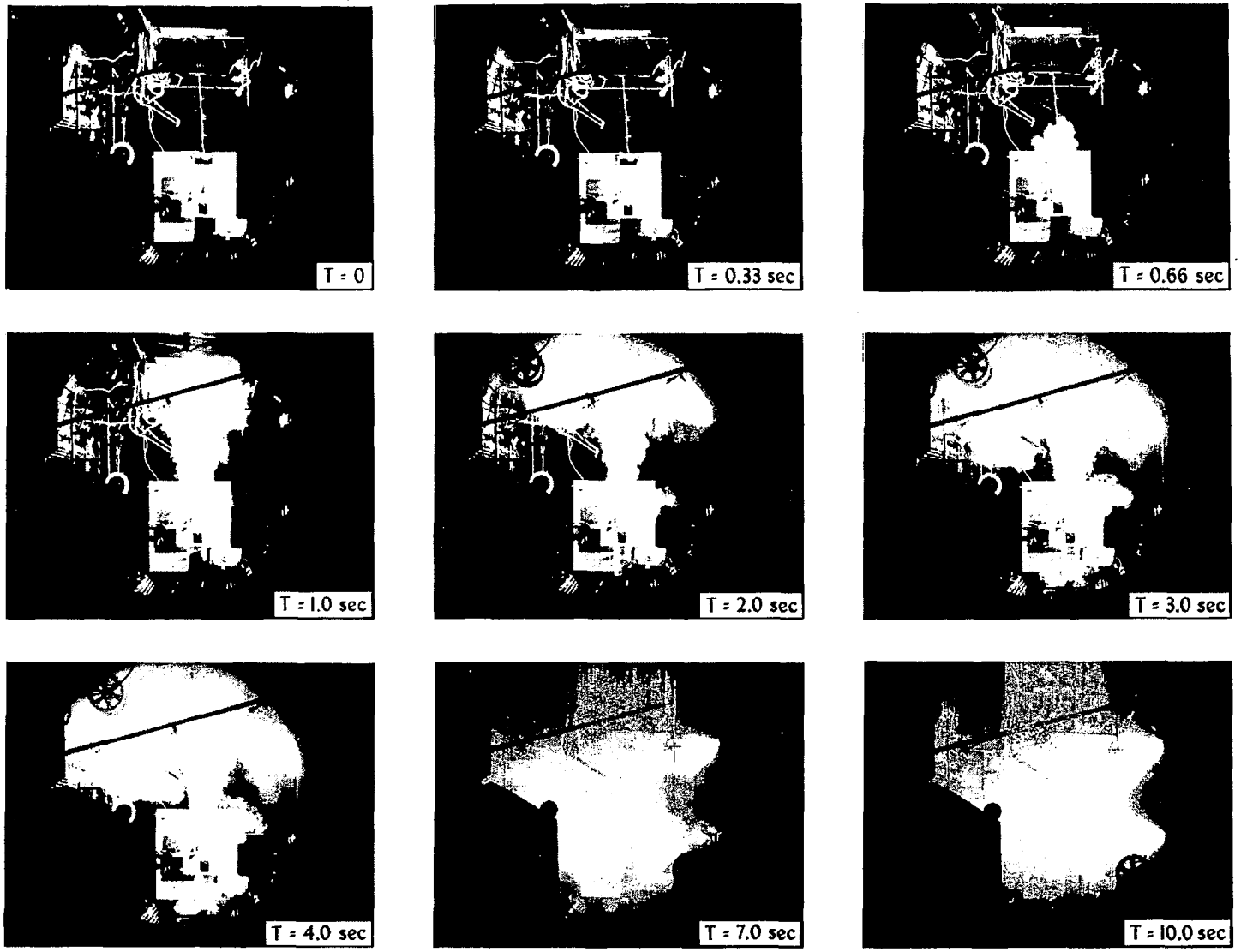

Figure 6. Top view of motor firing.

3.1.1 Coulometer

The coulometer used in these tests was supplied and operated by personnel from the USAF School of Aerospace Medicine, Brooks Air Force Base, Texas. It was used to monitor HCl concentrations during the first six test firings in the chamber and during two of the test firings at MSFC. It is a standard laboratory microcoulometric titrating system which has been modified to accept a continuous sample of gas bubbled through the electrolyte. The cell is composed of two pairs of electrodes immersed in a 70-percent (vol/vol) aqueous glacial acetic acid solution made approximately 1×10^{-7} molar in silver ions. One pair of electrodes is used to sense the concentration of silver ions, and the other pair is used to generate silver ions. When a sample of HCl is introduced into the cell, it reacts with the silver ions to produce silver chloride (AgCl) as a precipitate. As the concentration of the silver ions in the electrolyte varies, a change in the output voltage across the sensing electrodes is developed. This voltage is fed to an amplifier and after being amplified and properly phased is applied to the generating electrodes to replenish the silver ions.

The potential drop across a precision resistor in series with the generating electrodes is monitored by a recorder. Thus, the total charge needed to regenerate the silver ions appears as a peak on the recorder. The area under this peak is related by Faraday's Law to the Cl^- ion concentration. The threshold detection limit for batch injection of HCl is about three nanograms. The total quantity is calculated from

$$W = \frac{36.45}{96501} \frac{\text{gm/mole}}{\text{coulombs}} \times 10^6 \frac{A}{R}$$

where

W = weight of HCl, nanograms

A = coulogram peak area, millivolt-seconds

R = precision resistor, ohms

When the instrument is sampling a steady-state mixture of HCl and air, the resulting constant current supplied to the generating electrodes can be directly related to the HCl concentration. The range of HCl concentrations which can be measured by the instrument can be adjusted

by changing the rate at which the sampled gases are drawn through the electrolyte. However, there are limits, imposed by the excessive turbulence of the electrolyte caused by high flow rates and poor mixing at low sampling rates, which set the optimum instrument range from 0.1 to 20 ppm of HCl. A typical sampling rate is 0.1 liters/min.

3.1.2 Bubblers

The three types of bubblers used in these tests are shown in Fig. 7. The bubbler is commonly used as a gas scrubber and in this application was used to dissolve the HCl present in a known volume of sample gas drawn through the device. The amount of HCl was calculated from a measurement of the pH or chloride ion concentration of the distilled water in the bubbler after sampling.

Two of the bubblers were modified as shown in Fig. 7 to include a pH probe which could be used to determine changes in pH on a real time basis.

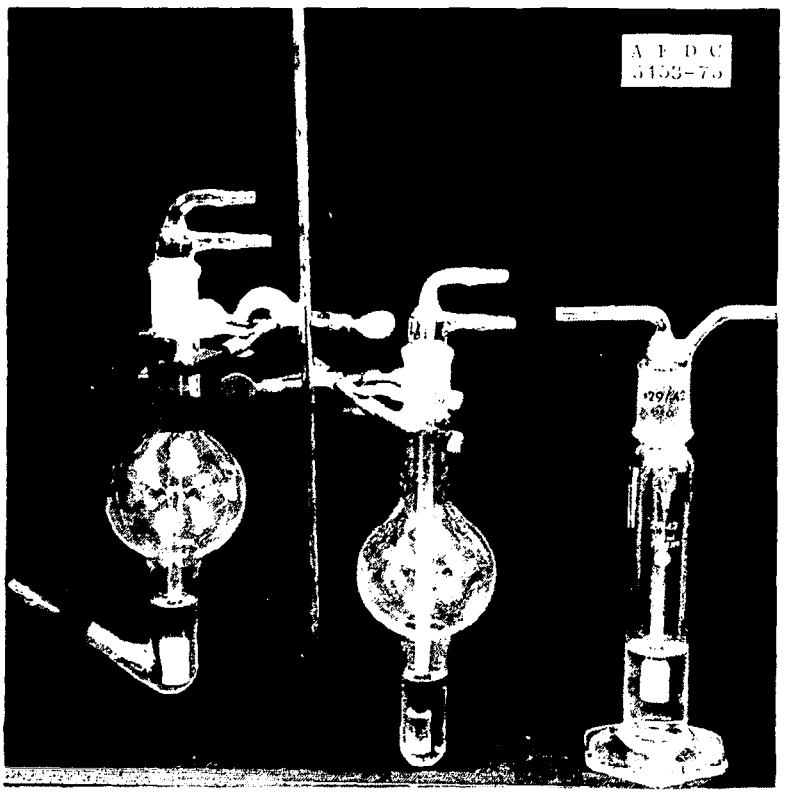

Figure 7. Types of bubblers used.

3.1.3 Millipore Filters

The millipore filters were initially procured and used to determine the particle mass loading in the exhaust cloud. However, part way through the test series it was found that these filters could also be used to measure HCl concentrations. These filters are supplied in a plastic housing and are designed for one-time use. A view of a complete unit and the individual components is shown in Fig. 8. The filter portion is a thin membrane which is supported by a cellulose backing pad. This backing pad is an effective absorber of HCl. When this pad is subsequently macerated in distilled water, the HCl is released into solution and the pH can be measured.

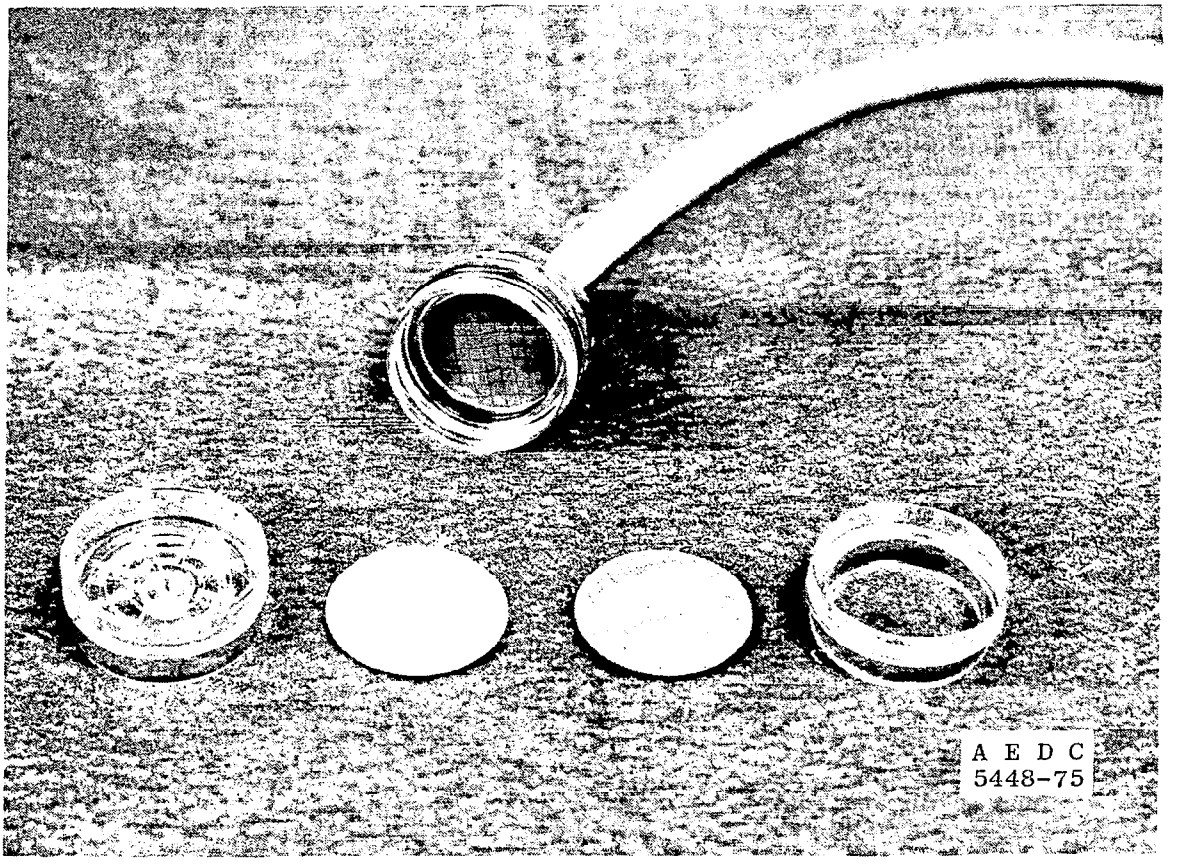

Figure 8. Millipore filter.

3.1.4 pH Papers

Several types of pH papers were used to monitor HCl. A general purpose paper with a range from 0 to 11 was deployed throughout the interior of the test chamber to determine whether the HCl reached the upper levels of the chamber. In all cases except one these papers registered pH0 upon recovery. The one exception was a piece of the paper which had fallen between two floor panels. It had barely changed color but did have some small spots, indicating that acid droplets were present during this test.

The papers were deployed throughout the grid network of detectors during the monitoring of the test firings at MSFC and did provide useful data to determine the general footprint of the cloud at ground level.

3.1.5 Chemiluminescent Detector (Geomet)

The chemiluminescent detector ingests the air sample through a ceramic tube coated with a sodium bromide-bromate solution. HCl gas in the sample reacts with this coating forming hypochlorite hypobromite, which travels down the tube to the reaction chamber. The reaction chamber contains a mixture of luminol and hydrogen peroxide. The hypochlorite and hypobromite act as catalysts to trigger the oxidation of the luminol, which in the process gives off visible light. The resulting photons are detected by a photoelectric detector. The signal from the detector is proportional to the quantity of HCl in the ingested sample and thus provides a continuous monitoring of HCl concentrations entering the instrument. Calibration was performed using the gas-mixing system shown schematically in Fig. 9. Cylinder A was filled with nitrogen containing approximately 60 ppm HCl. This gas was obtained premixed from a commercial gas supplier. Cylinder B contained dry N_2. The two gases were flowed through rotometers to a common mixing tube, where the HCl was thus further diluted. The chemiluminescent detector and the coulometer both sampled from this common supply of gas, and the excess was vented through valve C. Flows were established in the system and maintained until steady-state readings were obtained by both the coulometer and the chemiluminescent detector. Care was taken to assure a positive gas flow from the vent valve at all times, while at the same time not raising the pressures in the mixing-sampling tube above ambient by any significant amount. This precaution was necessary in order not to influence the flow rate through the sampling instruments. Flow rates through each instrument were monitored by

attaching a flowmeter to the exhaust port of each instrument's pumping system. The actual concentration of HCl in the sampled mixture was calculated from the data obtained from the coulometer. Data points from 1 to 50 ppm were obtained by adjusting the various gas flow rates.

Since this method of calibration refers to the coulometer as the absolute in determining HCl levels, several tests were made where the gas mixture was sampled by a bubbler also. A determination of the HCl concentrations using this instrument along with a pH probe yielded values within 5 percent of the coulometer values. In each case the bubbler values were lower than those from the coulometer.

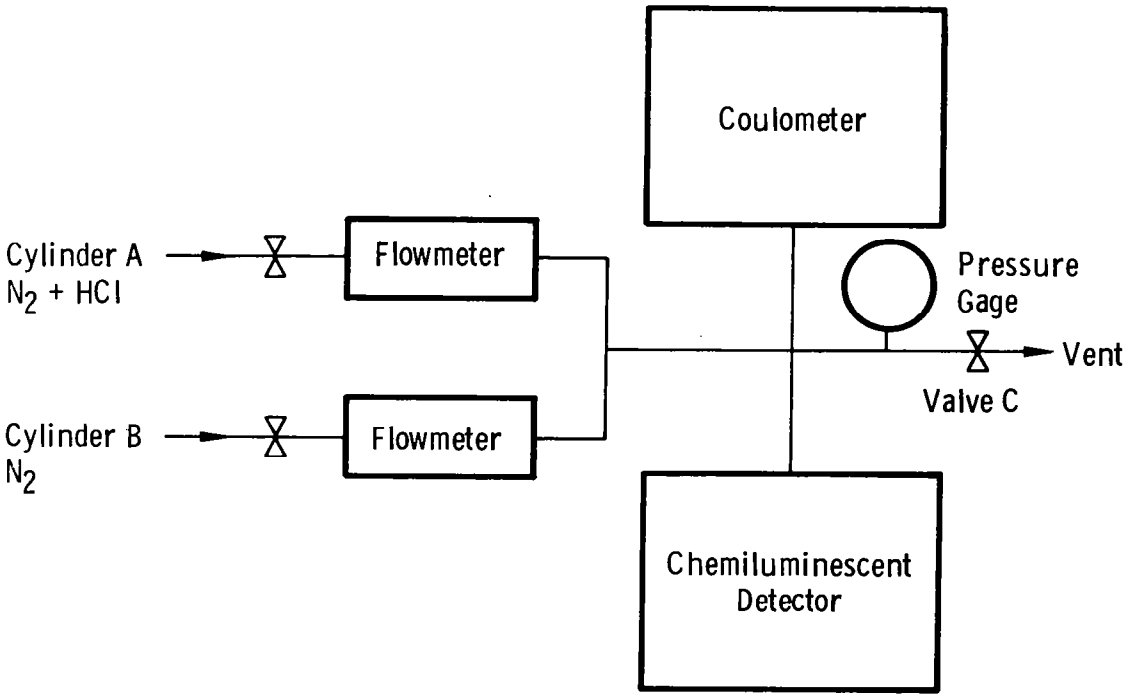

Figure 9. Calibration of chemiluminescent detector.

3.1.6 Modified Condensation Nuclei Counter

The condensation nuclei counter which was modified for these tests is a commercial instrument designed to monitor the concentration of particulates in the atmosphere.

The basic condensation nuclei counter (CNC) is shown schematically in Fig. 10. The sample, at a flow rate of about 100 cc/sec, is drawn in through a humidifier to bring it to 100 percent relative humidity. It then passes through the first section of a rotary, motor driven valve into the expansion chamber. After a brief dwell period, the second section of the rotary valve opens the expansion chamber to a source of regulated vacuum.

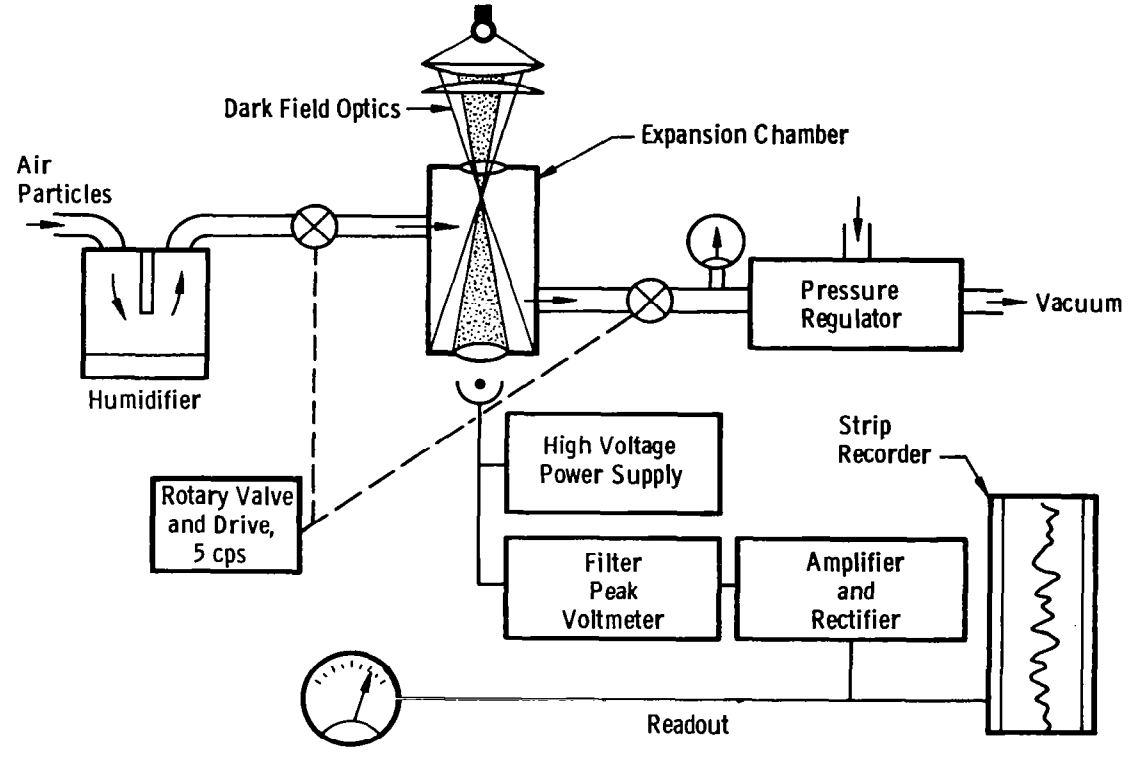

Figure 10. Schematic of condensation nuclei counter.

The sudden expansion results in adiabatic cooling of the sample, causing the relative humidity to rise about 100 percent. Water then condenses on nuclei present, and the resulting droplets soon grow to a size where they can scatter light. The expansion chamber contains a dark field optical system which produces no light on the photomultiplier tube in the absence of fog droplets. With droplets present in the chamber, they cause light to be scattered to the photomultiplier. The amount of light is proportional to the number of droplets (each containing one nucleus) and to their scattering area.

For most applications the vacuum is regulated to give an under-pressure expansion of 8 in. of mercury. The valve cycling rate is five times a second, producing an essentially continuous measurement of nuclei concentration. The response time is about 2 sec, due in part to flow delays, particularly in the humidifier. For applications requiring long inlet lines it is possible to connect the sample inlet through a tee connection to a second air pump, thus increasing the flow through the sample line to about 500 cc/sec; this reduces the trasnport delay and at the same time minimizes coagulation losses in the sample line.

In its normal operating mode the condensation nuclei counter is insensitive to HCl gas since it does not act as a nucleation site. Similarly, the counter is not sensitive to other gases such as ammonia (NH_3). However, if HCl and NH_3 are allowed to mix before entering the humidification chamber, they react to form particles of ammonium chloride, (NH_4Cl) which are extremely effective condensation nuclei. Thus the counter was modified by adding an ammonia addition system which could be pulsed on and off to the inlet of the sampling tube. In this configuration, when the instrument samples the exhaust product from the test chamber with the NH_3 off, it registers a particle count representative of the aluminum oxide particles.

When the NH_3 is pulsed on, if there is any HCl gas present, there is an additional count due to the NH_4Cl produced. However, if the HCl is adsorbed on existing Al_2O_3 particles, the NH_3 produces no additional count. The system was calibrated for HCl using a scheme similar to that described for the chemiluminescent detector, with the exception that compressed air was used to dilute the N_2-HCl mixture. This provided a background particle count in the instrument.

3.1.7 Copper-Coated Aerosol Detectors

At the beginning of the test series a dewpoint hygrometer was used to measure the humidity in the Aerospace Chamber (12V). This instrument operates on the principle of drawing a continuous sample of air over an aluminum mirror, which is slowly cooled. A photodetector looks at a collimated light beam reflected from this mirror and detects the change in reflectivity as the mirror cools to the dewpoint and water condenses on its surface. A thermistor detects the temperature of the mirror surface at this point.

During test number 6, in which the initial relative humidity was set at 89 percent, the dewpoint hygrometer sampling fan was left

on during the engine firing. After this test the hygrometer would not operate properly and upon disassembly it was found that the aluminized mirror surface had been pitted by acid droplets. In the following chamber test, several glass slides which had been vacuum coated with a thin layer of aluminum were located in the chamber to record acid droplets which might settle on them. This technique proved successful, and the slides did record evidence of acid droplets. It was noted that each circular etched spot contained a small, solid particle at the center. In most cases it was quite obvious that this nucleus was spherical, and thus was most likely an Al_2O_3 particle. However, the nucleus in some circles appeared to be a cluster of crystals. Analyzing these crystals by using a scanning electron microscope (SEM) with an electron probe and looking at the X-rays produced indicated the presence of aluminum and chlorine. Since the SEM instrument cannot detect the lighter elements, including oxygen, it was impossible to determine whether the aluminum detected came from the substrate coating on the glass slide or from an aluminum oxide particle. To avoid this problem a second set of glass slides was vacuum coated with copper, and in the tests which followed proved equally capable of recording acid droplet fallout. In subsequent tests in the 12V chamber a motorized carousel loaded with copper-plated glass disks was used to take a time sequence of droplet fallout. The carousel was programmed to stop at two-minute intervals and carried six disks. The carousel loaded with sampling disks is shown in Fig. 11.

In addition to being used in the 12V tests the individual copper-coated disks have been deployed in a grid network at the outdoor rocket tests both at the Arnold Engineering Development Center (AEDC) and the Marshall Space Flight Center (MSFC).

3.2 COLLECTION AND ANALYSIS OF Al_2O_3 PARTICLES

Several methods of collecting the Al_2O_3 particles were used in these tests. These included

1. Millipore filters (8.0-, 0.4-, and 0.2-μm pore size)
2. Cascade impactor
3. Rotating vanes
4. Settling plates

The samples collected by the filters were used to determine the gross mass loading of the Al_2O_3 and provided a bulk sample of the particulates. Additional investigation of the Al_2O_3 particles was conducted using a scanning electron microscope fitted with an energy-dispersive X-ray system which allowed a limited chemical analysis of the samples.

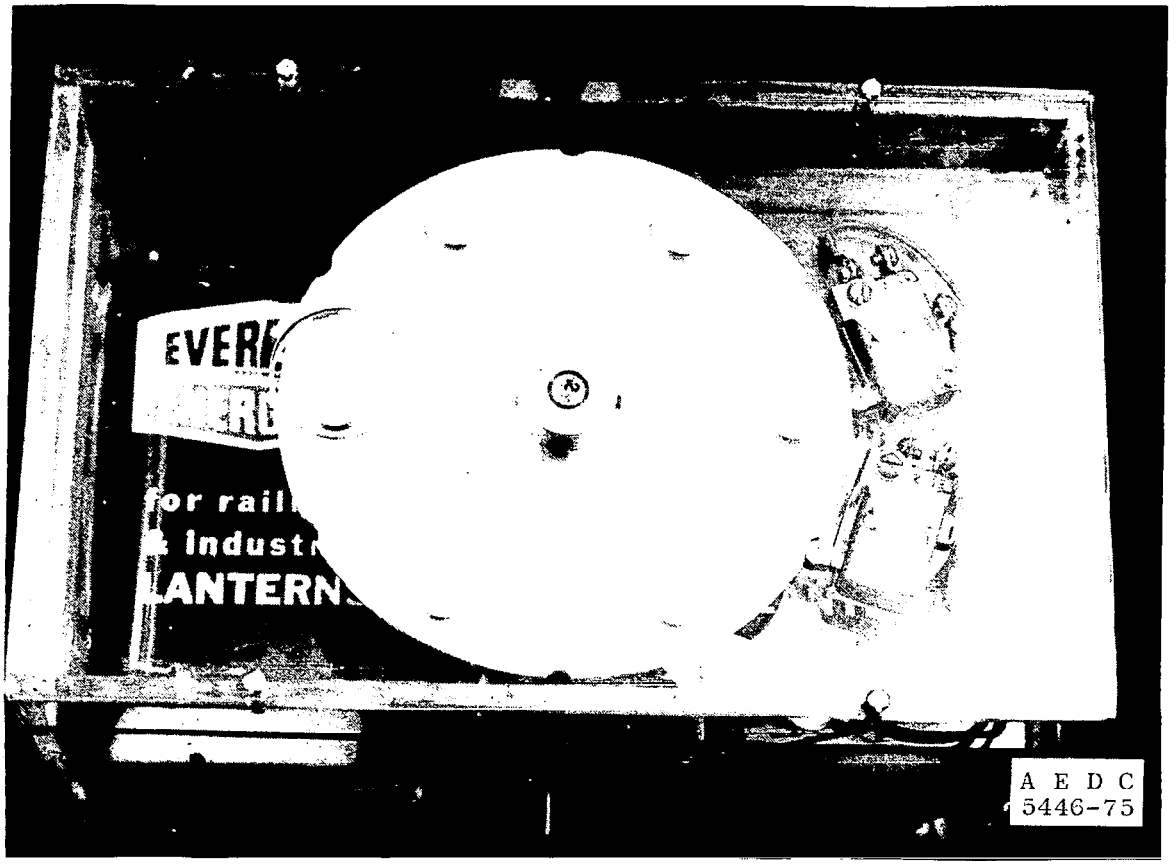

Figure 11. Copper-plated fallout disks and carousel.

3.2.1 Millipore Filters

The millipore filters, shown in Fig. 8, were used to measure the particle mass loading in the exhaust clouds produced in the test chamber. The filter membranes are available with various pore sizes. Membranes with pore sizes of 8, 0.4, and 0.2 μm were evaluated prior to the chamber tests. When these filters were used to sample smoke from free-burning fuel, it was noted that some of the Al_2O_3 did penetrate the 8-μm membrane and could be detected in the cellulose backing pad. Microscopic examination of the pads behind the 0.4- and 0.2-μm membranes did not reveal any aluminum oxide, even though some of the individual

smoke particles were determined to be less than 0.1 μm. The material collected on the filters showed considerable agglomeration; however, it is not clear whether this agglomeration occurred in the free atmosphere or after the Al_2O_3 collected on the filter membrane. The 0.4-μm filters were chosen for use in the 12V tests since these filters required a minimum of adjusting to maintain a constant flow rate through them during the collection period.

In the series of engine firings in the 12V chamber the filters were clustered in a group of five. Each filter was connected to a sampling pump via a solenoid valve, a needle valve, and a rotometer. The solenoid valves were operated sequentially by the master timing panel so that each filter sampled for a 10-min period. An indicator light was used to signal that a filter was sampling, and during the sample period the needle valve was manually adjusted to maintain a constant flow rate through the filter. Each filter membrane was weighed before and immediately after the test. The filters were then stored in a dessicator and weighed at a later date to check to see if any significant amount of the weight increase was due to the absorption of water by the Al_2O_3. The only set of filters which indicated any measureable weight loss after dessication were those used in the test conducted with a simulated misting rain.

3.2.2 Cascade Impactor

The cascade impactor used in these tests is designed to sample airborne particles in a size range from 200 to 0.5 μm. The instrument essentially consists of a system of four air jets impinging, in series, on glass disks. The jets are progressively finer, so that the speed and therefore the efficiency of impaction of particles onto the disks increases from jet to jet when air is drawn through at a steady rate. The cascade impactor is shown in Fig. 12. The sampling rate of 17.5 ℓ/min gives velocities through the four jets of 2.2, 10.2, 27.5, and 77 m/sec, respectively. The manufacturer's calibration indicates that the maximum particle sizes found on the second, third, and fourth disks are 20, 7, and 2.5 μm, respectively. The largest particle on the first stage is defined by the upper size limit of the sample.

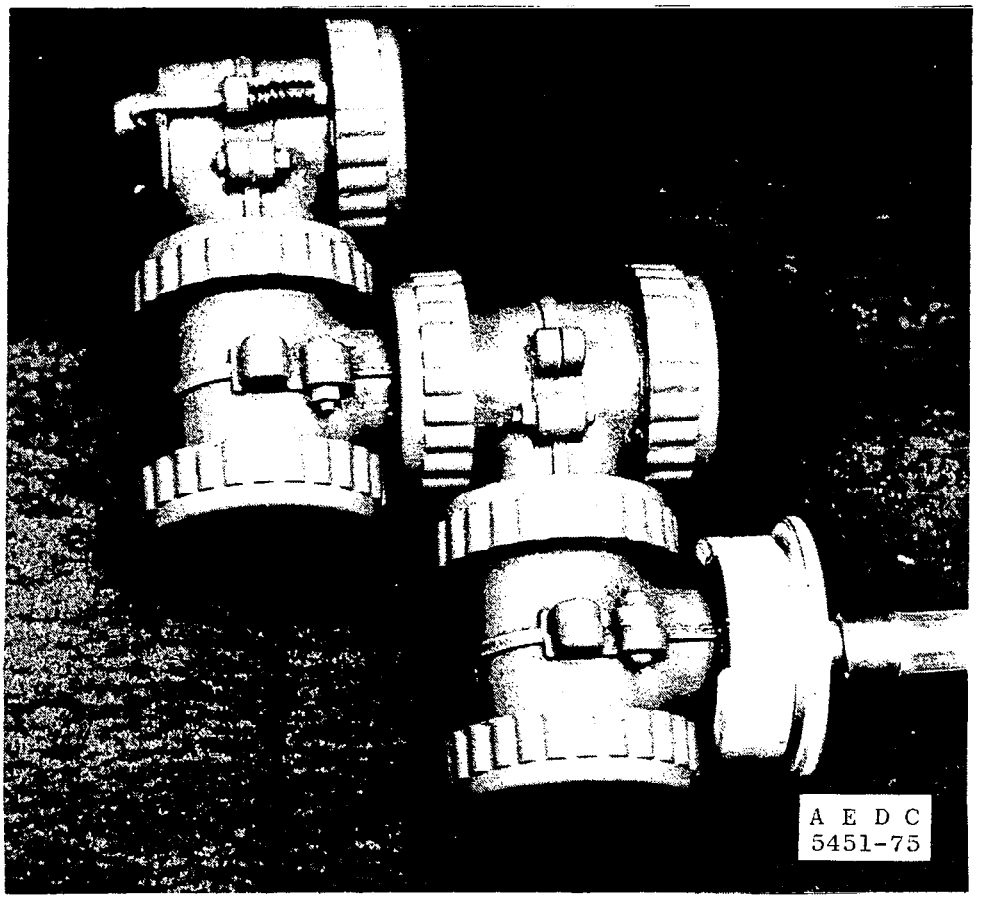

Figure 12. Cascade impactor.

3.2.3 Rotating Vanes

Several suggestions have been made as to possible methods of recovering samples from actual ground clouds produced by large solid-fueled rockets. The use of small radio-controlled aircraft is very appealing because of the ability of such aircraft to follow the cloud and penetrate it when desired. Since a wide variety of both radio control equipment and model aircraft have been produced for the hobby market, this equipment is readily available and relatively inexpensive. An obvious limitation is the size and weight of the instrumentation which could be carried. While there is some question about the possibility that an HCl detector could be developed for such a test bed, there is little doubt that it could serve to collect samples of Al_2O_3 particles. As a first step in evaluating the sampling capabilities of such a system, a model airplane propeller was mounted on the shaft of a high-speed

electric motor. A short strip of double-sided sticky tape was applied to both blades to collect the sample. Also, a short section of an airfoil representing the leading edge of a wing tip was attached to a rotating arm to simulate the forward velocity of a plane flying through the cloud. The leading edge of this airfoil was also covered with a sampling tape.

3.2.4 Settling Plates

The settling plates used to collect samples of the Al_2O_3 particles are described in Section 3.1.7, "Copper-Coated Aerosol Detectors."

4.0 TESTS IN AEROSPACE CHAMBER 12V

4.1 DESCRIPTION

A total of 18 test firings were conducted in the 12V chamber. The prime variables were the initial relative humidity and the addition of spray cooling water in the flame trench. The ambient temperature varied slightly from day to day and ranged from 23.9 to 27.5°C. A test matrix is presented in Table 1.

A typical test consisted of the following sequence. All bubblers were loaded with distilled water and located in the chamber. Millipore filters were also installed and connected. The high-speed camera used to photograph the flame trench was loaded and set on standby. The 35-mm sequence camera was loaded and also set on standby. If the test was to include spray water in the flame trench, then the reservoir was loaded with the required amount of water and pressurized. The rocket motor was then mounted on the test stand and the pressure transducer; thermocouples and ignition circuit were connected. The timing sequencer was then programmed and run through a cycle with all systems disarmed except the bubblers and the millipore filters. During this precheck the flow rates through the bubblers and filters were adjusted to the desired levels. The correct sequencing of other components was checked by observing the indicator lights. A typical sequence is shown in Fig. 13.

After the sequencer check, the cameras and rocket motor were armed and the chamber door locked. The humidity in the chamber was then measured with the remote hygrometer and a calculation made of

the amount of water which needed to be added to bring the humidity to the desired level. This quantity of distilled water was then added to the chamber via the pressure-atomizing spray system. The two mixing fans were then turned on to ensure complete evaporation of the spray and uniform mixing of the water vapor. The fans were then stopped and the humidity was again measured and recorded. The sequencer was then started, and the ignition and burn were monitored by viewing the TV display from the overhead camera.

After the rocket burn the exhaust products were monitored for periods from 30 min to 2 hrs, depending on the particular test. The coulometer, chemiluminescent detector, condensation nuclei counter, and continuously monitored bubbler were manually operated by test engineers.

After completion of the test, the valve to the exhaust ducts was opened and the main chamber door was released from its locks. As the remaining gases and smoke particles were swept from the chamber, the door was gradually opened wider. When the visible smoke had cleared completely, the chamber was entered and the bubbler, millipore filters, and fallout disks were recovered.

Table 1. Test Matrix

Coulometer	Geomet	CNC	Cont.	Bubbler	Run No.	Ambient Temperature, °C	Relative Humidity, Percent	Water Injection	Comments
		x		x	1	26.1	29		Deflector Plane Set at 48 deg
	x	x		x	2	23.9	31		Vent Fan on During Firing
x	x	x		x	3	25.0	71		Moved Coulometer Outside Chamber
x	x	x		x	4	27.2	45		Moved Geomet Outside Chamber
x	x	x		x	5	26.1	50	x	
x	x			x	6	26.7	89		
				x	7	24.4	67		
				x	8	25.3	69		
		x		x	9	26.7	72	x	
		x		x	10	24.4	67		Deflector Plate Lowered to 21 deg
		x		x	11	27.5	42		
		x		x	12	24.4	67	x	
				x	13	25.6	64		
				x	14	25.6	87	x	
		x		x	15	27.5	82		
		x		x	16	25.0	75		
				x	17	27.2	64*		Simulated Light Rain During Firing
				x	18	25.6	100		Reduced Chamber Pressure to Produce Fog

*Initial Humidity at t = 0

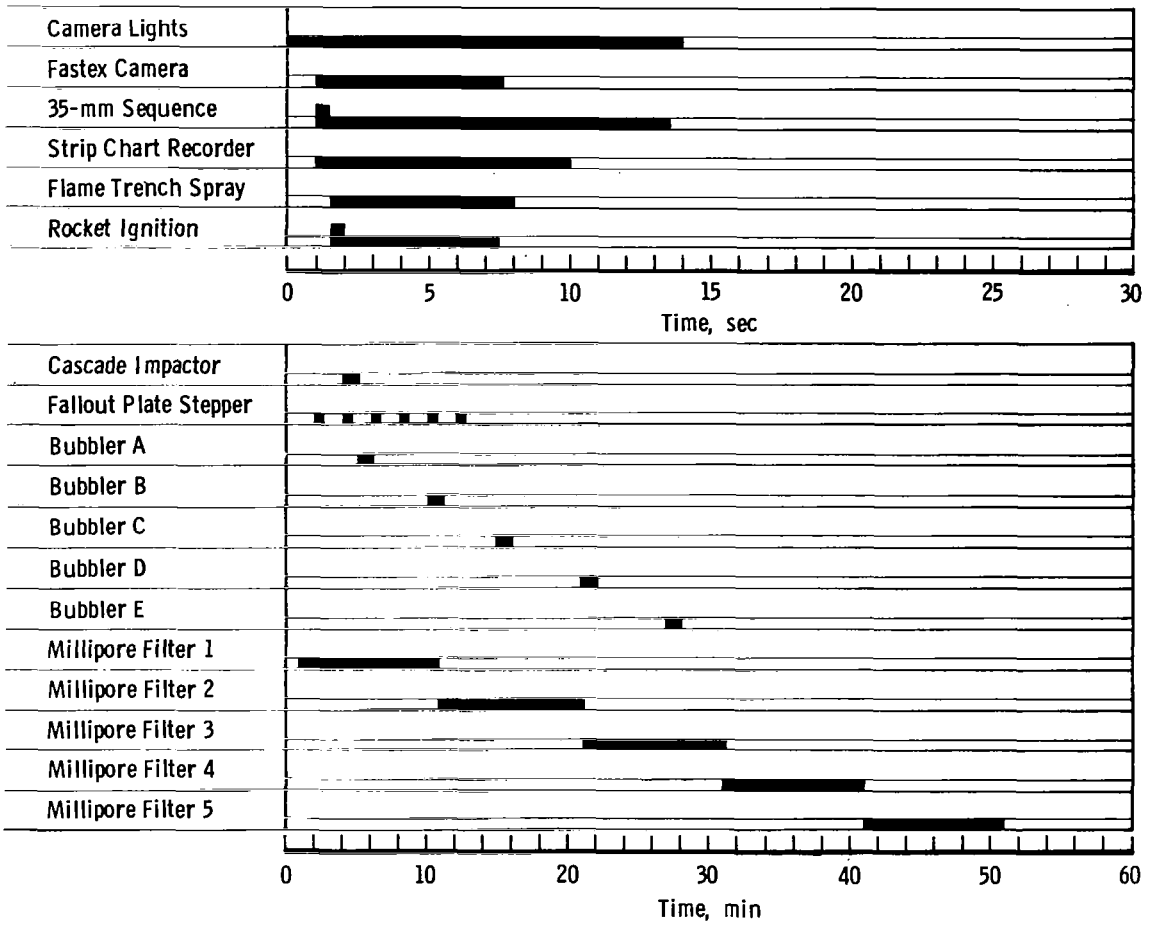

Figure 13. Typical timing sequence.

The last two tests differed slightly in that for test number 17 the humidification spray system was fitted with a coarse nozzle and the spray was left on during the firing and part way into the data-taking period. In test number 18 the chamber relative humidity was raised to 98 percent by the water system, and then a large Rootes blower was turned on which dropped the chamber pressure approximately 20 mm of mercury in a period of 30 sec. This adiabatic expansion of the air in the chamber produced a dense fog. The pump valve was then closed and the engine was fired into the fog.

4.2 RESULTS

A series of HCl gas release tests was conducted in which HCl gas was released into the environmental chamber. After the gas was released, the mixing fans were turned on for 20 sec to distribute the HCl throughout the entire volume. The HCl concentration was then measured at 10-min intervals to determine its decay rate. Data were obtained from four bubblers located in the center of the chamber. Each bubbler was operated for one minute at the appropriate time. Three tests were made, with the initial conditions of 30, 68, and 82 percent relative humidity. In each case 19 gm of HCl were released. Assuming uniform mixing of the gas within the chamber and no wall losses, this would yield a maximum concentration of 100 parts per million.

The results of these tests are presented in Fig. 14. It is apparent that there is a significant loss of HCl during the mixing process since the extrapolated concentration at t = 0 is lower than the calculated maximum. The data indicate that the decay is logarithmic and that there is no significant dependence on the initial relative humidity.

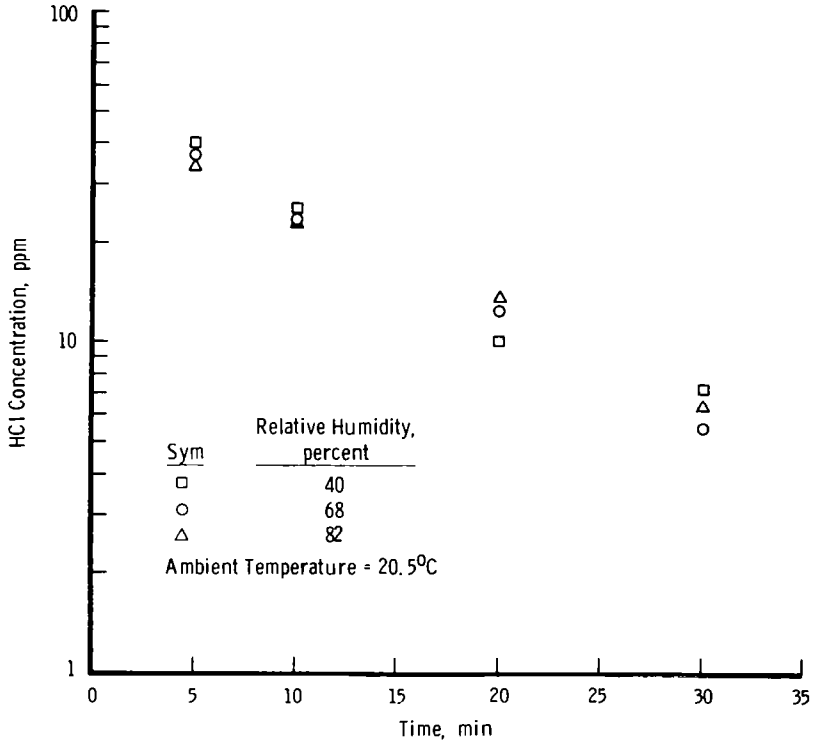

Figure 14. Decay of HCl gas released in chamber.

4.3 ROCKET MOTOR FIRINGS

Tests 1 through 17 were conducted with a rocket motor loaded with 85 gm of propellant. Assuming uniform mixing and no losses, these motors would produce a cloud with a maximum HCl concentration of ≈100 ppm and an Al_2O_3 particle loading of 1.97×10^{-4} gm/liter. Test No. 18 was conducted with a 170-gm propellant load. During the firing of the motors the environmental chamber pressure rose an average of 9 mm and then dropped back to ambient within two minutes. This agrees well with the prediction that with no wall losses, the added gases plus the heat of combustion would result in a maximum overpressure of 10 mm of mercury. In Test No. 18 the chamber pressure had been reduced to produce the fog. Firing the rocket motor brought the chamber back to atmospheric pressure. At this point a vent valve was opened at the top of the chamber and the chamber remained at atmospheric pressure for the duration of the monitoring period.

Miniature thermistors (1-sec time constant) located in the exhaust plume as it rose from the flame trench indicated a temperature rise to 70°C during firing (Fig. 15). Similar thermistors located in the top of the chamber indicated less than a 0.5°C fluctuation in temperature throughout the complete test period.

4.3.1 Measurement of HCl Concentrations

Measurements of HCl concentrations were made with several instruments. Comparative data from the Geomet chemiluminescent detector, the modified condensation nuclei Counter (CNC), the continuously monitored bubbler, and individual bubblers are shown in Fig. 16. Individual bubblers located at points 1, 4, 5, and 6 (Fig. 17) indicate that there was a significant gradient immediately after the engine burned but that this gradient had disappeared after 5 min. The absolute concentration of the HCl as determined by the bubbler was 38 percent lower than the Geomet. This can be explained by later tests which showed that the Al_2O_3 particles ingested in the bubblers buffered the HCl solution, thus raising the pH slightly. The most important aspect of this data is the fact that three instruments all recorded the same rate of decay. This decay compares well with the decay measured for pure HCl releases in the chamber (Fig. 14).

The data for the HCl decay for engine firings into atmospheres of various low humidities are presented in Fig. 18. At the higher humidities the HCl initially decays at a much faster rate, as is shown in

Fig. 19. A comparison of data obtained from the complete test series is presented in Fig. 20. This includes the special cases of an initial misting rain lasting approximately 10 min and a simulated ground fog. It will be noted that these data can be fitted with two linear decay rates.

The agreement between the HCl decay rate for the misting rain and the high humidity tests suggests that the more rapid removal of HCl is caused by a similar mechanism (i.e., adsorption of HCl by water droplets). In the case of the high humidity environment this would involve condensation and droplet growth in the exhaust cloud itself. Additional evidence of acid droplets produced during the high humidity tests was obtained on the copper-coated settling plates used in the later tests.

On several tests, spray water was added to the flame trench during the rocket motor firing. The total amount of water added was small when compared to the total quantity of water available in the ambient air in the test chamber (< 2 percent), yet, as is indicated in Fig. 21, there was a significant effect on the level of HCl recorded in the test chamber. The data obtained from the geomet indicate that adding the spray to the flame trench induces some condensation even when the ambient relative humidity is low. A comparison of two decay curves is presented in Fig. 22.

4.3.2 Aluminum Oxide Particulates

Assuming no losses and uniform distribution throughout the test chamber volume, the mass loading of Al_2O_3 particles produced by 85 gm of propellant would be 2×10^{-4} gm/ℓ. Filters operating in sequence were used to collect the Al_2O_3 particulates and monitor the mass loading. The average filter weighed approximately 0.05 gm before use, and during a 10-min collecting period averaged a weight gain of approximately 0.01 gm. All filters were oriented with their front face vertical so that they would not accumulate fallout before or after their sampling period.

Data from all the tests are presented in Fig. 23. There is no evidence of any effect due to initial humidity or addition of spray water to the flame trench on the long term concentration of Al_2O_3 particulates. The one set of data for the simulated misting rain does indicate that some depletion had occurred prior to the sampling periods.

On several test runs some filters were used to sample the Al_2O_3 particles during the first two minutes after firing. These data are

quite random, indicating the nonuniform distribution of the exhaust species at this time. All these filters indicated particle mass loadings in excess of 6×10^{-5} gm/liter with average values around 9×10^{-5} gm/liter. One interesting observation from these data is that the particle sizes on these filters range from submicron to 30 μ, whereas all the particles on filters operated from T + 2 min to T + 100 min are submicron. Scanning electron microscope (SEM) photographs of comparable sections of these two types of particle samples are shown in Fig. 24.

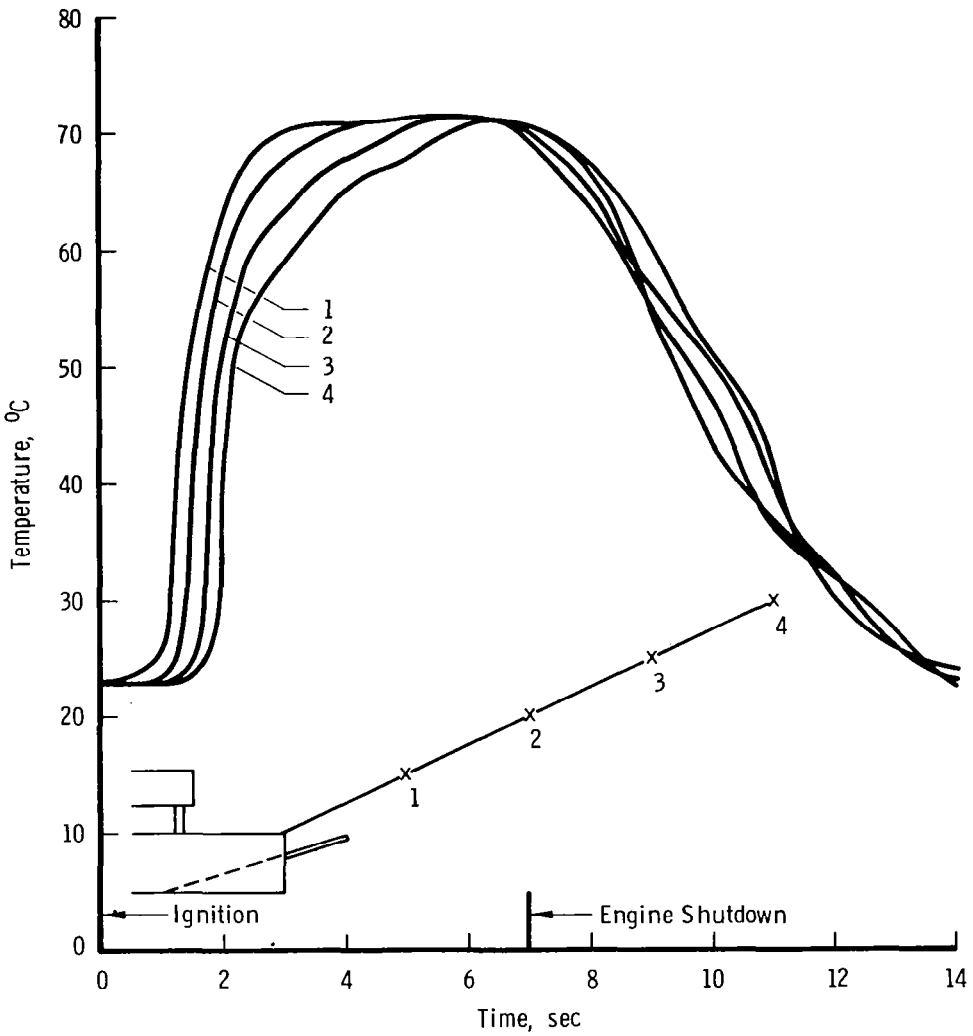

Figure 15. Temperature history of exhaust plume.

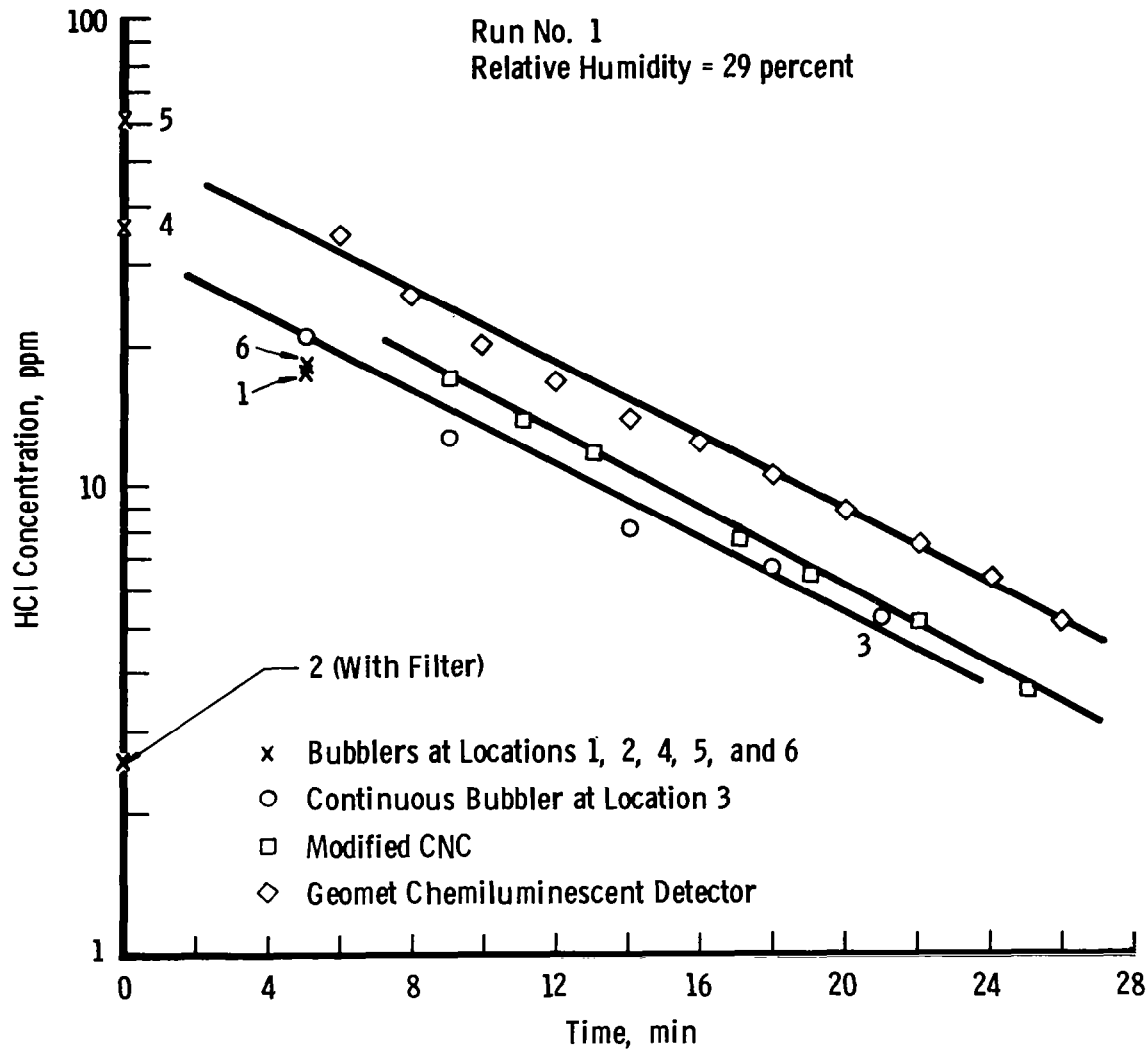

Figure 16. Comparison of HCl decay as determined by various instruments.

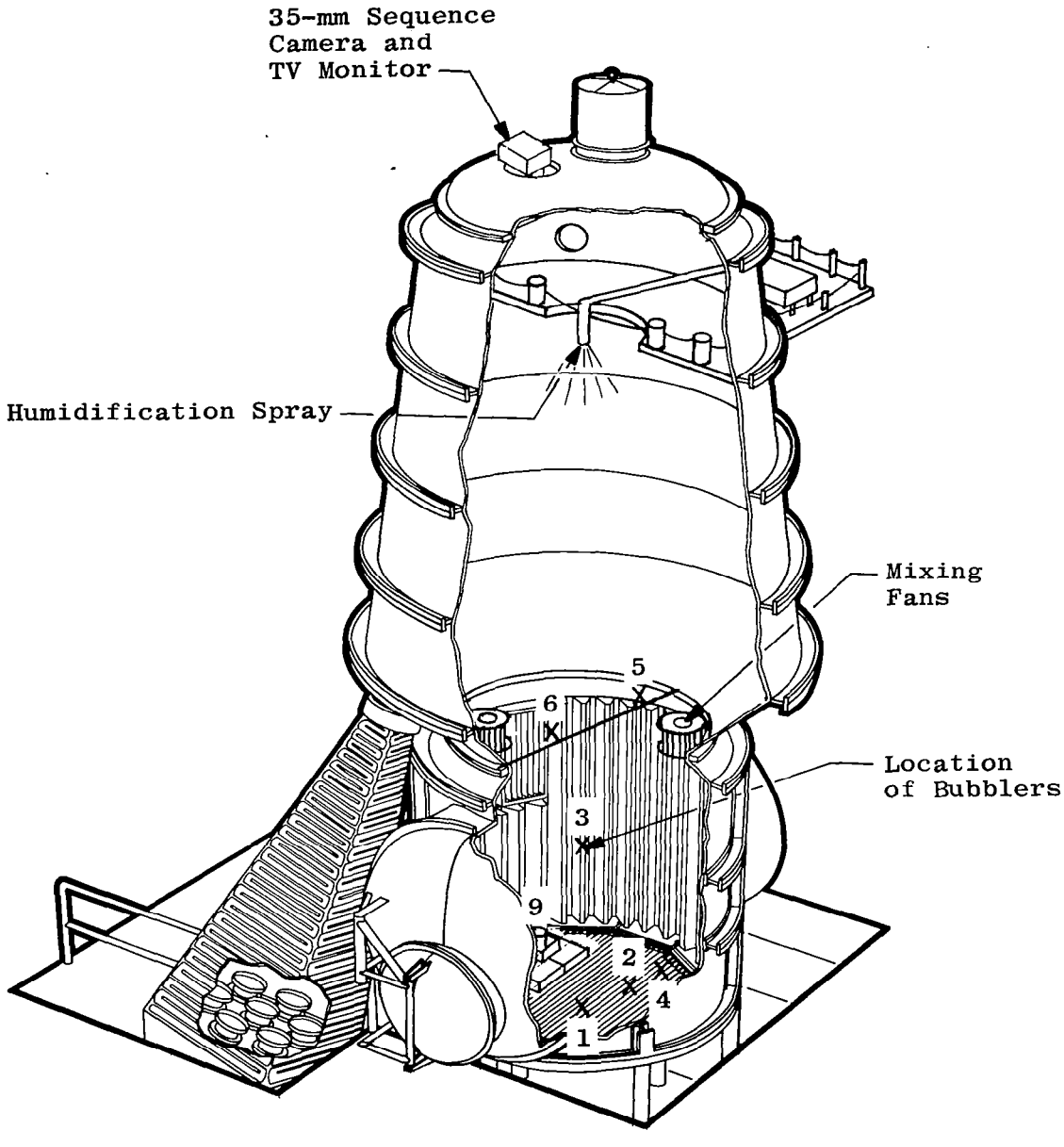

Figure 17. Schematic of Aerospace Chamber 12V.

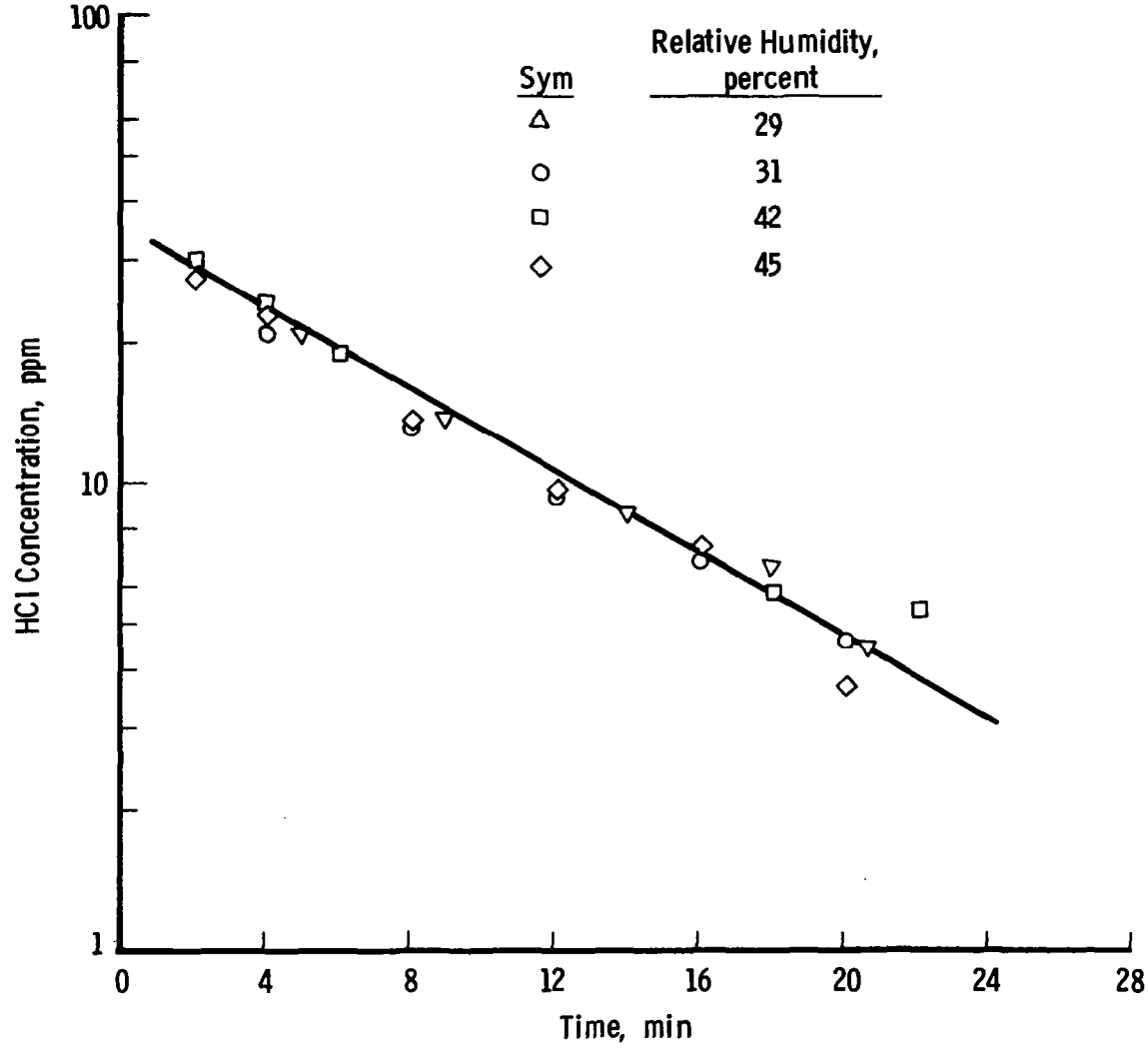

Figure 18. Decay of HCl (low relative humidity).

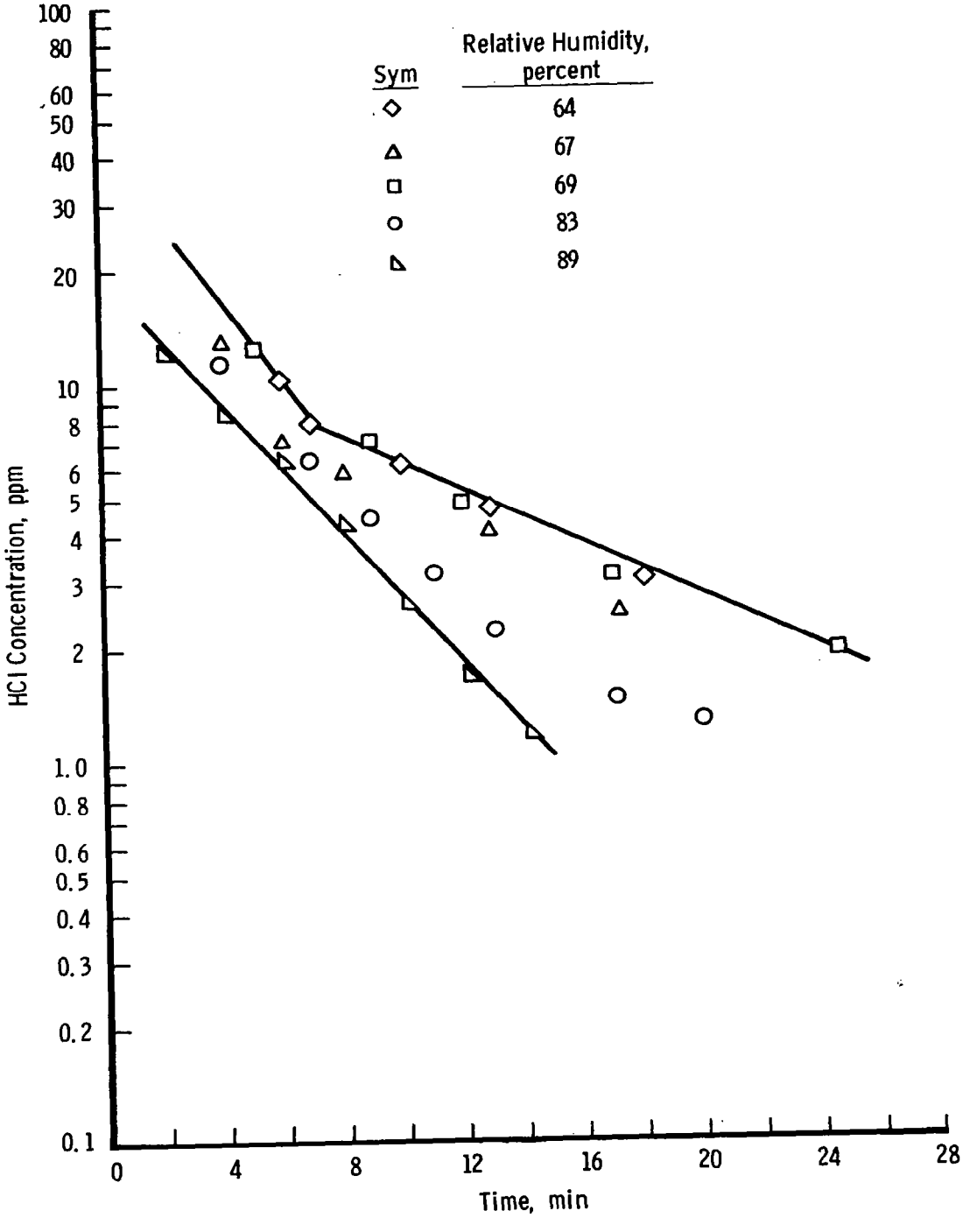

Figure 19. Decay of HCl (high relative humidity).

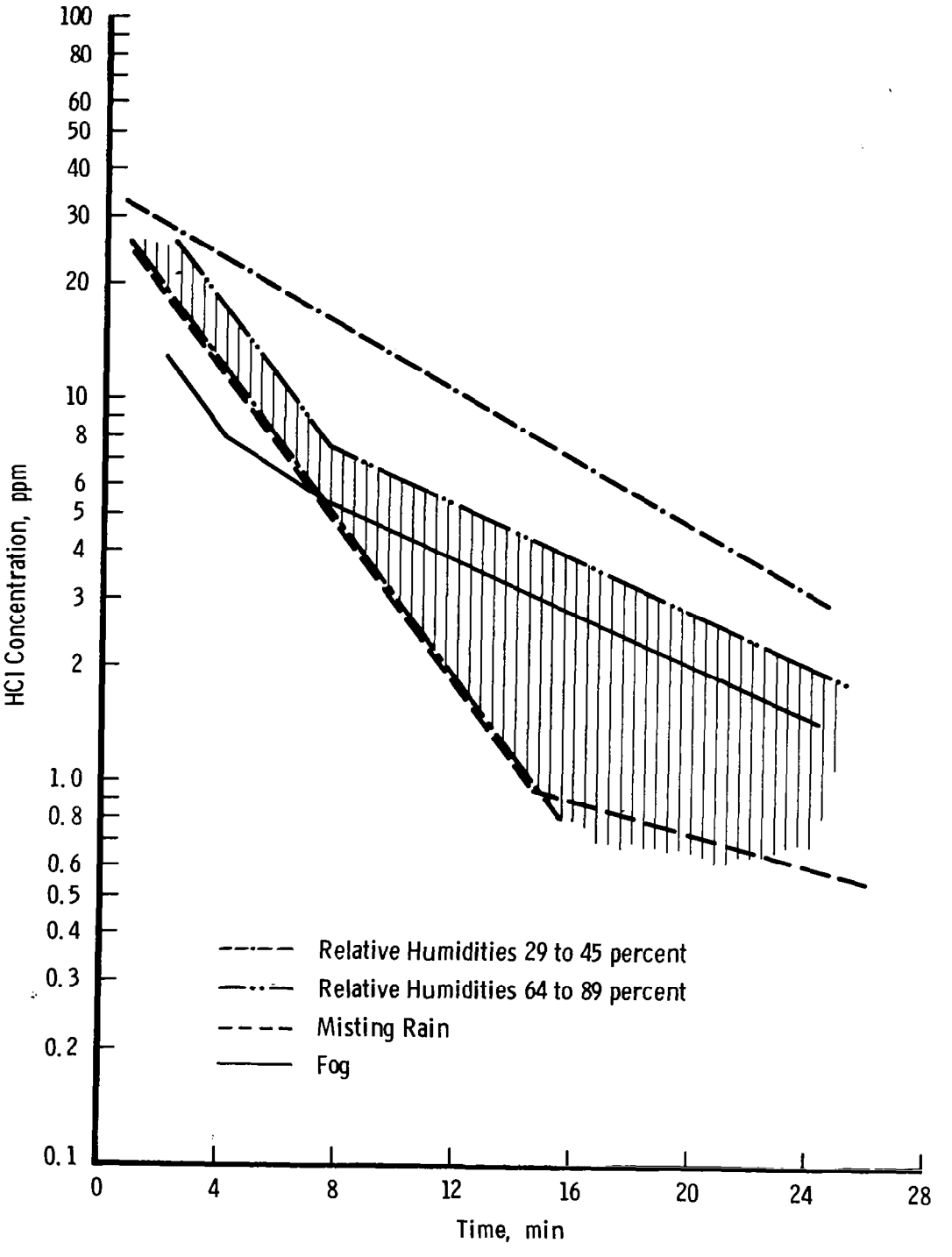

Figure 20. Composite of data including fog and misting rain.

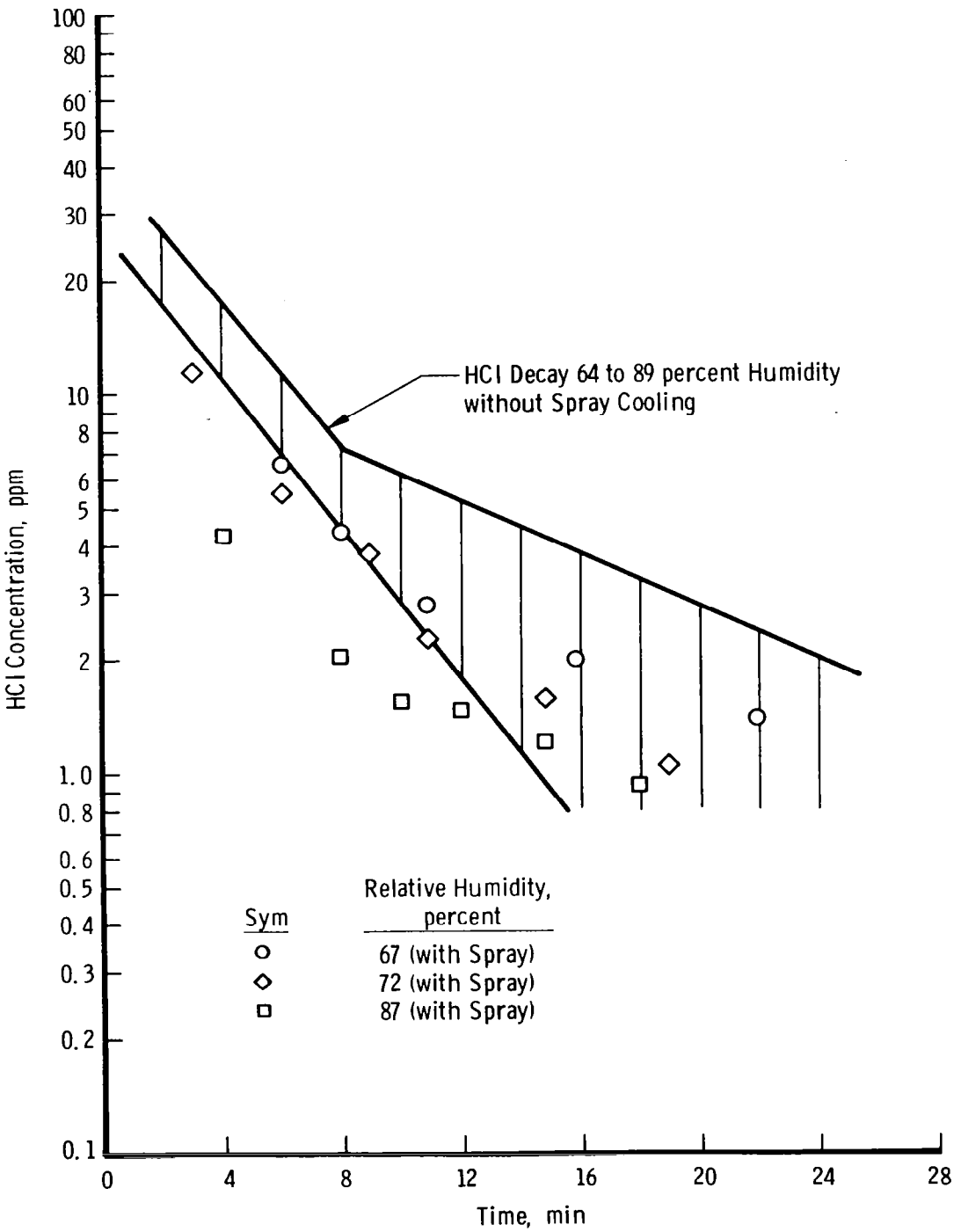

Figure 21. Effect of spray water in exhaust.

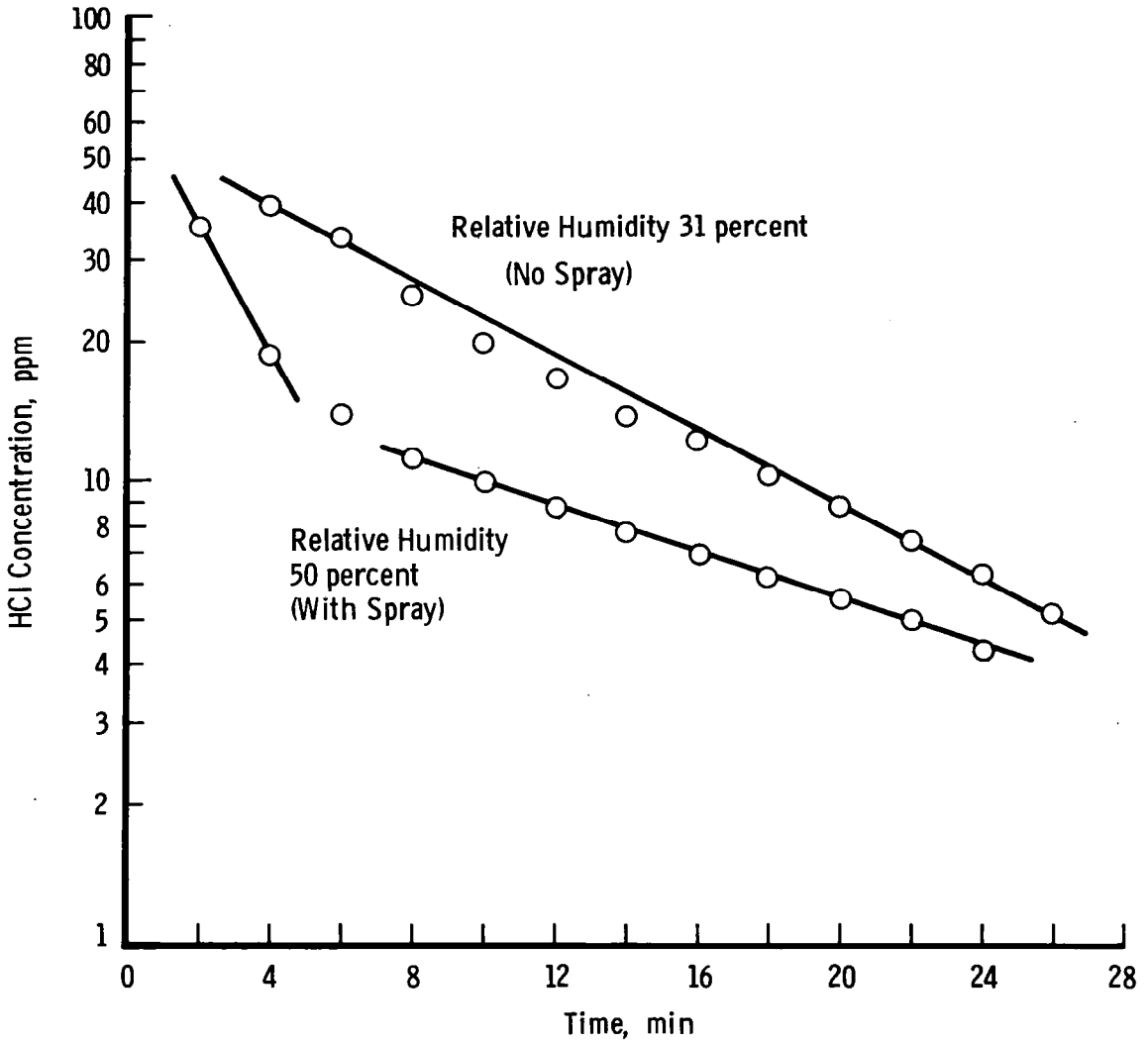

Figure 22. Effect of spray water (low relative humidity).

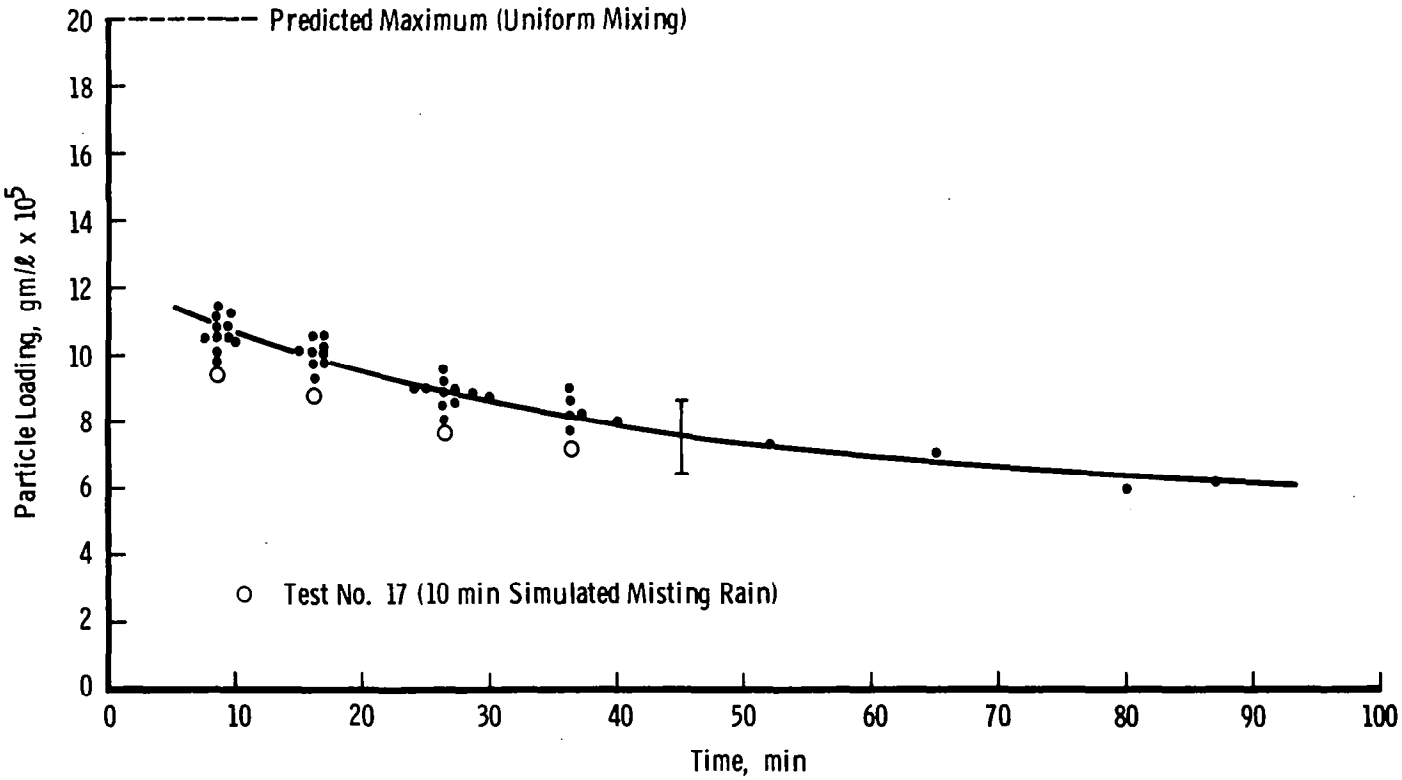

Figure 23. Aluminum oxide particle mass loading (Tests Nos. 1 through 17).

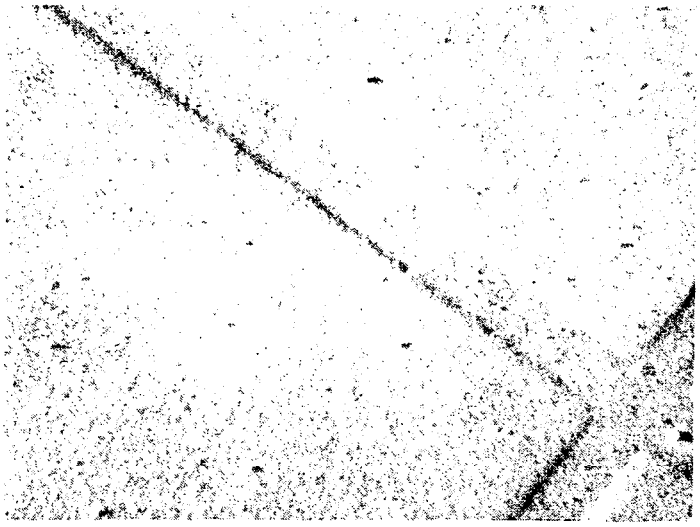

a. T = 0 to 2 min

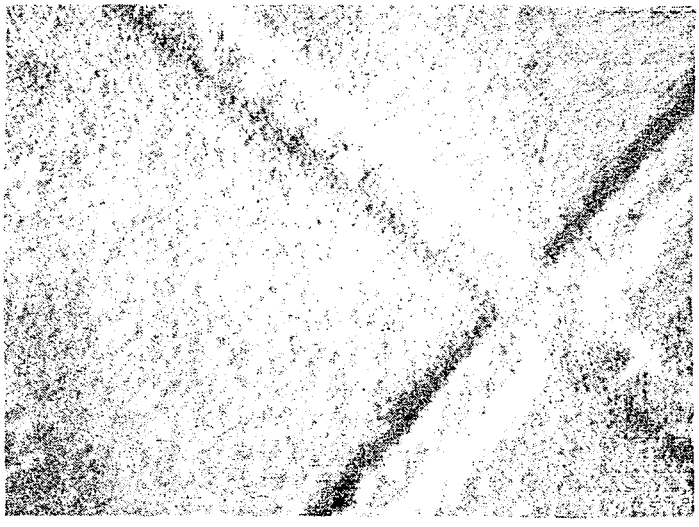

b. T = 10 to 12 min

Figure 24. Particles collected on filters.

5.0 SUPPLEMENTAL SMALL ENGINE TESTS

5.1 TESTS IN ROCKET PREPARATION BUILDING

These experiments were conducted to determine whether the data obtained from confined tests were significantly influenced by the nature of the enclosure. Of particular interest was the observed formation of an acid aerosol at relative humidities greater than 65 percent. In the 12V chamber tests the system was completely sealed, and during the test firing there was a slight overpressure (≈ 9 mm) transient. This set of two firings was conducted in a large metal building formerly used as a rocket motor preparation site. The internal free volume was 8,600 cubic feet. By the very nature of its construction, this building was not sufficiently airtight to sustain any overpressure.

The rocket motor and flame trench were installed at one end of the building, and instrumentation similar to that used in the previous tests was installed on temporary scaffolding. A framework measuring 8 by 6 by 6 ft high was constructed inside the shed and was covered and sealed with clear polethylene sheet. A duct was provided along with a blower to supply fresh air to this enclosure. Test personnel occupied this room and operated the sampling instrumentation during these tests. This arrangement proved to be quite useful in that it located the instruments well inside the test volume without long sampling lines, and at the same time provided immediate access to all operational controls (Fig. 25).

The first test was conducted with an ambient temperature of 80°F and a relative humidity of 68 percent. The motor was loaded with 255 gm of fuel. There was no significant difference between the results obtained and those recorded in the previous chamber tests. The copper-plated disks recorded an acid aerosol which persisted for the first few minutes. The decay rates of the HCl showed an initial rapid decay followed by a slower decay rate. The absolute level of the HCl and particulate concentrations were higher than in comparable ARC 12V chamber tests; however, this was expected since the predicted maximum level for uniform mixing was 150 ppm.

The second test was conducted with 170 gm of fuel in the rocket motor in order to set the exhaust concentration to a level comparable to the environmental chamber tests. The ambient temperature before

firing was 72°F with a relative humidity of 52 percent. There was no evidence of any acid droplets on the collection disks which were exposed during this test, although the edges of the disks turned a dark blue. This had been observed on previous occasions when the disks were exposed to fairly high concentrations of HCl gas. The HCl decay curves for these two tests are shown in Fig. 26. As can be noted in comparing these data with those from the chamber tests, Fig. 20, the pattern of the HCl depletion is similar.

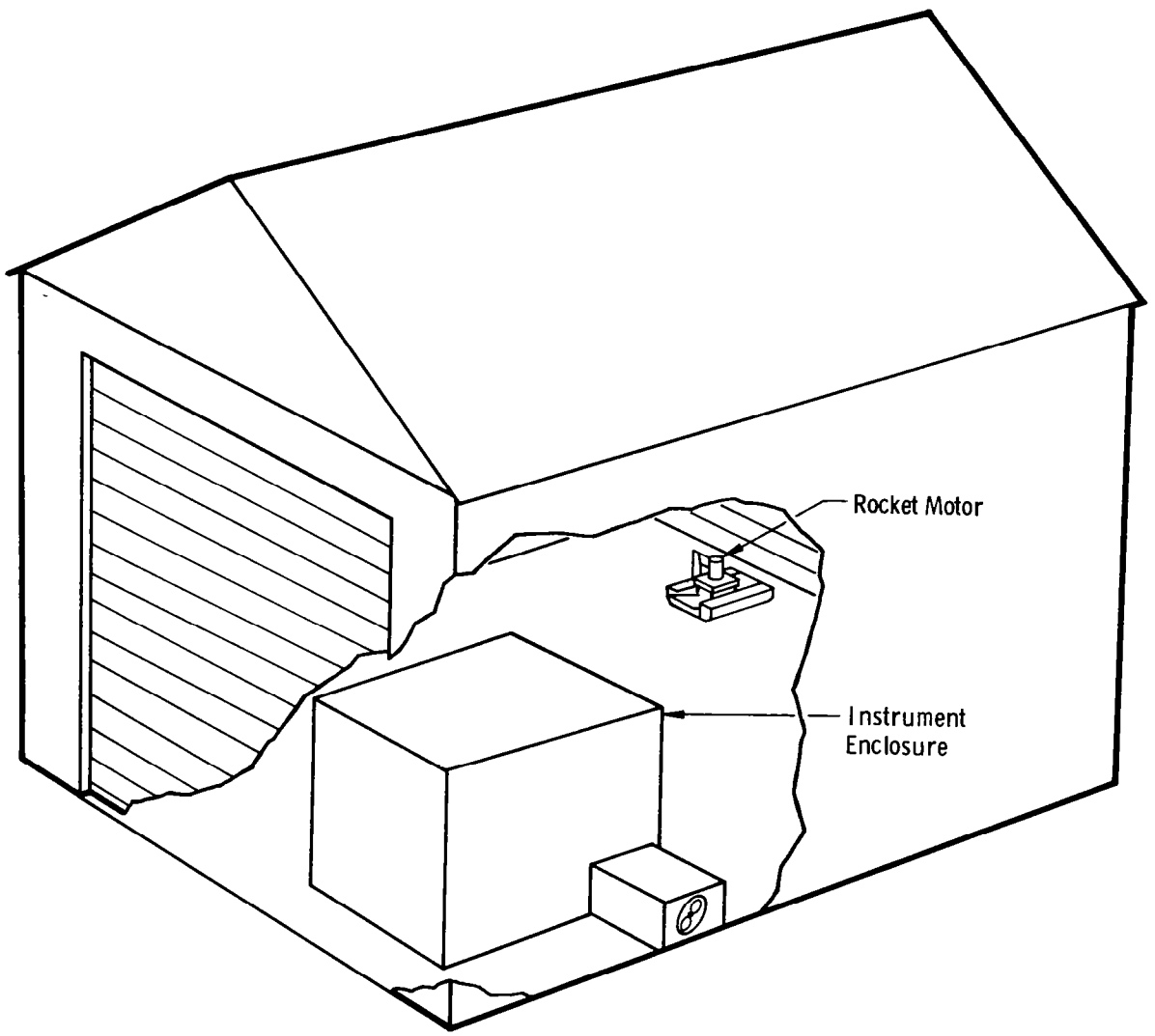

Figure 25. Schematic of rocket preparation building.

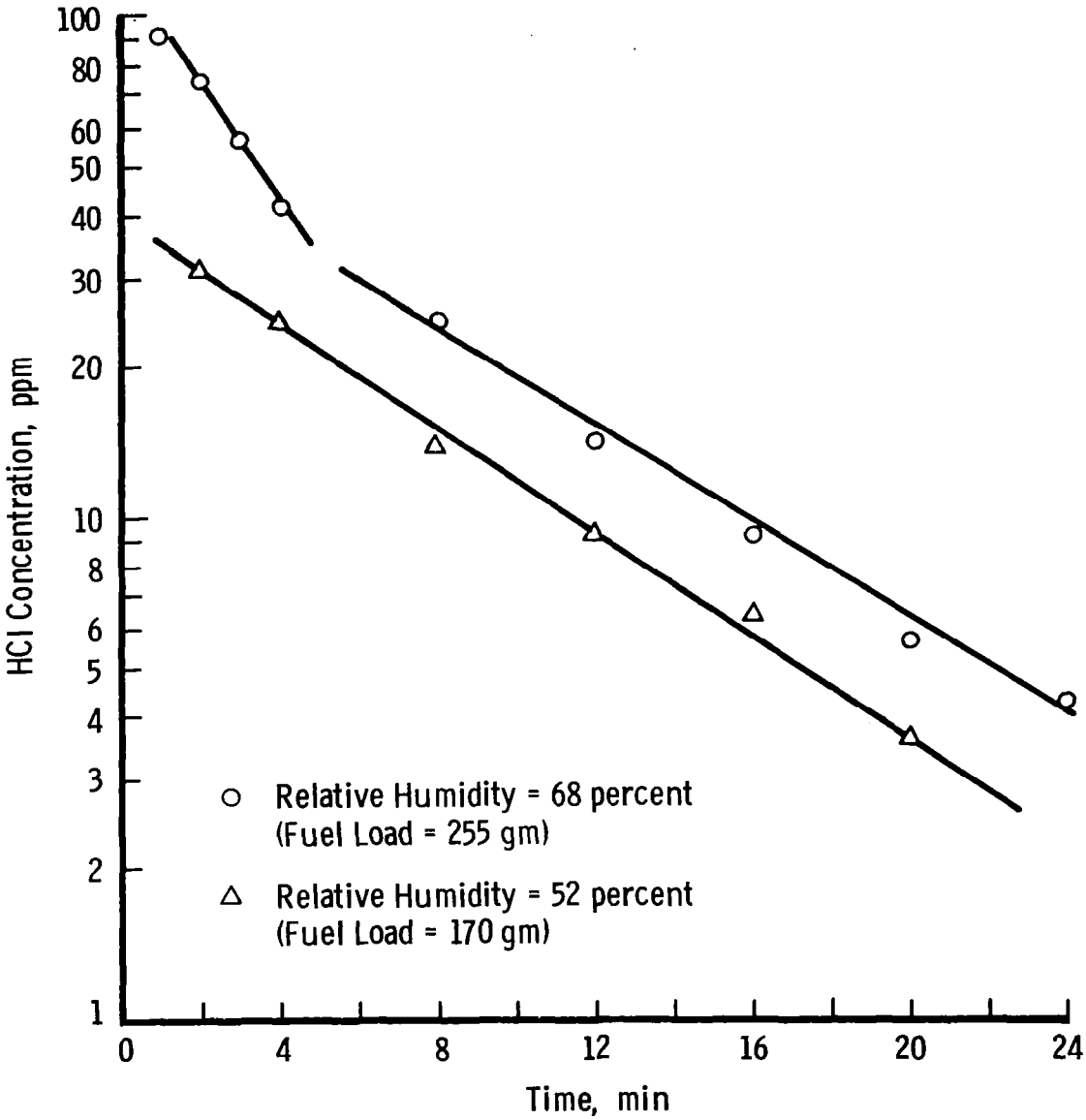

Figure 26. Motor firings in rocket preparation building (HCl decay rate).

5.2 OUTDOOR TEST FIRINGS

5.2.1 Procedure

Four tests were conducted in which the model of the rocket motor and launch pad was located outdoors on a concrete apron. These tests were conducted primarily to gain experience in preparation for monitoring the test firings at MSFC. A network of bubblers, millipore filters, and fallout disks was arranged in a 60-deg arc downstream of the flame trench. The gas samples were drawn through the HCl detectors using the water-driven pumping system shown in Figs. 27 and 28. The total volume of gas sampled can be set by filling the reservoir with the desired volume of water. The sampling flow rate is adjusted by setting the flow valve. In operation the unit is filled with water and the filter or bubbler attached to the suction port. The drain tube is held in the upright position with a small piece of polyethylene tape looped over a short nichrome wire. A small radio receiver and relay along with a heater battery are used to remotely trigger the sampler. At the desired time the power is applied to the nichrome wire, which melts through the polyethylene tape and releases the drain tube. The suction pressure of these pumps can be increased by raising the reservior and increasing the length of the drain tube.

5.2.2 Results

No data were obtained from the first two firings. On the first test the samplers were located too far downwind, and while the exhaust travelled in the direction of the samplers there was too little HCl at ground level for detection. On the second test a transient wind gust blew the exhaust gases to one side of the array of sensors. The third test was successful, and a sequence of photographs of the cloud passing through the first set of sensors is shown in Fig. 29. The average concentrations of HCl based on the dosage measured by the samplers and the exposure determined from the sequence camera data are presented in Fig. 30. The cloud front travelled through the sensors at 3.5 m per second, and the total burn time was 7.5 sec. From visual observations and the sequence photographs it was determined that the cross-sectional area of the cloud front as it passed by the first set of sensors was approximately 6 m^2. Thus approximately 150 m^3 of exhaust gases passed this point. Since the motor contained 170 gm of fuel, 38 gm of HCl would be expected in this cloud, yielding an average concentration of 155 ppm. Considering the uncertainties in estimating the dimensions of the cloud volume, the predicted and

measured values are in good agreement. The fact that the cloud path as defined by the photographs and the cloud path as defined by the HCl measurements agree indicates that at this point in the exhaust cloud history the HCl is contained within the visible cloud boundary.

The ambient temperature for this test was 69°F with a relative humidity of 55 percent. Aluminum oxide particles were collected on the fallout disks, but there was no evidence of acid droplets.

The fourth test was an attempt to reproduce test number 3 except with the relative humidity above 70 percent. However, the wind once again shifted as the engine was fired, and the cloud was blown to one side of the array.

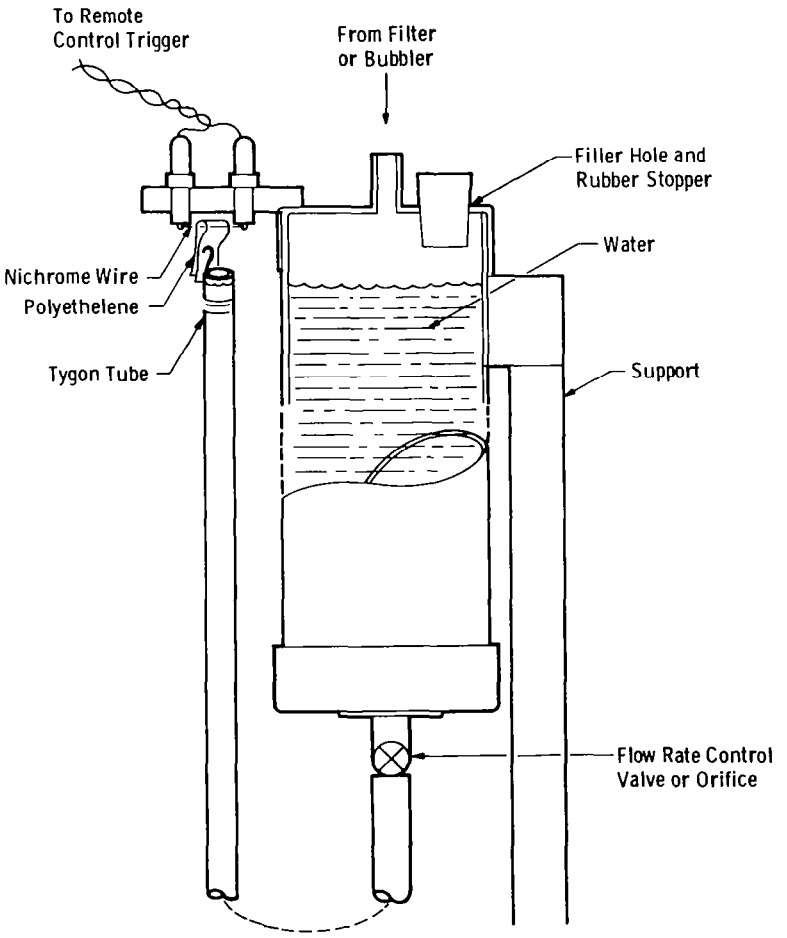

Figure 27. Water-driven sampling pump.

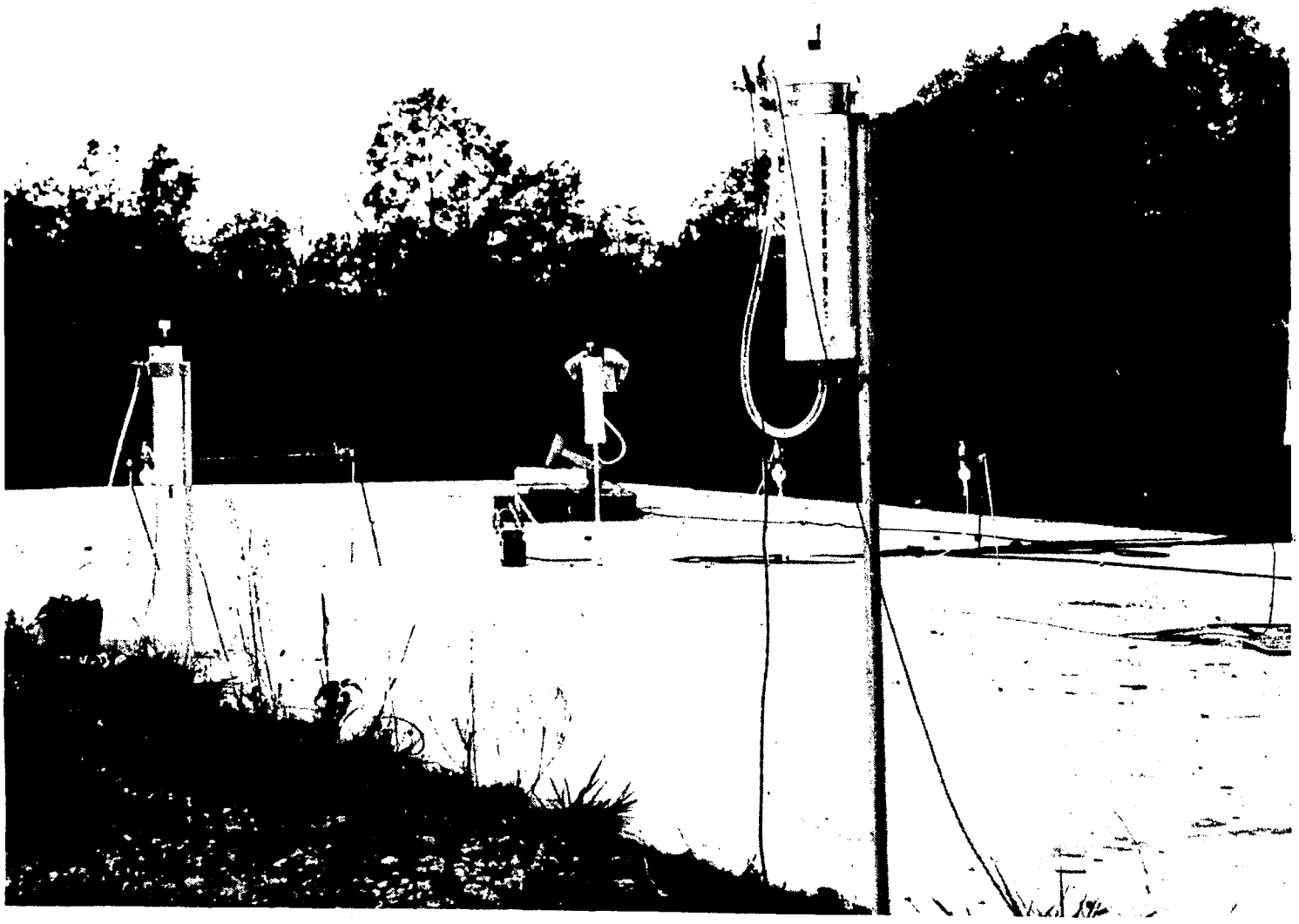

Figure 28. Outdoor test site.

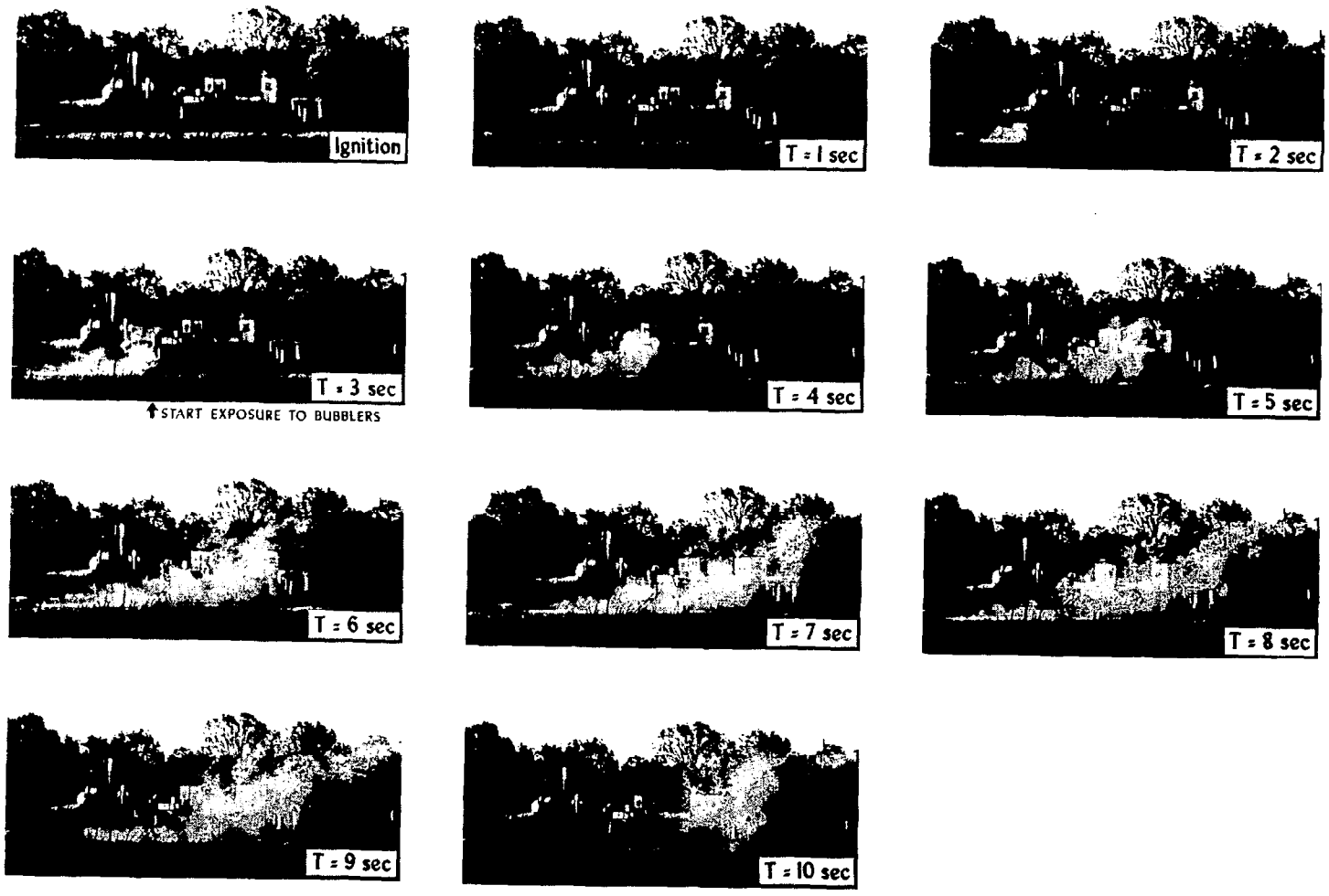

Figure 29. Photo sequence of outdoor firing.

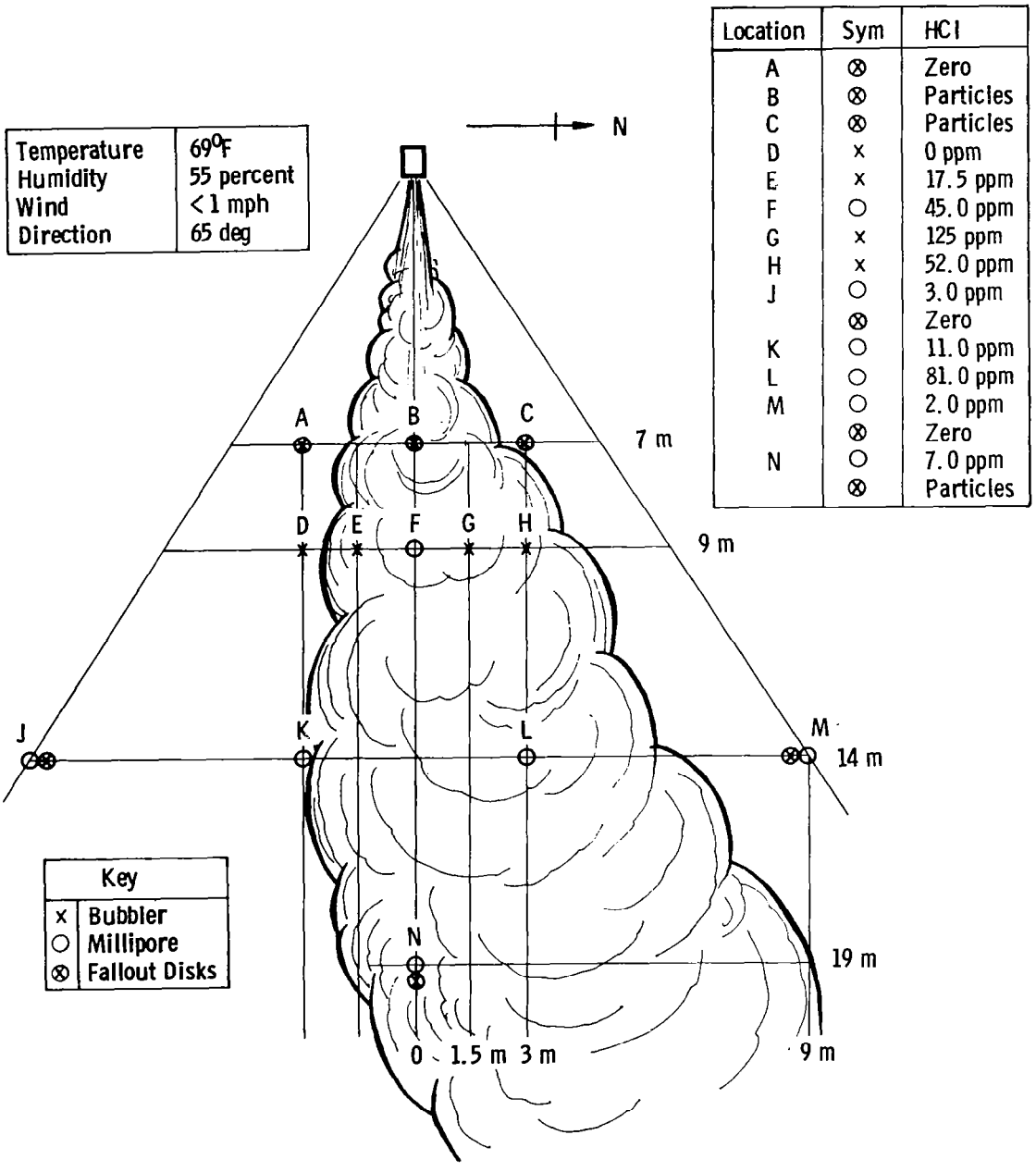

Figure 30. Results from Test No. 2 (AEDC).

6.0 MONITORING OF 6.4-PERCENT-SCALE SSV TEST AT MSFC

6.1 DESCRIPTION

These tests were conducted at the open air test site number 4540 at the Marshall Space Flight Center (Fig. 31) and utilized a detailed 6.4-percent-scale model of the space shuttle vehicle and launch complex. Two TE-M-416 rocket motors were used as the strap-on solid boosters. The solid motors each contained 175 kg of fuel and burned for approximately 8.5 sec. The propellant contained 20.4 percent aluminum, and the combustion chamber pressure was 1,000 psia. The nozzles had an 8.38-cm-diam throat with an expansion ratio of 6.66 and a half angle of 15 deg.

Some of the tests consisted of firing only the solid rocket motors. Others consisted of firing the solid motors and a set of liquid H_2, LOX engines located in the model of the shuttle vehicle. Seven tests were monitored, and the dates and atmospheric conditions are listed in Table 2.

Table 2. Marshall Space Flight Center Tests

Test No.	Date	Temp, °F	Humidity, Percent	Spray Cooling	Camera	Wind Speed, mph	Wind Direction, deg	LOX Engine
1	08-16-74	82	74	No	Yes	< 1	300	No
2	11-22-74	53	90	No	Too Dark	< 2	Variable	No
3	01-09-75	56.5	94	No	Too Dark	4	180	No
4	01-16-75	51.5	72	Yes	Yes	5	360	Yes
5	02-08-75	48	74	Yes	Yes	< 1	215	Yes
6	03-25-75	55	55	Yes	Yes	25	315	Yes
7	10-13-76	81.5	56	Yes	Yes	5	225	Yes

6.2 RESULTS

A schematic of the test site is presented in Fig. 31. A summary of the data obtained from these tests is contained in Figs. 32 through 38, which show the general path of the exhaust cloud and the measured HCl concentrations and dosages at ground level.

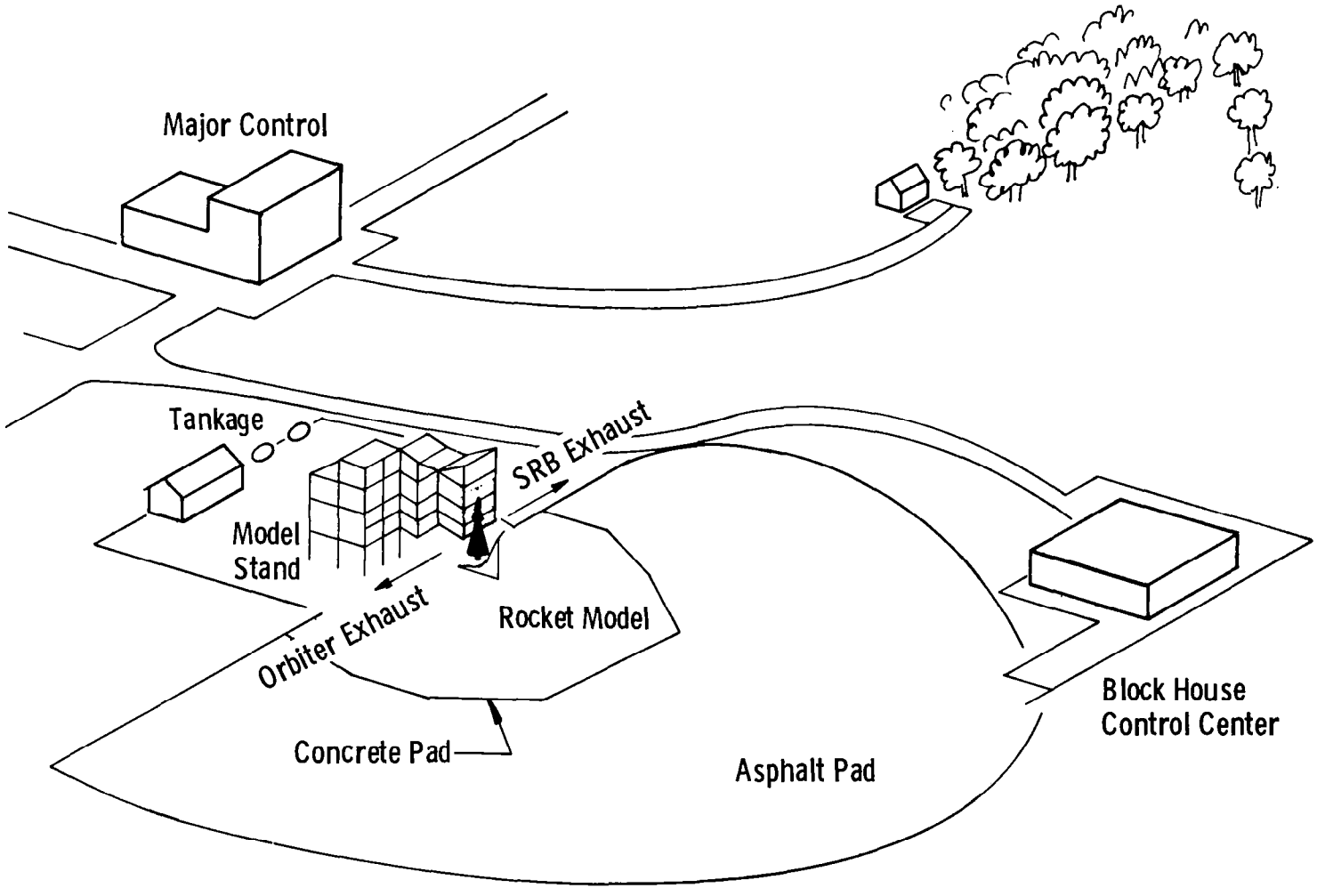

Figure 31. Acoustic Model Test Facility (MSFC).

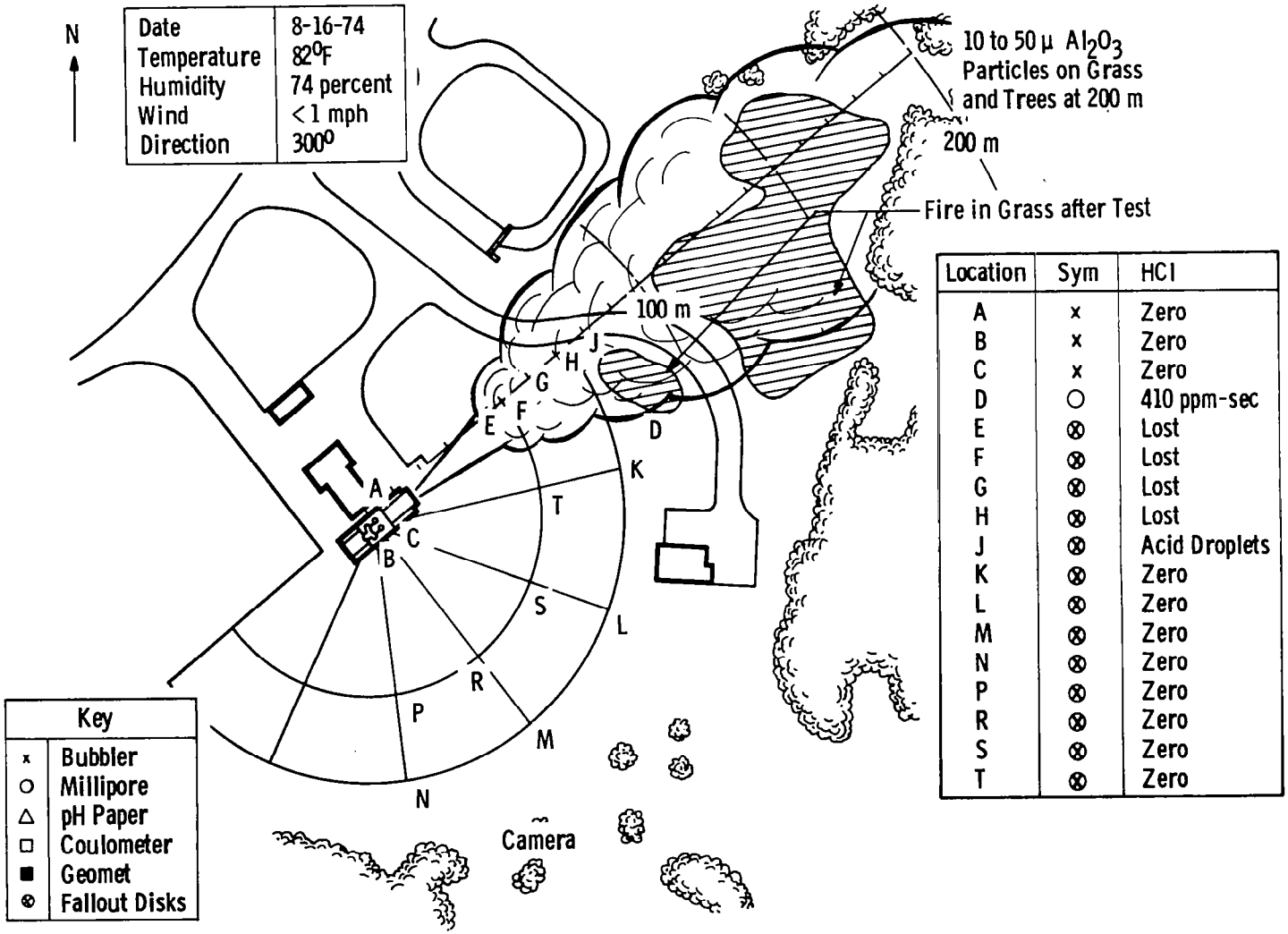

Figure 32. Results from Test No. 1.

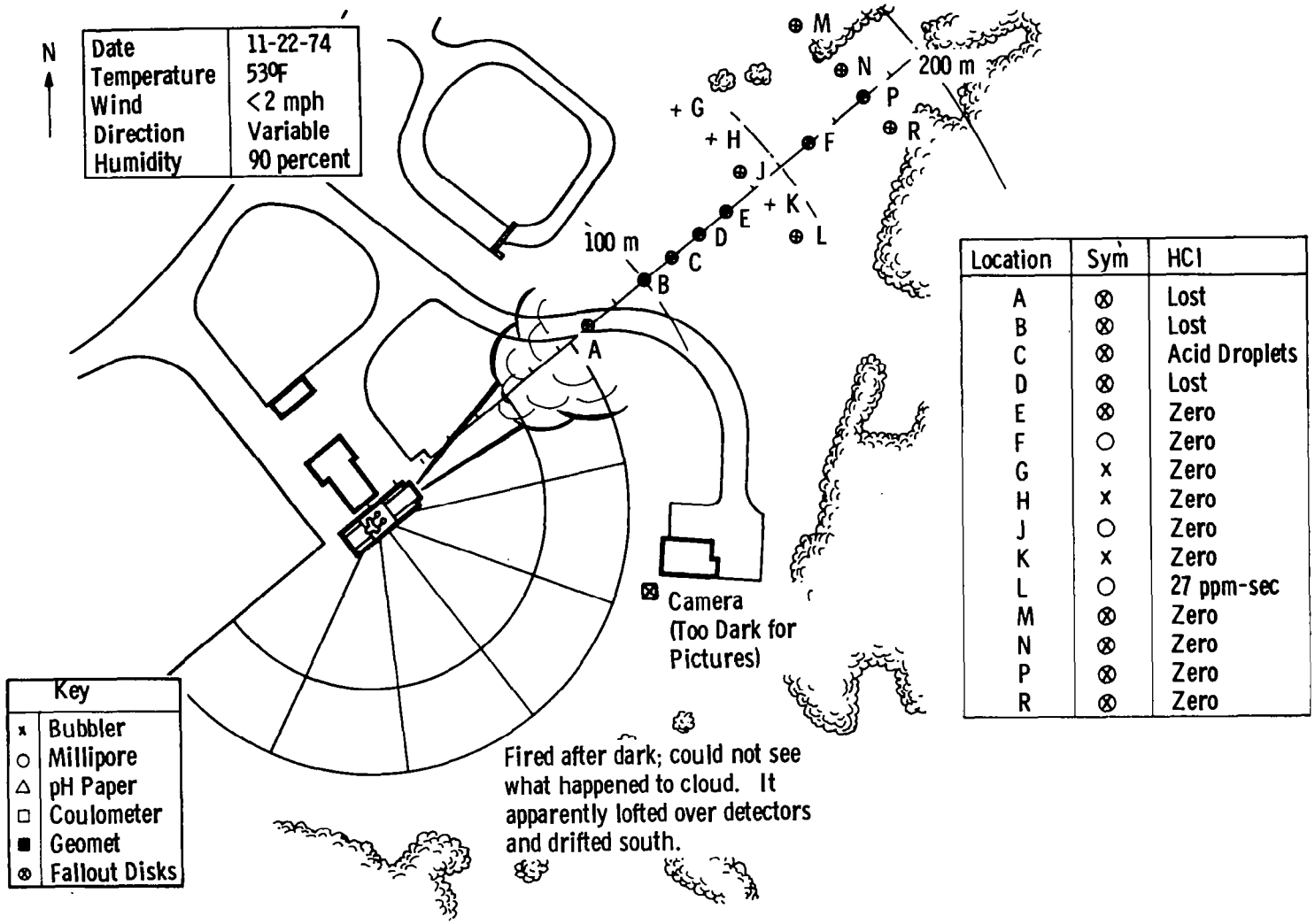

Figure 33. Results from Test No. 2.

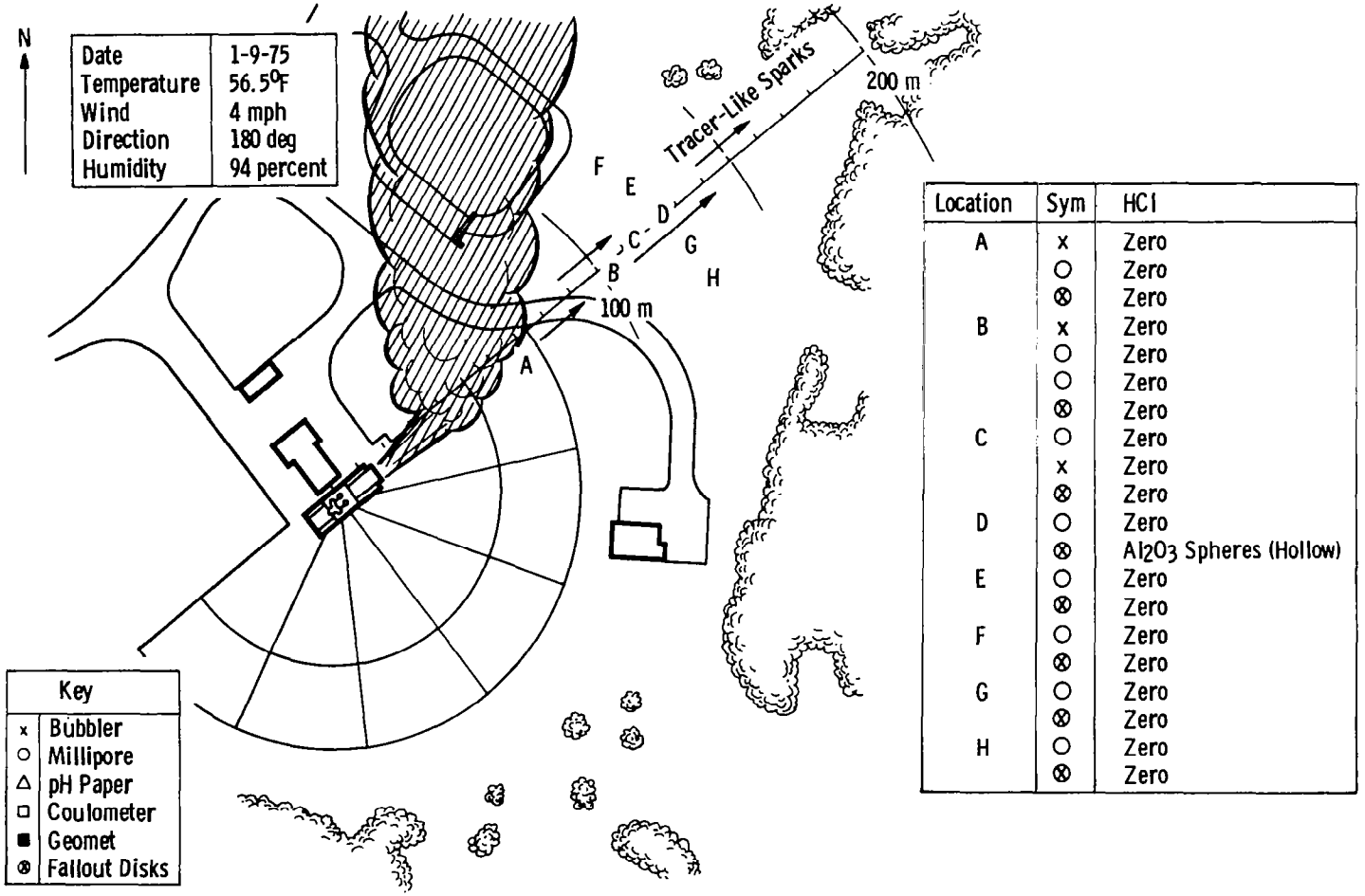

Figure 34. Results from Test No. 3.

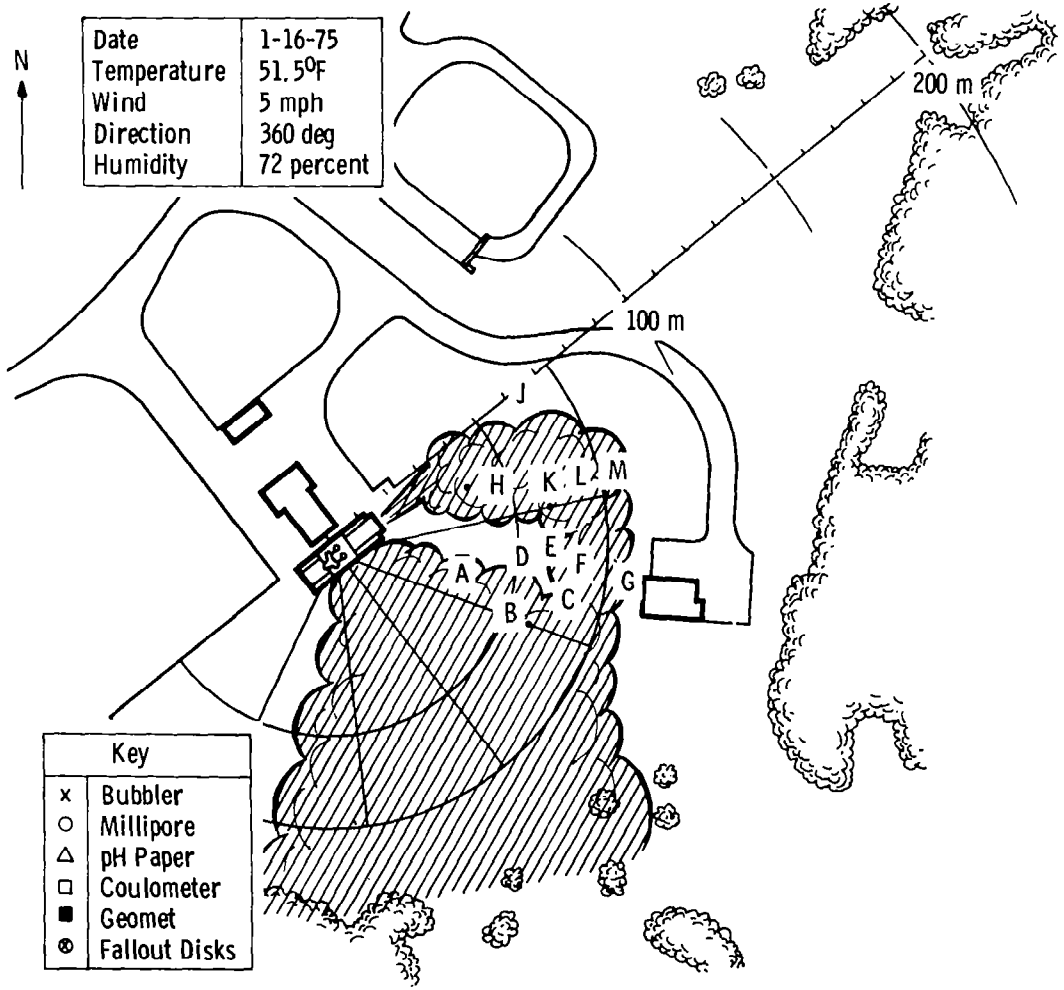

Location	Sym	HCl
A	x	57 ppm-sec
	△	pH 2
	⊗	Aerosol
B	○	62 ppm-sec
	△	pH 2.5
	⊗	Aerosol
C	○	62 ppm-sec
	△	Lost
	⊗	Lost
D	○	70 ppm-sec
	△	Lost
	⊗	Aerosol
E	○	43 ppm-sec
	△	pH 4.5
F	○	100 ppm-sec
	△	pH 2.5
G	○	32 ppm-sec
	△	pH 3.5
	⊗	Aerosol
H	○	Contaminated
	△	pH 2
	⊗	Aerosol
J	x	Zero
	△	pH 5.5
	○	Zero
K	△	pH 3
L	△	pH 4
M	△	pH 4.5

Figure 35. Results from Test No. 4.

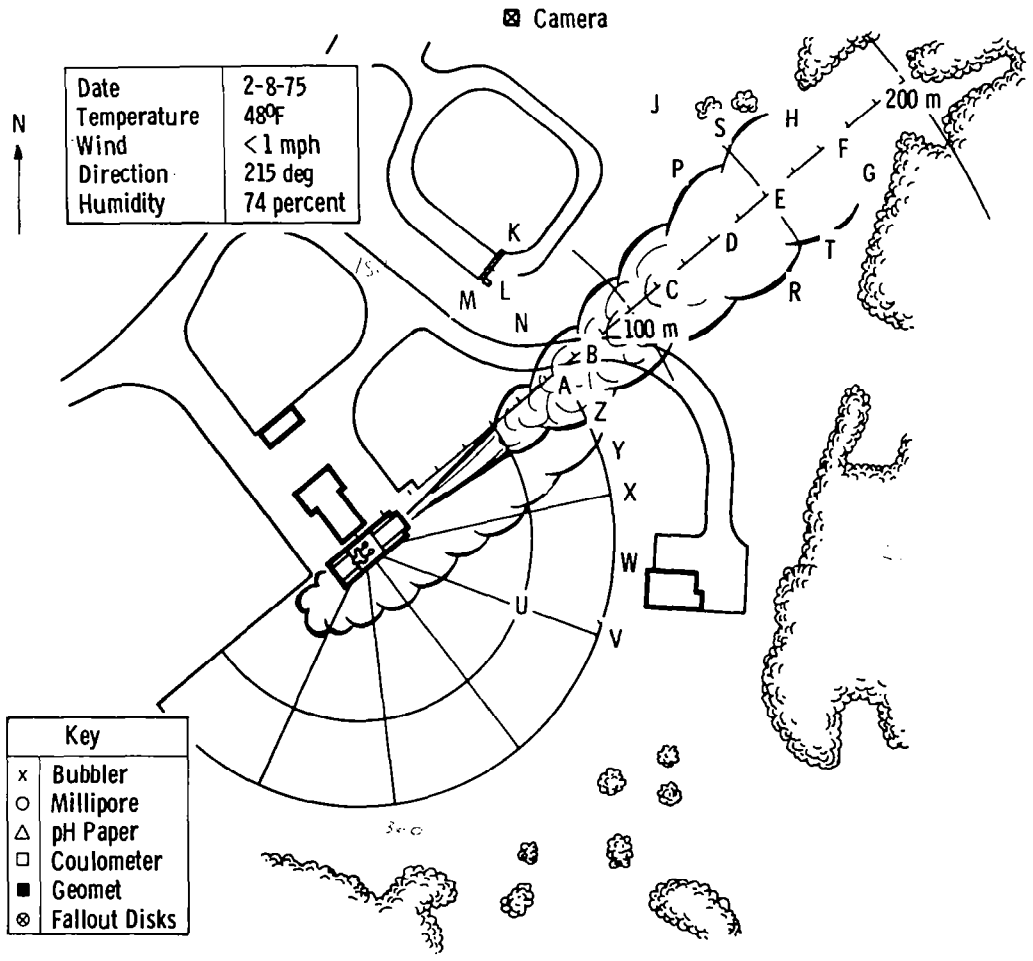

Location	Sym	HCl
A	x	9,000 ppm-sec
	⊗	All Copper Removed
B	x	Destroyed
	⊗	All Copper Removed
	△	pH 1
C	⊗	Aerosol
	△	pH 2.5
	○	81 ppm-sec
D	⊗	Slight Oxidation
	△	pH 3.5
	○	78 ppm-sec
E	⊗	Zero
	△	pH 4.0
	○	32 ppm-sec
F	⊗	Zero
	△	pH 4.0
	○	36 ppm-sec
G	⊗	Zero
	△	pH 4.5
	○	36 ppm-sec
	□	<1 ppm
H	⊗	Zero
	△	pH 4
	○	50 ppm-sec
	■	5 ppm
J→X	⊗	Zero
	△	Zero
Y→Z	⊗	All Copper Removed

Figure 36. Results from Test No. 5.

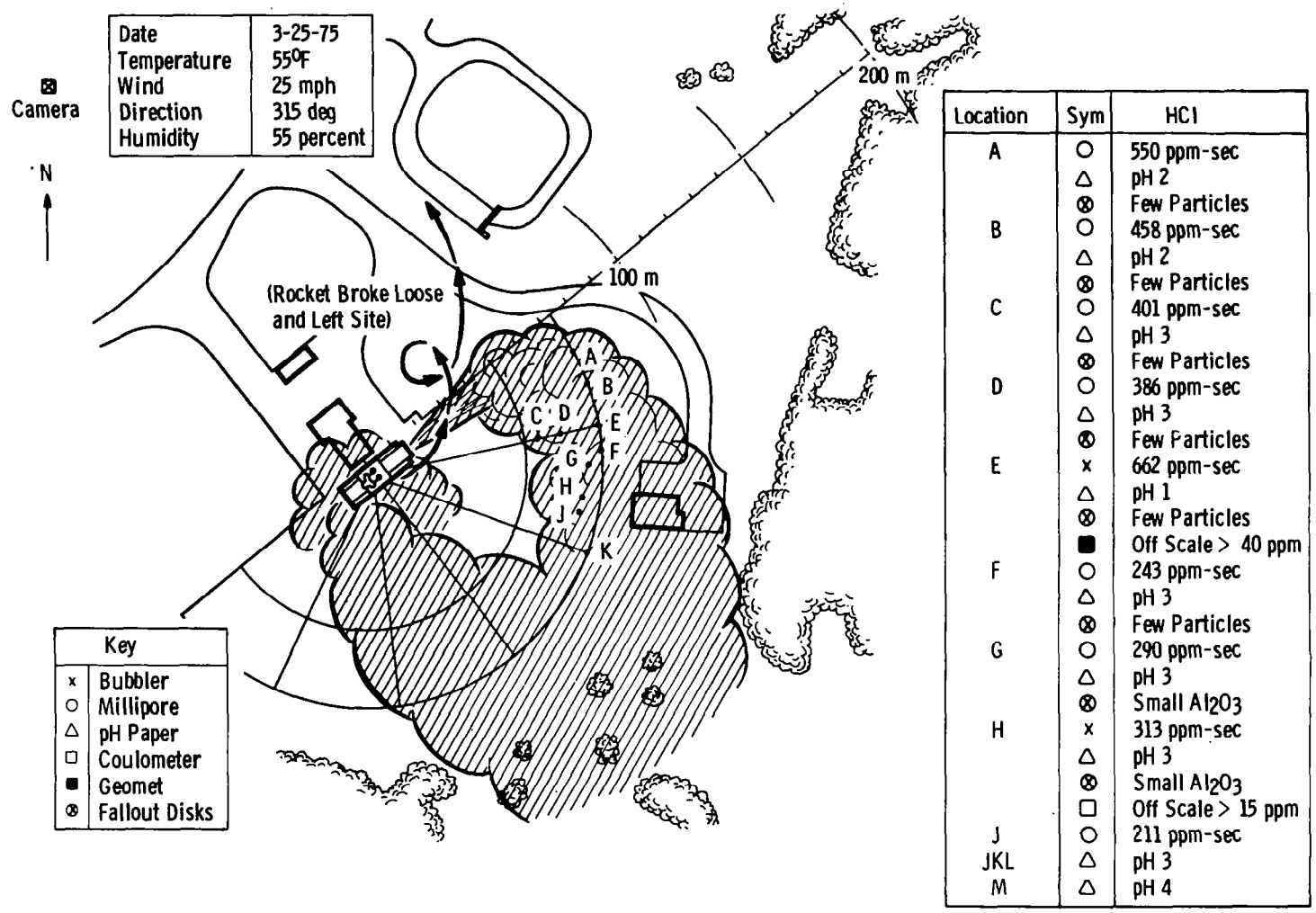

Figure 37. Results from Test No. 6.

6.2.1 Test Firing No. 1

The HCl samplers were located in the superstructure above the test pad. This location was chosen for two reasons. First, there was a radio blackout delcared for all tests, which precluded using the remote samplers with the radio-controlled triggers, and the alternate sampling pumps required a 110-v a-c power source. This was readily available at all levels in the test tower. Second, it was thought that, with such low winds, a significant quantity of the exhaust would rise through the superstructure.

This firing provided several surprises. First, the bulk of the exhaust gases left the exhaust deflector at ground level and stayed on the ground well beyond the perimeter of the asphalt apron. The small portion of the exhaust plume which did rise from the motor burn was swept to one side of the superstructure and bypassed the samplers.

All of the sampling disks located in line with the flame trench except one were swept away by the force of the exhaust. This one, however, produced some good data showing that there was an acid aerosol already present in the exhaust cloud about 80 m from the flame trench. More detailed data from this detector are presented in Section 8.0. Grass samples were taken from the hillside at the 200-m point and were examined under the microscope. Several 10- to 50-μ Al_2O_3 spheres were found on these samples. The grass was kept in water for several days, and it was observed that several brown spots appeared on the surfaces about the same time that the edges of the blades also showed evidence of necrosis. Unfortunately, the Al_2O_3 particles had been shaken off by this time, and it was thus not determined if the spots were coincident with the particles.

One remote HCl detector located in line with the flame trench was used during this test and was triggered via a long cable strung to the blockhouse. This detector measured an HCl dosage of 410 ppm-sec. A sequence camera recording at 3 frames per second indicates that the HCl cloud passed by this detector in approximately 10 sec, yielding an average concentration of 41 ppm. One of the sequence frames from this test is shown in Fig. 38.

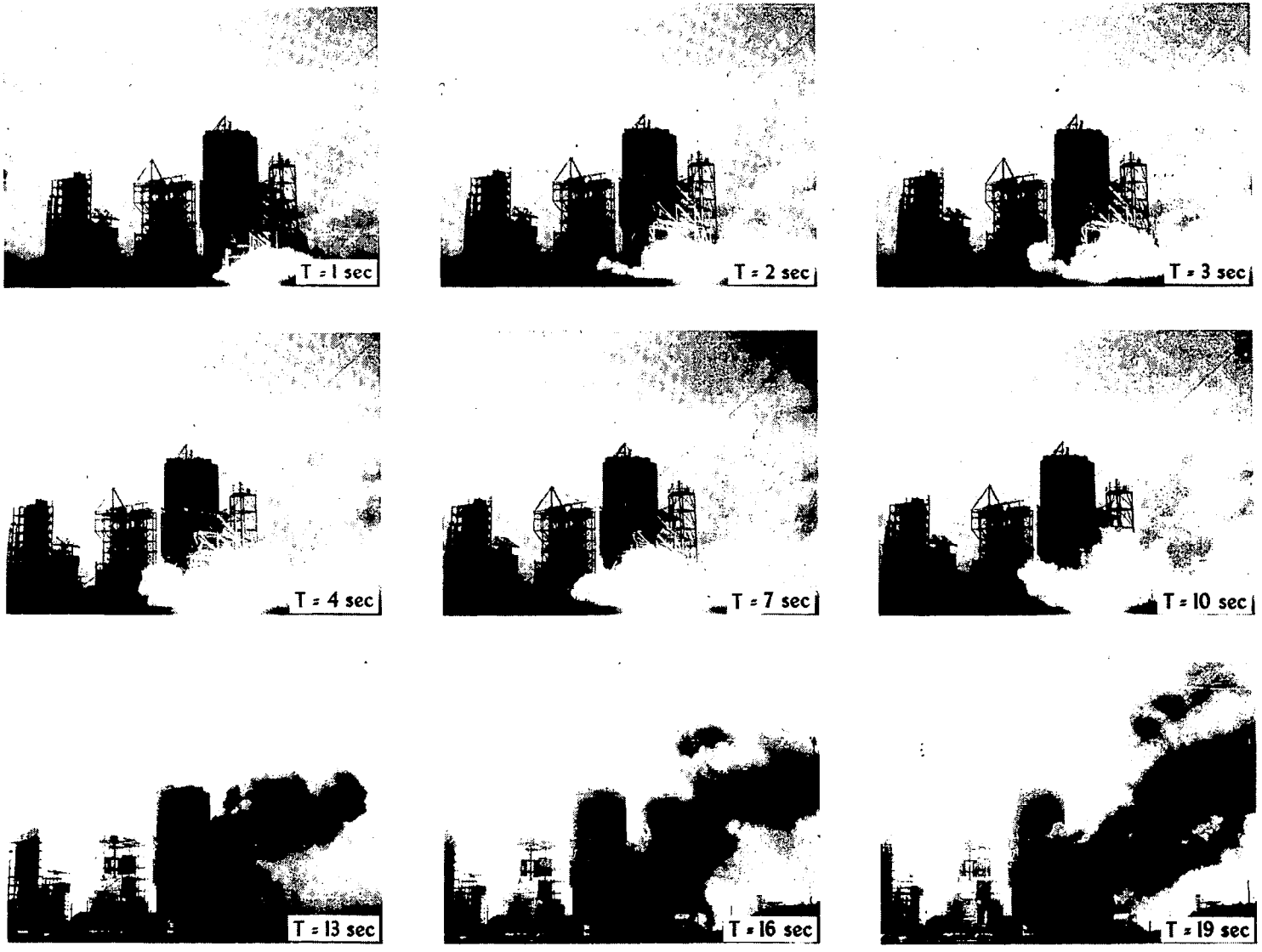

Figure 38. Photo sequence MSFC Test No. 1.

6.2.2 Test Firing No. 2

For this test the instrumentation was located in line with the flame trench and well beyond the edge of the asphalt apron. A long extension cord was used to provide power to operate two small sampling pumps for the bubblers and the filters. The firing was delayed until after dark, preventing camera coverage of the cloud. Earlier in the evening there was a slight ground fog at the edge of the wooded area.

The sensors at locations A and B were again lost due to the force of the exhaust. The mounting brackets held, but the copper-coated glass covers were blown off. Only two samplers detected any evidence of the exhaust cloud. The disk at location C recorded acid aerosol droplets. These stains are shown in Fig. 39. As was noted in the AEDC chamber tests, these droplets all have relatively large (5 to 20 μ) Al_2O_3 spheres which served as condensation nuclei.

The detector at L was the only one to record any HCl, and, as is noted, this was only a trace amount. Since the winds were so light, it seems most probable that the exhaust cloud lofted over the samplers, possibly drifting in a southeasterly direction.

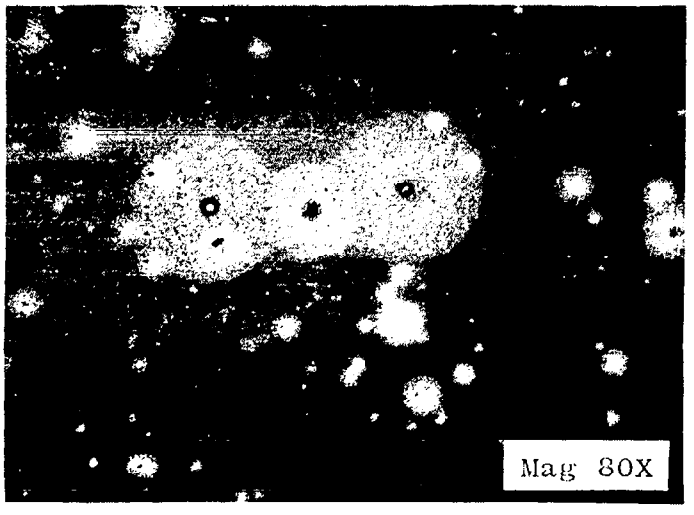

Figure 39. Optical microphotographs of acid droplet stains.

6.2.3 Test Firing No. 3

At the time the HCl and Al_2O_3 monitors were deployed, the wind was steady at 240 deg. However, at the time of firing it had shifted to 180 deg, with the result that the cloud missed the monitor array completely. This firing was also at dusk, and thus there were no photographs taken of the cloud. It was observed that long tracer sparks travelled from the exhaust deflector at the pad well over 150 m down the center of the detector array. Several Al_2O_3 spheres were found on the sample disk at location D, but there were no indications of acid droplets. These spheres were hollow and transparent and 10 to 30 μ in diameter. It is most likely that these particles were produced from the burning fuel ejected from the rocket motor. Similar particles have been observed in samples collected in the 12V chamber tests and also in free-burning fuel in the laboratory.

6.2.4 Test Firing No. 4

This test was scheduled for 3:30 p. m. and the initial development of sensors was made at 2:00 p. m. with a prevailing wind at 330 deg. However, there was a "hold" due to arming problems on the rockets, and during this time the wind shifted to 360 deg. During the delay as many of the detectors as possible were relocated. This last minute change resulted in getting all the sensors under the exhaust cloud, although the sampling grid was somewhat random.

This particular firing was made with the solid rocket motors raised approximately three nozzle diameters above the launch complex. Thus, while most of the exhaust travelled through the flame trench a significant amount spilled out around the pad. The footprint of the resulting cloud, as shown in Fig. 35, is based on the photographs from the sequence camera and visual observations from the major control building (Fig. 31). The measured dosages of HCl agree fairly well with these visual observations. The dosages range from 32 to 100 ppm-sec with the cloud passing across the detectors in approximately 12 sec. All of the fallout detectors recovered indicated both Al_2O_3 particles and acid aerosol. Again, the particles falling out on the copper-coated disks were in the 5- to 30-μ size range, with both solid and hollow spheres. All stains, indicating the acid droplets, had a large Al_2O_3 sphere as a nucleus.

6.2.5 Test Firing No. 5

This test was scheduled for an early morning firing. The wind was slight and from the southwest. There was a light frost on the ground. The sensors were located as in Fig. 36. The solid engines were installed with their nozzles directly over the launch pad exhaust holes, and thus very little spillage around the sides was expected. This firing also included burning the LH_2-LOX engines and spraying cooling water in the flame trench. The launch was delayed, first due to a frozen water line at the launch pad and then due to a LOX vent valve failure. During this period it was noted that water had condensed in the inlets of the bubblers and the Geomet flowmeters were full of water. The inlets to the bubblers were dried out and the Geomet was disassembled and dried. The rocket motors were fired at 12:55 p.m., and the visual cloud passed directly down the line of sensors. However, the cloud started to rise slightly sooner than expected and was well above the ground as it arrived at the Geomet and the coulometer. It is possible that this cloud was a little more bouyant since the ambient temperature was so low (48°F).

The photographs from the sequence camera show that the LH_2-LOX engines fired at t = 0 and the solid motors were ignited at t + 3.3 sec. The exhaust cloud travelled along the ground to the 100-m mark and then started to rise. The leading edge of the cloud arrived above the Geomet and the coulometer at t + 15.6 sec and was approximately 30 ft above the ground. By t + 25.6 sec a trailing edge of the cloud had drifted into the location of the Geomet and the coulometer. This trailer lingered for approximately 25 sec and slowly dissipated. A second cloud from the LH_2-LOX engines moved into the sensors at approximately t + 70 sec and took about 10 sec to disperse. The fact that the second cloud contained HCl was at first surprising since the liquid engines do not produce HCl, and their exhaust is ducted into a separate flame trench. It is obvious, however, that some mixing of the exhausts must occur just below the main support pad before the gases enter the separate flame ducts.

Records of the Geomet response are presented in Fig. 40. The recorded peaks of 5 and 3 ppm along with the exposure time agree well with the closest millipore filter, which measured a dosage of 50 ppm-sc

The coulometer appears to have had response problems, possibly due to moisture condensing in the inlet. The raw data trace presented in Fig. 40 shows that it did not sense the HCl until well after both the

Geomet and the sequence camera indicate that it had arrived. The long sensing period after the HCl cloud had passed and the seemingly random peaks which follow are all indicative of HCl having been adsorbed on the inlet, and subsequently of its being released into the instrument as air was continually drawn through. The inlet problem was probably aggravated during this test because the instruments were deployed early in the morning when the temperature was below 40°F, with the firing being conducted approximately four hours later, when the temperature had risen to 48°F. The total dosage can be obtained by integrating under the response curve. This yields a value of 72.5 nanograms of HCl or a dosage of 26.8 ppm-sec. This again agrees well with the nearest millipore detector, which measured 36.0 ppm-sec.

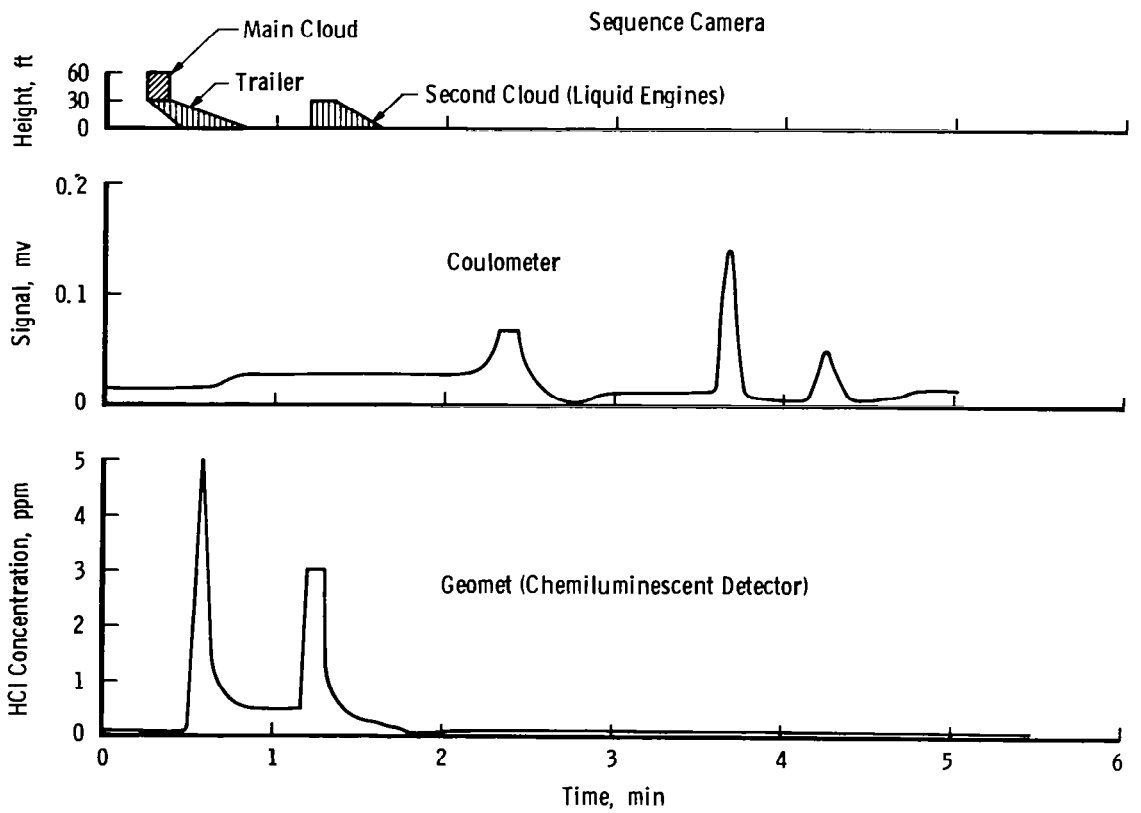

Figure 40. Comparison of HCl data MSFC Test No. 5.

The copper-coated fallout detectors located at A, B, Y, and Z were etched clean of all copper. Thus, these detectors did not have the spot patterns normally observed. However, the residual copper chloride crystals were clustered in circular patterns around large Al_2O_3 spheres, indicating that the initial HCl arrived as aerosol droplets. The disk at location C had a collection of acid aerosol droplets similar to those observed both in the AEDC chamber tests and the previous MSFC tests (Fig. 41). Once again the droplets were all associated with the relatively large Al_2O_3 particles. Sample disk D showed a slight discoloration at the edges of the copper plating, indicating exposure to HCl gas and water vapor, but there were no droplets or large Al_2O_3 particles on this collector. The rest of the disks were clean and the copper coatings showed no evidence of discoloration.

During this test several large pieces of concrete (10 by 5 by 1 cm) were blown out of the flame trench and into the detectors. One bubbler at location B was destroyed. The surviving bubbler at Location A indicated a total dosage of 9,000 ppm-sec with an exposure of 10 sec in the tailings. The average concentration in the main cloud at this point was therefore close to 900 ppm.

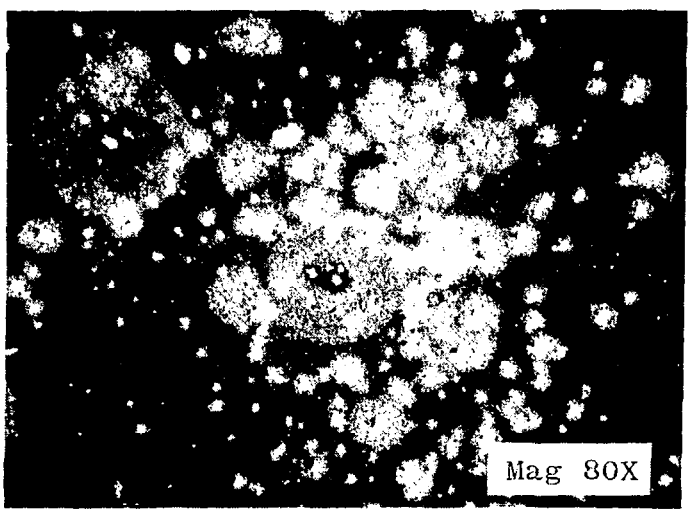

Figure 41. Variety in size of acid aerosol droplets.

6.2.6 Test Firing No. 6

This test was conducted with winds gusting to 25 mph. Shortly after ignition, the solid rocket motors broke loose from their mounts. One caught in the top part of the framework of the test stand, and the other left the test site and arced over into a nearby wooded area. A sequence of photos from this test is presented in Fig. 42. Because of this sequence of events the instruments were exposed to a much larger concentration of HCl than was anticipated, with the result that the Geomet and the coulometer both saturated and went off scale. Dosages at various locations on the asphalt apron ranged from 211 ppm-sec to 660 ppm-sec. The average exposure time as observed from the block house was approximately 10 sec. The pH papers indicate a large footprint on the asphalt apron. The papers located near the bubblers and millipore filters agree in general with the dosage received at those locations. The paper at location M was unchanged, indicating that the cloud did not reach this point at ground level.

The copper-coated aerosol detectors collected Al_2O_3 particles at all locations. The maximum particle size was 25μ, with one or two of this size on each disk. The detector at location G had one well-defined acid droplet stain with a 25-μ Al_2O_3 particle as its nucleus. Detectors at C, E, and J also had one or two acid aerosol stains; however, the complete etched stain was less than 150 μ in diameter, indicating an extremely small aerosol droplet.

One unexpected observation from this test was the persistence of the ground cloud as a visible entity. With the prevailing winds it was expected that the cloud would dissipate quickly. However, the cloud remained relatively close to the ground and was still well defined 10 min after the firing.

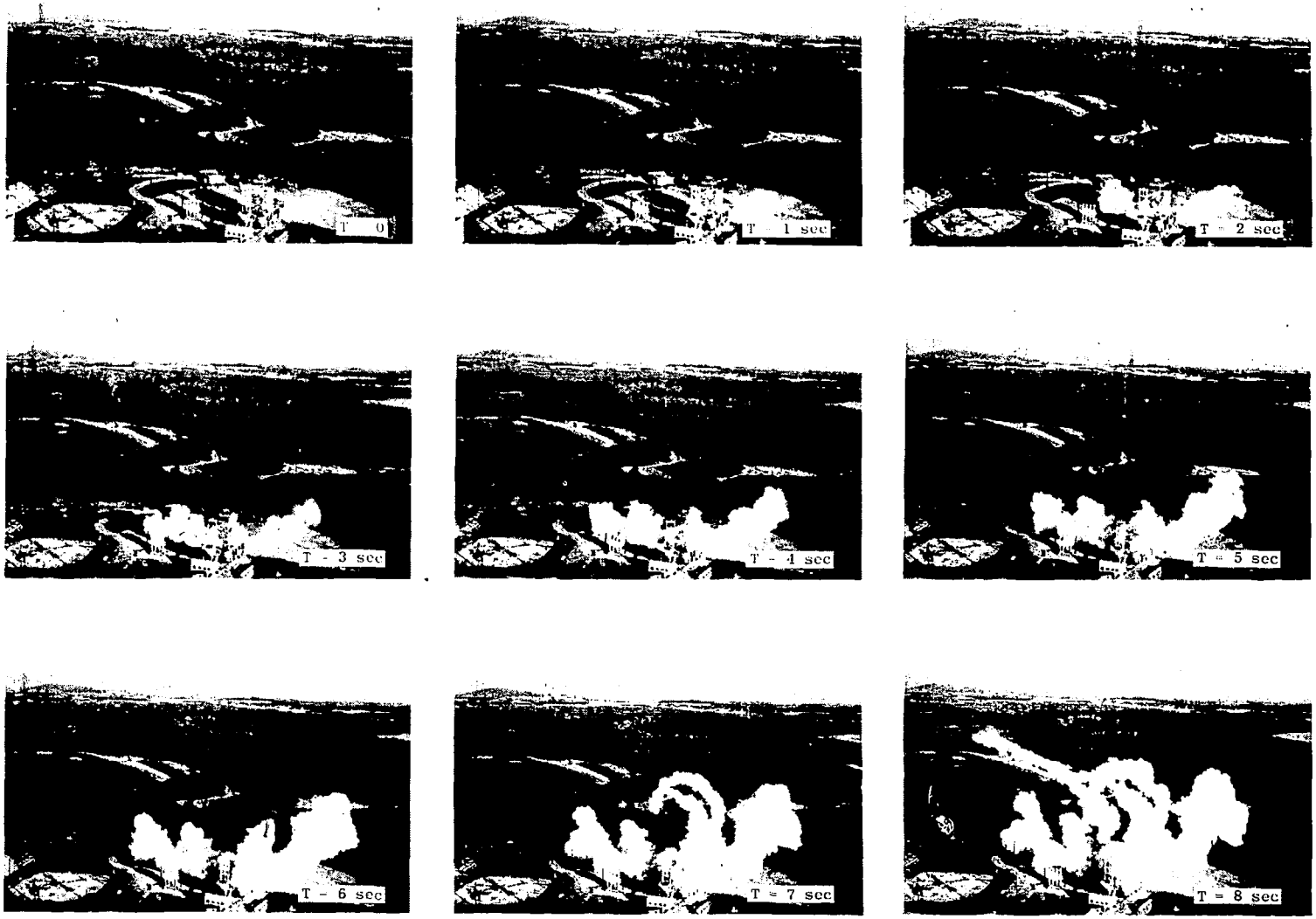

Figure 42. Photo sequence of MSFC Test No. 6.

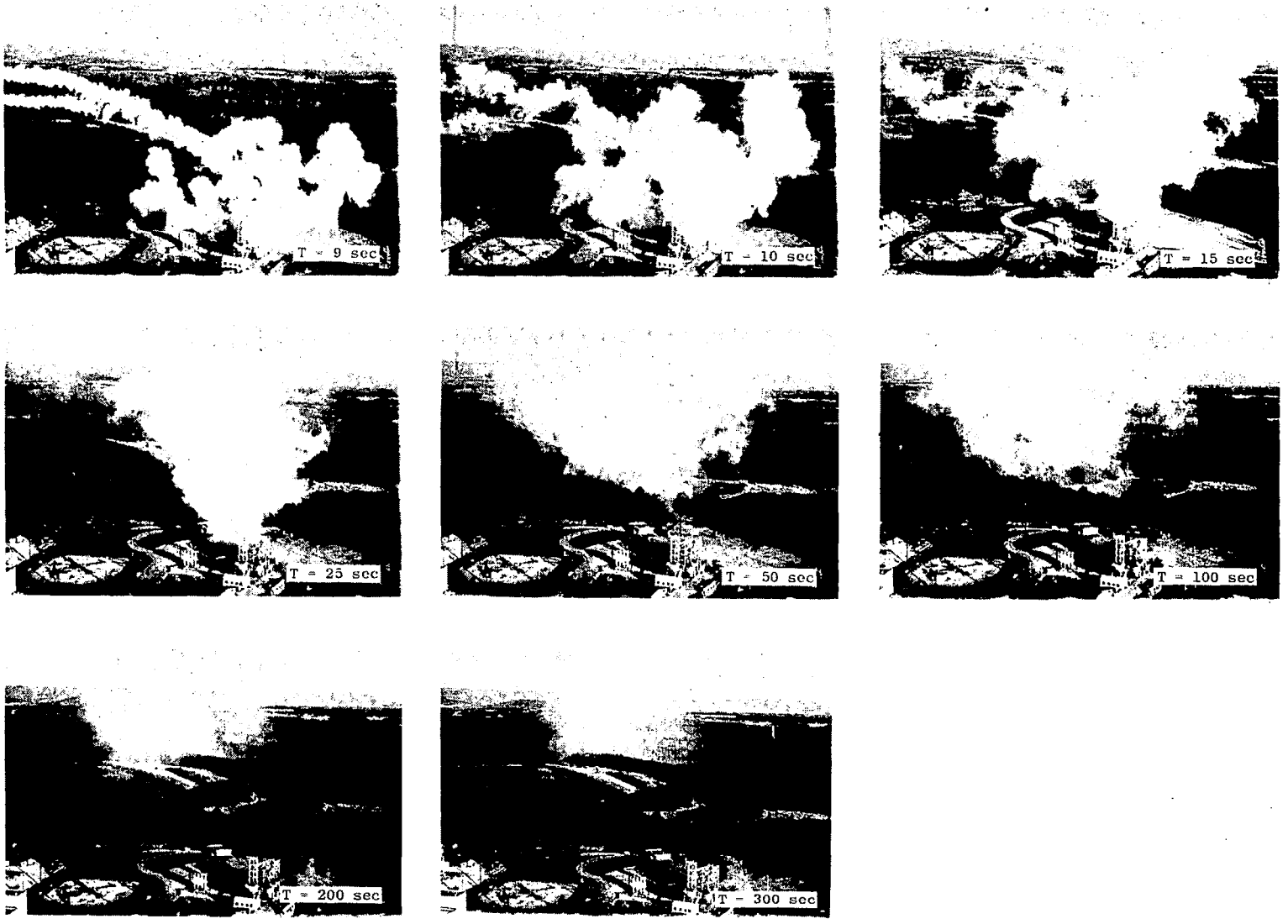

Figure 42. Concluded.

6.2.7 Test Firing No. 7

Al_2O_3 PARTICLE SAMPLING EXPERIMENTS

The prime objective of this test firing was to determine the feasibility of using spray water for acoustic vibration suppression. Thus the test conditions consisted of the model of the shuttle with its strap-on boosters mounted above a scaled version of the proposed Vandenburg flame trench with spray water added to the exhaust ducts. The Al_2O_3 collection experiments were permitted as a peripheral test with the proviso that they were to be conducted on a noninterfering basis. The excess water used during the test was undesirable insofar as particle sampling was concerned, although not unrealistic compared to the actual launch conditions which will be experienced.

Various Al_2O_3 collection techniques were used to compare the types of samples obtained. These included

1. An "isokinetic" probe
2. Millipore® and Nuclepore® filters
3. Petri dishes
4. Cascade impactor (four stage)
5. Sticky tape impactor (single stage)
6. Acid aerosol sampling disks

The locations of the various probes and samplers are indicated in Fig. 43. In addition to the Al_2O_3 sampling, several potted plants were located around the test site. These were collected after the test firing and were observed for a period of 12 weeks.

The test was scheduled for 1700 hours, and the motors were ignited at 1705 hours. The wind was light from the southwest, and the temperature was 27.5°C (81.5°F). The relative humidity was measured at 56 percent. A self-generated acid aerosol caused by condensation would not be expected under these conditions.

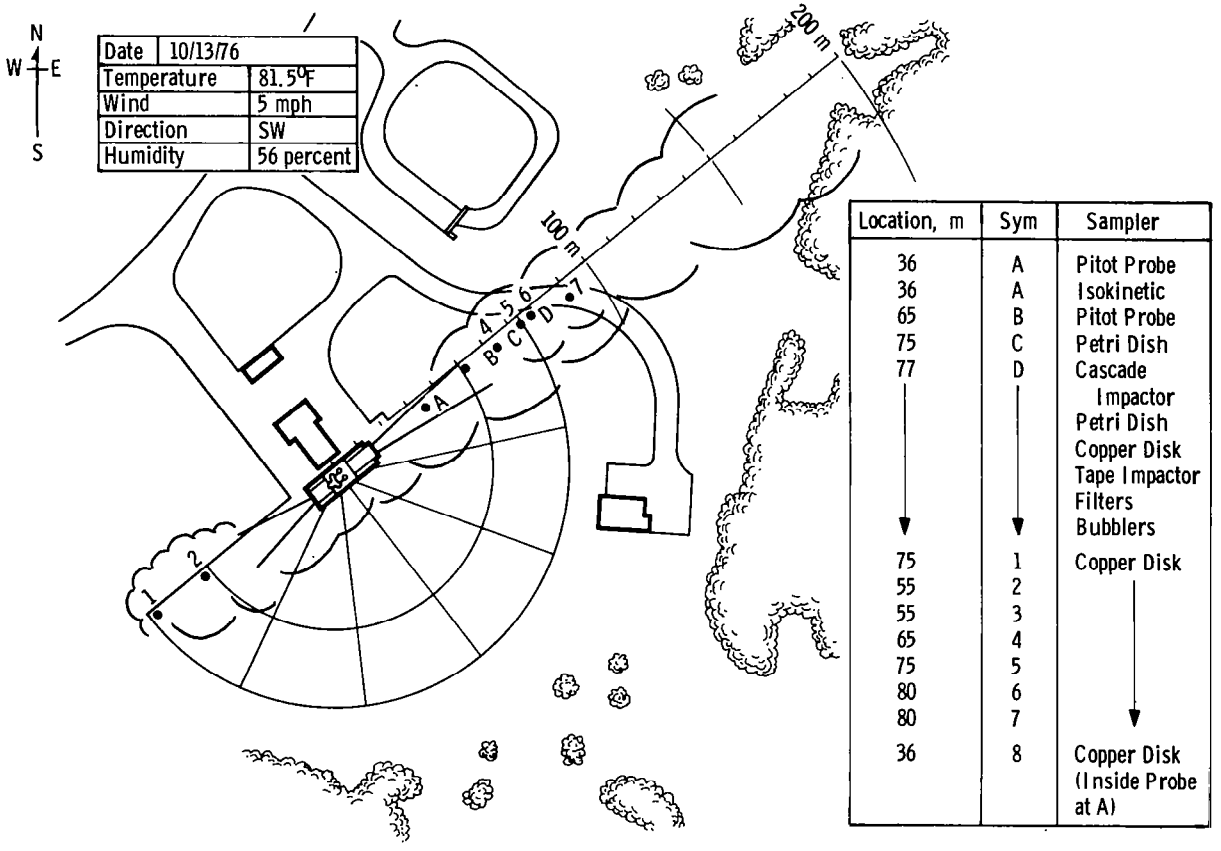

Figure 43 MSFC Test Site.

Isokinetic Probe

This probe was built following the general pattern of the UTC probe used to collect Al_2O_3 samples at the Titan III-C launch platform (Ref. 12.) The sampling disk used in the probe was a 1.27-cm (0.5-in.)-diam scanning electron microscope stub. A pitot probe located by this probe indicated that the sample was taken in a 193-km/hr (120 mph) exhaust flow. The sample disk was unevenly coated with Al_2O_3 particles. The particles were sized and counted from photographs taken on the scanning electron microscope. Several parts of the disk were excluded from analysis because of overlapping particles.

Millipore® and Nuclepore® Filters

The Millipore® and Nuclepore® filters were located in line with the flame trench duct at the 75-m mark. The air sampling rate was set at 5 ℓ/min, and the filters were mounted in pairs, one facing toward the flame trench and the other facing away. After the firing it was noted that the plastic housing of the rearward-facing filters had been broken by flying debris, with resulting damage to the filter membranes. The forward-facing filters had collected a heavy sample; however, subsequent analysis showed that a large portion of the sample was material ablated from the flame trench. No attempt was made to sort out the Al_2O_3 particles to size them.

Petri Dishes

Two petri dishes were located at the 80-m mark. One of these dishes was anchored to the floor and because of the raised rim saw only material settling out of the exhaust. The other was fastened in a vertical position facing the exhaust. The horizontal dish contained some sand and concrete; however, the sample was sufficiently dispersed that the Al_2O_3 was easily identified. The vertical dish was heavily coated, and once again the intermix of ablation material and Al_2O_3 precluded any particle counting.

Cascade Impactor

The sampler was located at 80 m, and the pump was set to sample at 17.5 ℓ/min. The sampling stages were loaded with copper tape so that besides collecting particles the samplers would exhibit an etched stain from any acid droplets which contacted the copper. After the firing it was noted that the final stage of the impactor had plugged solid. Since the efficiency of the separation of particle sizes requires a constant sampling flow rate, this buildup in the last stage resulted in a gross distortion of the samples on the other stages. These data were not used in determining a size distribution of Al_2O_3 particles.

Sticky Tape Impactor

The tape collectors at 36 and 65 m were heavily eroded. The collector at 80 m was fully saturated with Al_2O_3 and ablation debris and was considered unsatisfactory for analysis. The tape at 100 m had a sufficiently dispersed collection of particles so that the Al_2O_3 could be identified and sized. The results of these tests are presented and discussed in Section 8.5.

Acid Fallout and Plant Specimens

At previous test firings on this rocket site, small copper-coated disks had been used to detect acid droplets which had condensed and settled from the cloud. During this test it was decided to set out some small potted plants to see the effects of the acid fallout (Fig. 44). No attempt was made to duplicate the variety of plants in either the Cape Kennedy or Vandenburg areas. The plants included geraniums, begonias, coleus, chrysanthemums, periwinkle, wandering Jew, and sweet williams. Eighteen plants were located downwind of the test stand, and an equal number of similar plants were set aside as control plants. Copper-coated sampling disks and strips of pH paper were also distributed along with the plants.

Figure 44 Potted plants used as acid aerosol detectors.

RESULTS FROM TEST

Copper Sampling Disks

The acid droplets collected on the copper disks were quite different from previously observed aerosols . Whereas the previous acid droplets were quite small (< 500 μm) with a single Al_2O_3 nucleus, the majority of these droplets were several mm in diameter with an assortment of solid material in each droplet. A typical residue from a droplet as collected on the copper-coated sampling disks is shown in Fig.45. As can be seen, there are several of the hollow Al_2O_3 spheres, one relatively large white solid sphere of Al_2O_3 ($\approx$100-μm diameter) and a large quantity of smaller Al_2O_3 spheres and silica particles. Examination under the scanning electron microscope (SEM) and analysis of the x-ray spectra showed the complete deposit area saturated with chlorine. The large dark grey particle toward the top of the figure showed no indication of any metallic element and has been tentatively identified as a carbon particle. The accumulation of such a variety of particles in large droplets suggests that they originate from the spray water and have collected particulates by washout rather than having been formed by a condensation process.

Figure 45 Residue from acid droplet on sampling disk.

The acidity of the droplets, which was estimated from the spotting on the pH papers, ranged from 2 to 0. The spots were correlated to droplet sizes by spraying dilute HCl droplets of known pH and catching the spray on pH paper and in silicon oil. A relationship was determined between the range of spot sizes on the pH paper and the acid droplets caught in the oil. Using this rough calibration technique it was determined that the size of the acid droplets at the test site ranged from 500- to 2,000-μm diameter. The HCl dosage from the cloud through which these droplets passed was measured by bubblers. At ground level this dosage was approximately 3,800 ppm-sec. The cloud swept by the bubblers in 15 seconds, thus indicating an average concentration of approximately 250 ppm. The droplets therefore had adsorbed some HCl but were not even close to equilibrium with the HCl gas available in the cloud.

Qualitative Results from Plant Exposures

At the time the plants were recovered from the test area, all the droplets which might have settled on their leaves had evaporated. However, traces of the droplets in the form of clustered residues were quite evident. No obvious damaged spots or burns were noted at this time. As the plants were transferred to the greenhouse, several brown spots were starting to appear. The following morning the burn spots were quite obvious, and typical damage is shown in Fig. 46. Leaves with extensive damage eventually dropped off; however, all the plants survived and in most cases suffered minimal setback due to the exposure. Comparison of the exposed plants to the control plants indicated the primary difference to be cosmetic spotting.

In addition to the burn spots, there was an appreciable number of Al_2O_3 particles which had been deposited on the leaves with no apparent harmful effects. Several experiments were conducted with the plants to determine the effects of controlled HCl exposure.

CONTROLLED HCl-PLANT TESTS

Exposure to Diluted HCl Droplets

In this test a leaf was set on a microscope stage and a droplet of dilute HCl was placed on its surface. It was noted that for diluted acids (pH 4) the droplet did not appear to damage the leaf until it had almost evaporated. More acidic droplets (pH 0) caused observable damage within 30 minutes. It is to be noted that due to the relative partial pressures of H_2O and HCl over a dilute acid droplet, as the droplet evaporates, its acidity increases. Thus mildly acidic raindrops which of themselves might not damage vegetation could cause spotting if they were to evaporate while on the leaves or fruit of the exposed plants. Continued rainfall which washed off the acid droplets would result in no observable damage.

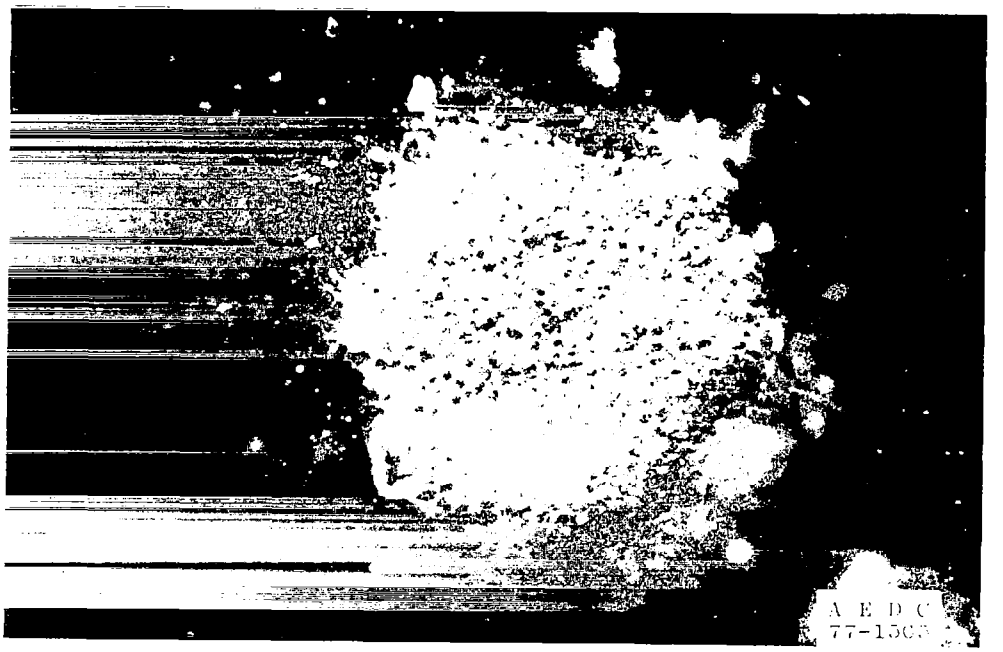

Figure46 Damage spots on leaves.

Exposure to HCl Gas

These tests were conducted to provide some qualitative idea of what might be observed by the average home owner if some of the plants around his house were exposed to an "acceptable" level of HCl for a period which could conceivably be experienced from the passage of an exhaust cloud. The observation of the plants was superficial insofar as it was confined to such obvious factors as spotting and leaf shedding.

Plants were exposed to an atmosphere containing 2 ppm HCl for a period of 30 minutes with no apparent ill effects. However, plants sprayed with water droplets, exposed to the same atmosphere, and then removed and allowed to dry off, sustained some spotting. This would suggest that a dry cloud containing low levels of HCl can cause cosmetic damage if the vegetation is previously watered by either rainfall or irrigation sprays.

Exposure to Al_2O_3 Particles

Plant leaves were dusted with Al_2O_3 particles which had been collected from rocket motors fired in a dry environmental chamber. The plants were kept in a greenhouse maintained at 85 percent RH, and all water was applied to the soil. No damage was apparent during the six-week observations.

At the end of this period a small quantity of HCl gas was introduced into the greenhouse (approximately 2 ppm). It was noted that many of the Al_2O_3 particles adsorbed water and formed droplets. These droplets evaporated when the plants were placed in a desiccating atmosphere, and the leaves once again showed evidence of an acid burn.

A more detailed look at this process was achieved by collecting some of the Al_2O_3 on a microscope slide which had been vacuum coated with a thin layer of copper. This slide was then inserted into a small plastic housing attached to the stage of a microscope. Preconditioned air was slowly passed through the sample housing and over the Al_2O_3. First the air was saturated with water vapor, and the particles were observed over a period of 15 minutes. There was no observable adsorption of water vapor by the particles. The reservoir was then charged with water-saturated air with 2 ppm HCl, and this mixture flowed over the Al_2O_3. Figures 47a, b, and c are sequenced at 5-minute intervals. The flow was from right to left, and it is noted that the Al_2O_3 adsorbed sufficient water to form droplets. The fact that these droplets dissolved the copper substrate is indicative of the fact that they were acidic. All of the particles shown in Figs. 47a,b, and c participated in this nucleation; however, this is a small section of the sample and was chosen to illustrate the process. Many of the other Al_2O_3 particles in the sample were inert and did not form droplets.

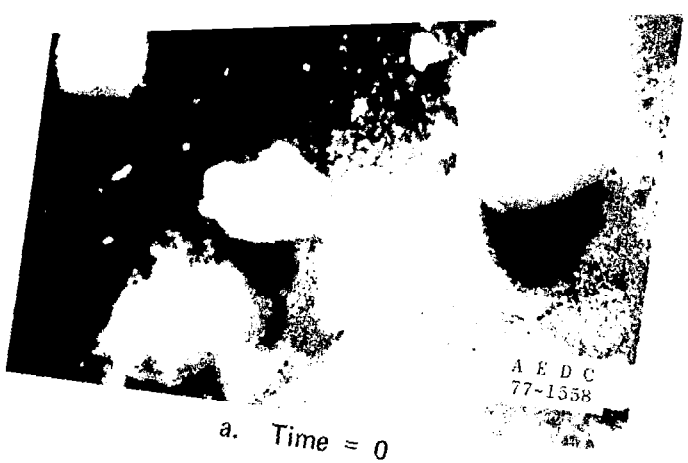

a. Time = 0

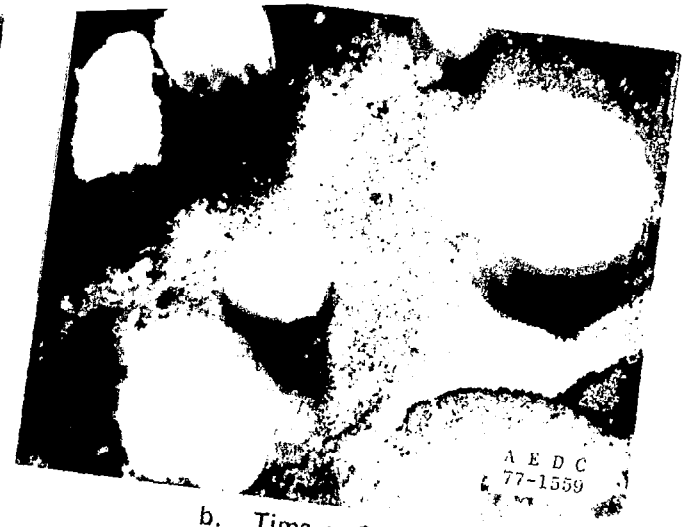

b. Time = 0 + 5

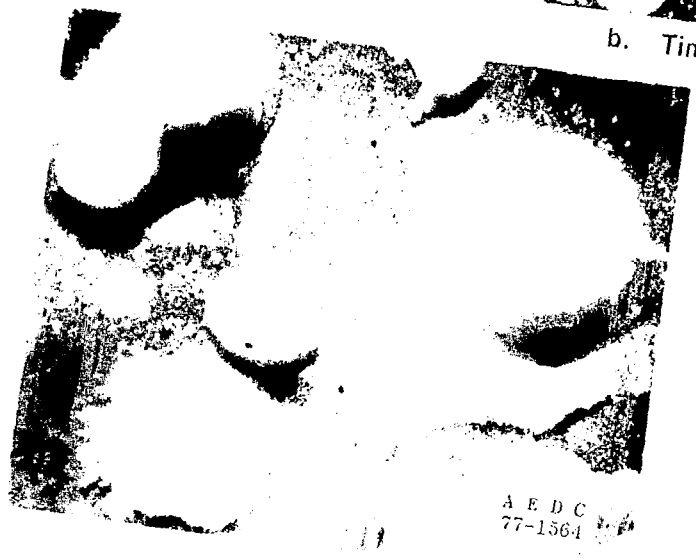

c. Time = 0 + 10 min

Figure 47 Adsorption of H_2O and HCl by Al_2O_3.

Qualitative Summary of Plant Studies

The qualitative work conducted with the plants during this phase of the study was initiated with the idea that if specific types of leaf spotting could be identified with passage of the exhaust cloud, then examination of foliage after cloud passage would result in inexpensive acid aerosol detection. In this regard the plants were able to record acid droplets only if the droplets were allowed to evaporate from the plant surface, or if the droplets were highly acidic. The observation that plants previously wetted by rain or sprays and then exposed to relatively low concentrations of HCl gas could sustain cosmetic damage would suggest that this mechanism should be investigated further, especially with plant species peculiar to the Kennedy and Vandenburg launch sites.

The effects of Al_2O_3 particles settling on vegetation and the associated condensation of HCl and H_2O would not appear to be of any great environmental concern. However, this should be considered in controlled environmental tests where plants are repeatedly exposed to rocket plume effluents, since Al_2O_3 particles from one test can be inadvertently activated in a subsequent exposure to HCl and water vapor.

6.3 SUMMARY OF MSFC TESTS

The main problem encountered in monitoring this series of test firings was in prelocating the monitoring instruments. Even in this relatively controlled test series where one of the test constraints was wind conditions, it was extremely difficult to predict the cloud path. A further complication was introduced by the safety requirement that all personnel must evacuate the area one hour before the scheduled firing time. This, coupled with a prohibition on any type of radio transmission, meant that all sampling instruments had to be started long before the actual firing and in some cases continued sampling well after the firing until the area was declared safe for access.

The millipore filters, copper-plated fallout disks, and pH papers provided an inexpensive network of sensors for these tests. The one test (2-8-75) in which the more sophisticated Geomet provided real time HCl concentrations which agree with the millipore data gives confidence in the results from the filters.

Monitoring this test series provided an opportunity to evaluate various sampling techniques and incidentally pointed out specific problem areas which can be encountered by certain instruments. One example is the water condensation in both the Geomet and the coulometer operating at temperatures close to freezing. The test monitoring also provided a baseline of data indicating the range of expected dosages of HCl around the test site during this type of rocket firing. However, possibly the most significant result from this portion of the program is the fact that the acid aerosols observed in the small-scale environmental chamber tests were also observed during these firings under similar atmospheric conditions. As in the chamber tests, these aerosol droplets are always associated with relatively large Al_2O_3 spheres which evidently act as condensation nuclei. A more detailed analysis of the types of Al_2O_3 particles and their size range is presented in Section 8.0.

7.0 EVALUATION OF INSTRUMENTATION

7.1 GENERAL COMMENTS

In this section comments are presented on experiences with the instruments used during these tests. The most convenient working conditions for instrument evaluation were found in the short test series in the large rocket preparation building. The small polyethelene-covered igloo was very flexible in that with a razor blade and tape, instruments could be mounted quickly and simply with their controls and internal components easily accessible in the clean environment and their sampling probes exposed to the simulated cloud without requiring special feedthroughs or extended inlet tubulation.

For short test periods requiring small gas samples the 30-in. Plexiglas® smokebox provided the most economical siumlated exhaust cloud having a reasonable mixture of gases and particulates. With the initial relative humidity set high, this arrangement also produced a self-generated acid aerosol in the test volume. The added side

effect, however, of free-burning fuel in a high humidity atmosphere, is an excess of hollow aluminum oxide particles. However, it is felt that, if necessary, the hollow particles could be suppressed by burning the fuel in a small cavity fitted with a restricted orifice.

7.2 EVALUATION OF COULOMETER

The coulometer shares a problem common to the bubbler, and that is adsorption of HCl on the walls of the glass inlet tube leading to the glass frit. If the coulometer is sampling from a steady source, then the walls of the glass tube eventually saturate, and the final steady-state value recorded by the instrument is representative of the HCl concentration in the source. It was determined experimentally that this process could be speeded up by injecting a small quantity of HCl directly into the inlet tube just prior to use in order to precondition the inlet tube. The response of the instrument is limited by the fact that the incoming sample has to be dissolved and distributed throughout the volume of the electrolyte. Thus for a step input of sample there is a gradual buildup of signal which takes from 5 to 80 sec, depending on the HCl concentration and the sample flow rate.

An example of the response of the instrument is shown in Fig. 48. These data were obtained by establishing a steady-state concentration of 10 ppm HCl in an enclosed volume. At t = 0 the instrument which had been sampling room air was connected to the test volume via a 6-in. length of heated glass tubing. After sampling for approximately 5 min, the coulometer inlet was disconnected from the test volume and once again sampled HCl-free room air. Under these conditions the instrument took 48 sec to attain a 10-percent recovery. The coulometer therefore can monitor changes in HCl concentrations, but one must be aware of the natural lag in response due to the system inertia.

For the first tests conducted in the 12V chamber, the coulometer was located inside the test volume in order to reduce the length of glass tubulation in the sample line to a minimum. However, the initial sample of HCl during the first engine firing was so large that it completely saturated the electrolyte. Subsequent tests were made with the instrument located outside the test cell and a 1.5-m by 2-mm ID glass tube used to withdraw the sample. Operated in this fashion, the sampling could be started and stopped when desired, and the sample flow rate could be changed as needed. This additional tubulation was preconditioned prior to each test but still resulted in an attenuated response.

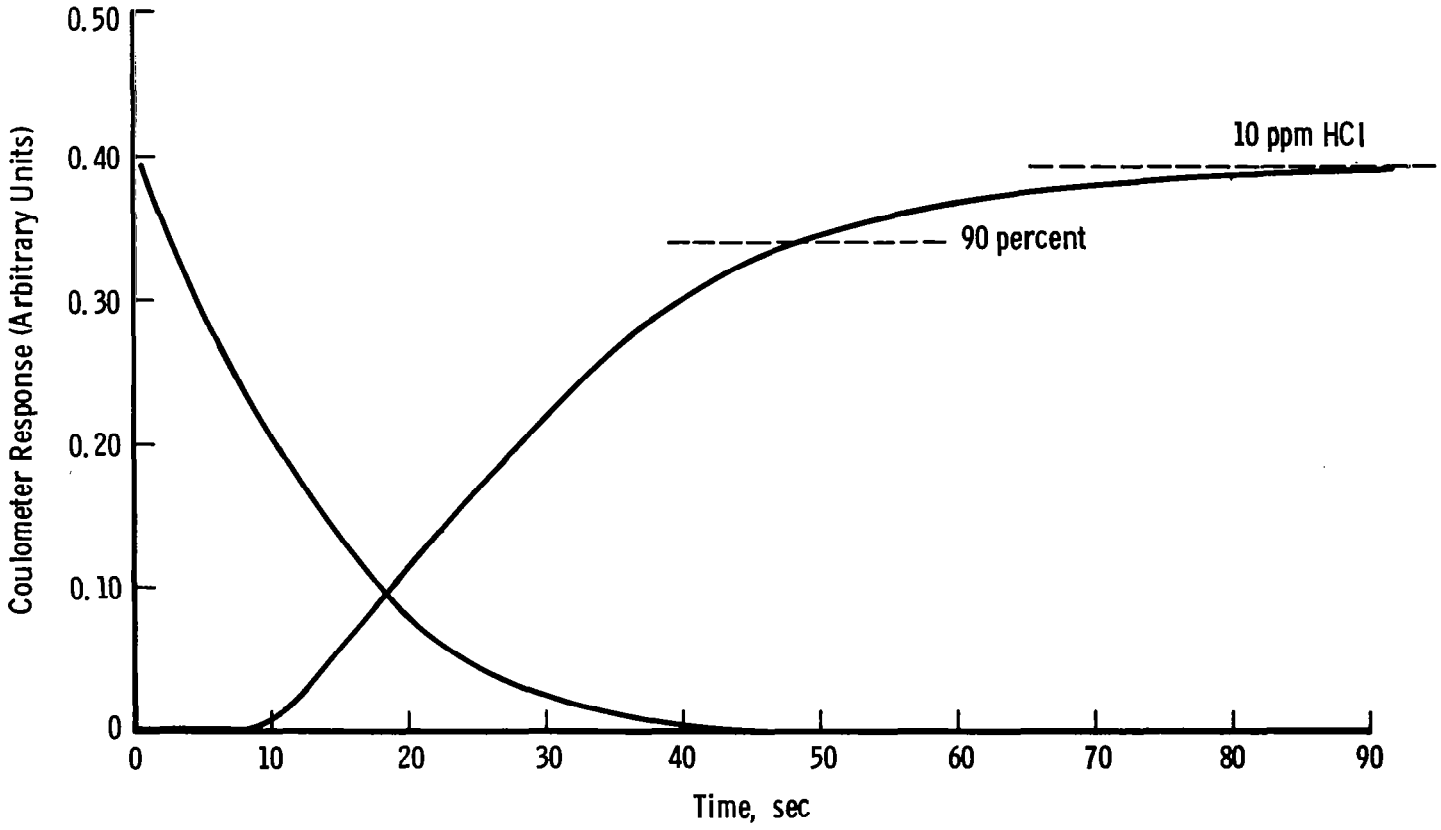

Figure 4.8. Response of coulometer.

When the high humidity test were made, it became obvious that water was condensing on the walls of the glass sampling tube. A heater tape was wrapped around the tube, and the temperature was maintained at 30°C for the final environmental chamber test. Thus, because of inlet problems, the data produced by the coulometer during these tests are questionable.

The coulometer was also used to determine the chloride concentration in samples obtained from bubblers. This was accomplished by injecting several microliters of the liquid from the bubbler directly into the coulometer electrolyte. The quantity of electricity required to rebalance the cell was measured and the amount of chloride in the sample was calculated. This technique was used to compare the results obtained via pH probes and chloride ion selective probes described in Section 3.1.2. The instrument is ideally suited for this type of analysis and is capable of determining quantities of chlorides as low as 3 nanograms per sample.

The coulometer has been employed as a standard to check HCl mixtures used as calibration gases for other instruments. In this role the coulometer samples the mixture for a specific time; from the determination of the weight of the total chloride ion sensed, the flow rate of the gas through the electrolyte, and the time interval, the concentration of the HCl is calculated. Using a Taylor series analysis with estimates on the precision of each measured quantity indicates an expected uncertainty of ±6 percent when the coulometer is sampling at its upper limit of 17 ppm.

7.3 EVALUATION OF BUBBLERS

Several comments should be made concerning the care and feeding of bubblers when they are used under these circumstances. Some of these points are well known and may be considered self-evident, but others are possibly peculiar to this specific type of test. In order to obtain the maximum sample and yet maintain some time resolution, it is desirable to set the flow rate through the bubbler as high as possible and keep the sampling time as short as possible. This can lead to two problems. The first is a carryover of water spray from the bubbler to the vacuum pumping system. The bubblers designed with the enlarged center section help to reduce this problem. The second is incomplete scrubbing and a resulting loss of HCl as it is carried through the bubbler. In order to assure that this was not occurring for the flow rates used in these tests, several runs were made with two bubblers in series. There was no detectable quantity of HCl collected in the second unit.

Besides being readily dissolved in water, HCl is strongly absorbed on the inlet tubes and internal surfaces of the glass bubblers. Thus it is necessary that the bubblers be backflushed to be sure that all of the HCl is in solution before the pH or the chloride ion concentration measurement is made. Besides backflushing the inlet tube it was also found necessary to bubble a little dry nitrogen through the glass frit to clear the HCl from it and ensure its complete mixing in the bubbler.

After using the bubblers for these tests it was noted that the normally white glass frits had turned dark grey. No amount of washing or backflushing helped in trying to remove this discoloration. Subsequent analysis of these frits indicated that they were loaded with aluminum oxide particles.

Tests of the Al_2O_3 particles have shown that both the α and γ phases are present. Therefore, it can be expected that a glass frit loaded with the Al_2O_3 particulates will have an effect on the pH of the solution in the bubbler, especially if there is a delay between taking the sample and then analyzing it. In order to determine the order of magnitude of this effect an HCl-air mixture was sampled with a bubbler containing a frit which was filled with Al_2O_3 but which had been thoroughly rinsed in distilled water. The concentration of HCl calculated from the pH reading immediately after sampling was 114 ppm. After sitting with the frit immersed in the sample for 2 hrs the pH had increased and the apparent concentration was calculated as 82 ppm (28-percent decrease). It is therefore recommended that bubblers which are used in future tests have replaceable frits.

The bubbler which was modified to include a pH probe worked successfully although there were some operational limitations. The first was the signal noise generated by the bubbles rising past the pH probe and causing streaming potentials. This was overcome by operating the system in a pulsed mode and taking readings when the gas flow stopped. The second problem was the inlet adsorption of HCl. This required that after every sample period the bubbler be slowly pressurized until the water backfilled the inlet tube and then depressurized to draw this water back around the pH probe. This proved to be a delicate procedure and required visual observation of the water level as the system was pressurized. The technique worked successfully although this operational method limited the placement of the bubbler to a location directly in front of the chamber viewport. In future applications this bubbler could be automated with an optical sensor used to control the back-flushing cycle.

Three methods of analysis of the solution in the bubblers were used. The simplest was a pH probe which had been precalibrated with standard buffer solutions. A second, similar type of measurement was made using a chloride ion sensitive probe. This produced results parallel to those of the pH probe. It was not used in the continuous-sampling bubbler because it was not convenient to mount it and its reference electrode in the bubbler. The third method involved taking small samples from the bubbler and adding them to the coulometer and electrically titrating to determine the chloride concentration. For bubbler samples obtained from pure HCl gas releases in the chamber, the HCl concentration calculated from the chloride determination and those from the hydrogen ion measurement (pH) agreed within 5 percent. However, when samples were taken from actual rocket fuel burns, the results obtained from pH measurements were consistently lower by 20 to 25 percent.

This could indicate that some of the Al_2O_3 also ingested in the bubbler is γ-alumina and is reacting with the HCl.

Considering the precision of the individual measurements required for the determination of the concentration of the HCl in the atmosphere using a bubbler as the sampling device leads to an estimate of the uncertainty as ±11 percent at concentrations of 27 ppm with sampling rates of 1 ℓ/min.

7.4 EVALUATION OF THE MILLIPORE FILTERS

The ability of the millipore filters to serve as HCl dosage monitors was discovered after several bubblers were equipped with them in an attempt to separate the Al_2O_3 particles from the gas sample so that the particles would not accumulate in the glass frits. After these bubblers were operated in the exhaust cloud, it was found that there was only a trace of HCl in the bubbler. However, the HCl concentrations determined from an analysis of the filter and backing pad matched the HCl concentration levels as measured by other instrumentation. Subsequent tests with these filters have shown that unused filters and cellulose pads are neutral and do not interfere with a pH determination. However, there is a chloride contribution from the cellulose material. This precludes analysis of the HCl dosage from a chloride ion determination.

These filters coupled with the pumping system described in Section 5.2 could provide a relatively inexpensive sampling system for field use; therefore, further tests were conducted to better define their advantages and their limitations.

These tests consisted of flowing gas from a bottled mixture of dry N_2 containing 60 ppm HCl through the filters at various flow rates. In addition, tests were conducted in a Plexiglas smoke box, shown in Fig. 49. The box has a volume of 15.28 ft^3, and 0.325 gm of fuel burned in this enclosure produces a cloud density equivalent to that produced by the 85-gm rocket burn in the 12V tests. The smoke box is fitted with two mixing fans and a venting system along with a humidifier. Appropriate feedthroughs and support stands allow installation of gas and particle monitors as required. A remote ignition system using an electrically heated nichrome element is used to burn the fuel samples.

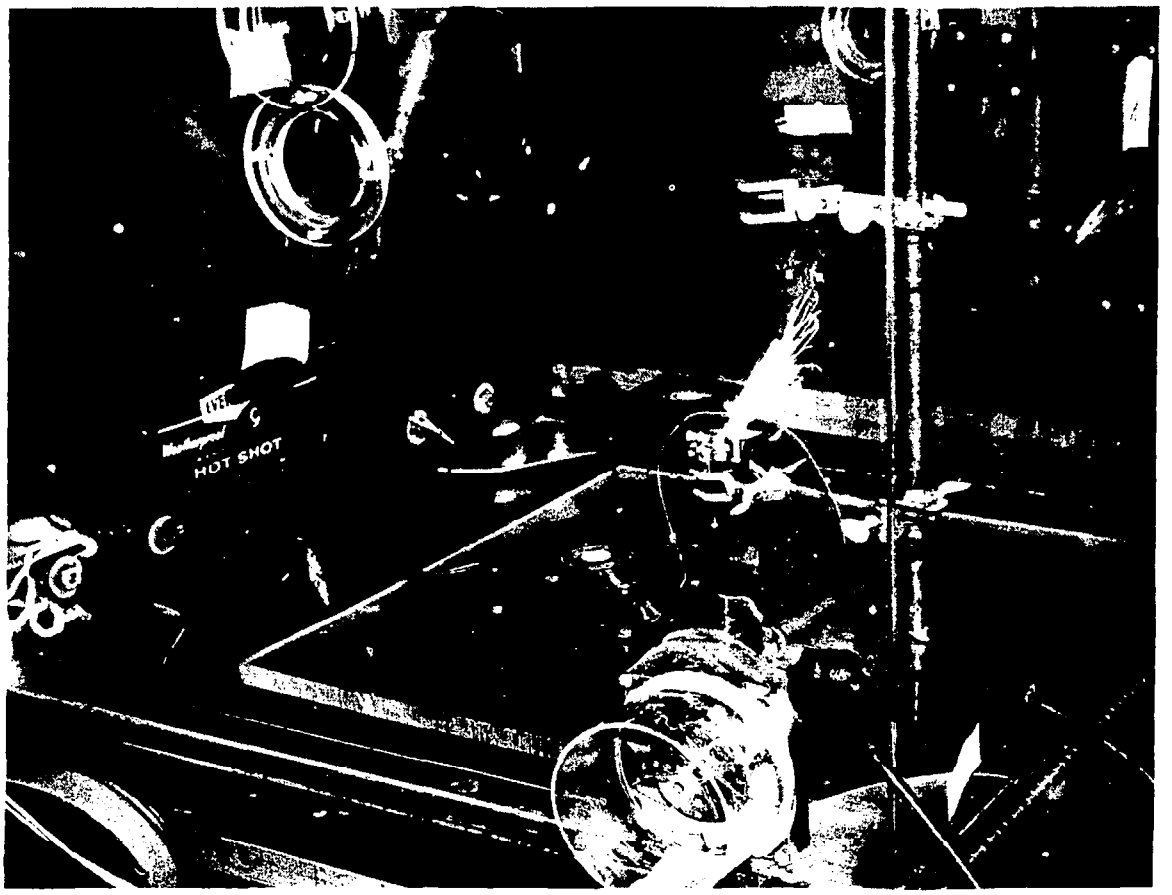

Figure 49. Burning fuel in Plexiglas® smoke box.

7.4.1 Permeation of HCl through a Filter Assembly

The first use of these filters to measure HCl concentrations indicated that there was no measurable permeation of HCl through the filter pad. However, this was a single data point with only one flow rate. Thus a series of filters was used to measure the HCl concentrations using a gas mixture of N_2 and HCl (60 ppm). The gas mixture was passed through two filter assemblies mounted in series and then exhausted through a rotometer which was used to determine the flow rate. Flow rates were varied from 0.5 to 6.5 ℓ/min, and sample times were set at 60 sec. A final run was made with the flow rate set at 5.5 ℓ/min in which the first filter pad had been moistened with several drops of distilled water. The data from these tests are presented in Fig. 50. The results with the moistened filter pad indicate that when practical, this is a preferred method of operation. Since all sample times were set at 60 sec with the flow rate variable, these data could indicate a carry-through caused by either over-saturation of the first pad or inefficient trapping at the higher flow rates. Noted in Fig. 50 is a single test point taken at 5 ℓ/min for 12 sec, which would indicate that the carry-over is caused by a combination of both of these factors. Thus future use of the single filter pads as HCl detectors should be limited to maximum flow rates of 1 ℓ/min to minimize bleed through losses, and sampling times set to limit the dosage to less than 3,600 ppm-sec to avoid saturation.

7.4.2 Filter Makeup and Performance

As was mentioned previously and can be seen in Fig. 8, the filter assembly consists of a filter membrane and a cellulose support pad. Several filters were exposed to samples of the N_2-HCl mixture, and the membranes and the support pads were processed separately to determine the distribution of the HCl between the two elements. The data presented in Table 3 indicate that the membrane has a rather limited capacity for adsorbing HCl, and depending on the flow rate and total exposure, it retains from 3 to 9 x 10^{-6} gm HCl. The relative consistency of the amount retained on the membrane when compared with the wide variation in the total dosage of these experiments (15 to 450 x 10^{-6} gm) indicates that in each instance the membrane has reached saturation.

The accuracy of the determination of an HCl concentration using this device is defined by the various measurements which must be made (i.e., time of exposure, flow rate through filter, quantity of

water used in the analysis, and the hydrogen ion concentration). Assuming reasonable uncertainties for each of these, measurements yield a net uncertainty of ±15 percent in the HCl concentration.

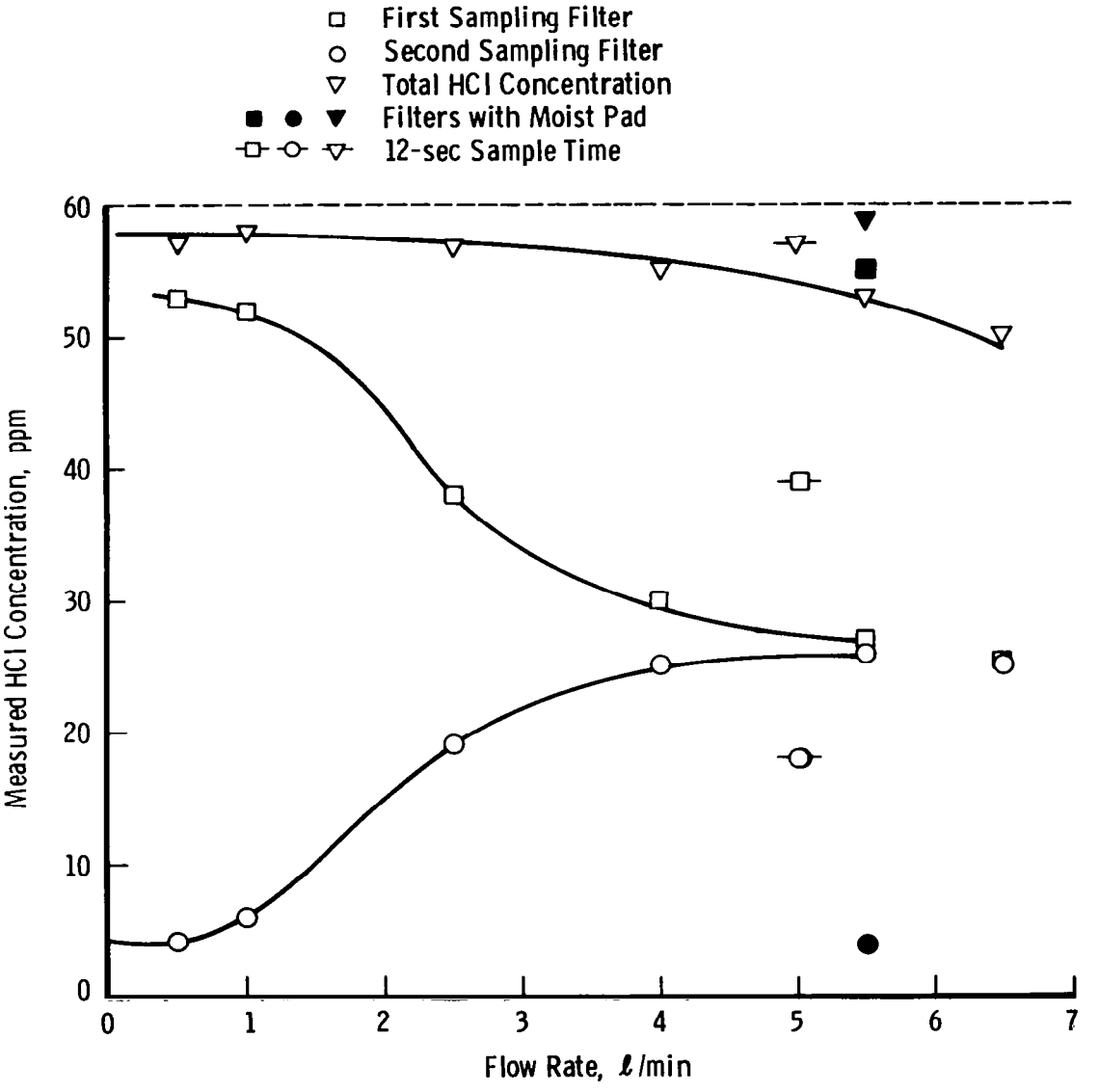

Figure 50. Evaluation of millipore filters as HCl detectors.

Table 3. HCl Distribution

Flow Rate, ℓ/min	Sampling Time, sec	HCl Collected	
		Membrane ($gm \times 10^6$)	Support Pad, ($gm \times 10^6$)
0.89	10	5.5 ± 2.5	8
0.89	60	6.3 ± 2.3	77
0.89	120	6.5 ± 3.5	150
5.0	10	4.5 ± 1.5	72
5.0	60	6.5 ± 2.5	427

7.5 EVALUATION OF pH PAPERS

General purpose pH papers with an effective range from 0 to 11 were obtained for evaluation as low-cost HCl dosage monitors. Pretest evaluation of these papers consisted of exposing them to various concentrations of HCl in a saturated air-water atmosphere. These ambient atmospheres were obtained by partially filling large glass containers with various concentrations of hydrochloric acid, the equilibrium vapor pressure and the resulting ppm concentration of HCl in the gas phase then being defined by the concentration of the acid and the temperature.

The results of these tests indicated that if the pH papers were exposed for 15 sec and their color change noted immediately, then they could be calibrated to give reasonably reproducible results. Sufficient color changes occurred to permit an estimate of the HCl concentration as yellow <5 ppm, gold 5 to 20 ppm, peach 20 to 50 ppm, and red >50 ppm. However, it was noted that four times the exposure in a sample atmosphere at one quarter the HCl concentration did not produce an appropriate color change to permit calibrating the pH papers as true dosage monitors for use where both the exposure time and the HCl concentration were unknown. Further tests with the pH papers exposed to the combustion products from rocket fuel indicated random responses. One important observation was made with a fuel burn test conducted at 89-percent relative humidity. One of the pH papers removed from the bottom of the test chamber was covered with spots, indicating that acid droplets possibly had settled on it.

In general, it is suggested that pH papers might be usefully deployed over a large area downwind of a rocket launch to provide some indications of acid droplets. It should be noted, however, that the pH papers can record such an acid droplet only when the color change of the total pH paper caused by the ambient HCl gas dosage is less than that caused by the droplet. It has also been observed that if the pH paper is exposed to droplets of distilled water and then to dry HCl gas, a reverse spotted pattern is recorded.

7.6 EVALUATION OF THE CHEMILUMINESCENT DETECTOR

The chemiluminescent detector responded rapidly when exposed to HCl-air mixtures and dropped to background level within a few seconds after the HCl source was removed. The response time was affected when a 1-m glass tube was added to the inlet, and thus for the first tests in the 12V chamber the complete instrument was located in the test volume, and no extension tube was used.

Some operational problems were encountered during the test series which should be noted. The first occurred after sampling exhaust products which had been produced in a relatively dry environment (29 percent relative humidity). The symptom was erratic readings, and the cause was determined to be a partial blockage in the reference cell flow system caused by an excessive ingestion of Al_2O_3 particles. This was corrected by connecting the reference cell inlet to a clean air supply outside the test cell. In later tests, where initial relative humidities were high (>70 percent), it was noted that there was a large noise signal superimposed on the HCl signal. At first these noise spikes were thought to be an electronics problem; however, further investigations indicated that they were definitely associated with the initial humidity conditions in the chamber and were caused by the presence of acid aerosol droplets.

Subsequent calibration studies on this instrument performed after the rocket motor tests conducted in the 12V chamber have raised some questions concerning the validity of calibrating with dry gas mixtures in the laboratory and then using the instrument at a later time in a high humidity environment with possible acid aerosols present.

The following studies were conducted using the smoke box shown in Fig. 4.9. The initial calibration was performed as described previously with a dry N_2-HCl gas mixture. The following day the instrument, along with the coulometer, was attached to the smoke box. Both

instruments sampled simultaneously from this source. The HCl concentrations in the box were maintained by circulating the air over a shallow glass base pan containing a dilute solution of hydrochloric acid. The HCl concentrations were established at the appropriate levels as indicated by the coulometer by varying the concentration of the hydrochloric acid. In all these tests the inlet tube to the coulometer was heated to prevent loss of HCl in the sample line. Under these conditions the HCl-air mixture was saturated with water vapor. The data presented in Fig. 51 show the shifts in calibration that were observed.

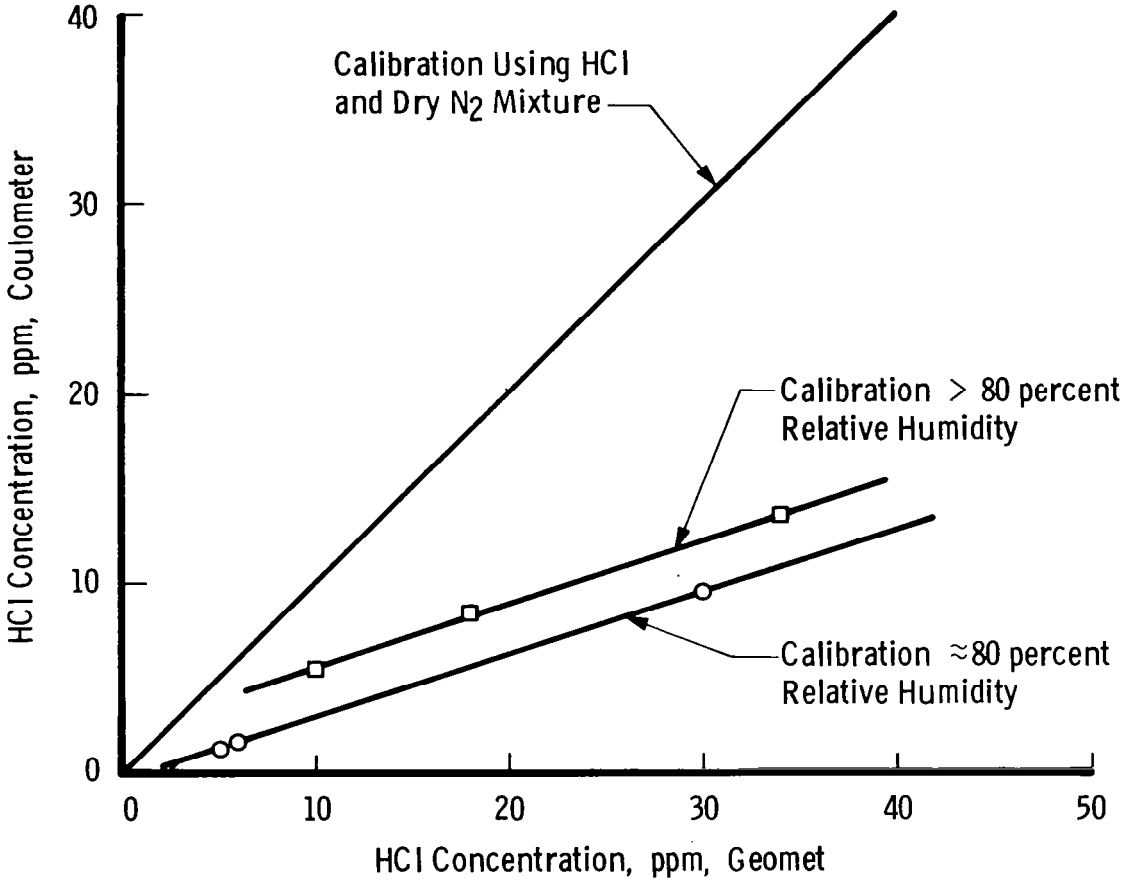

Figure 51. Calibration of Geomet.

A further test was conducted in which a small glass nebulizer was installed in the smoke box. The nebulizer was filled with a dilute solution of HCl (pH 1) and operated to produce an acid mist in addition

to the already water-saturated HCl-air atmosphere. The coulometer indicated a slight increase in HCl with the nebulizer operating (5 percent). The chemiluminescent detector produced erratic results. The first notable feature was the appearance of noise spikes superimposed on the basic signal. However, the base signal did not remain steady but slowly increased and decreased in a random fashion (Fig. 52). It is tempting to suggest that the baseline represents the HCl in the gas phase and the spikes can be analyzed to determine the HCl dissolved in liquid droplets. However, the experiments conducted to date are not sufficient to support such a hypothesis. At this time it has been determined that when noise spikes appear this is indicative of an acid aerosol in the sample. It is also suspected that the usable lifetime of the bromide-bromate coating on the inner surface of the ceramic tube may be significantly reduced when it is sampling gas mixtures with an aerosol present. Further tests should be made to determine the magnitude of this effect. Insofar as the chemiluminescent detector is calibrated against the coulometer, its accuracy is defined as ±6 percent when sampling under the same conditions under which it was calibrated. Large changes in these conditions could increase this uncertainty, as indicated by data in Fig. 51.

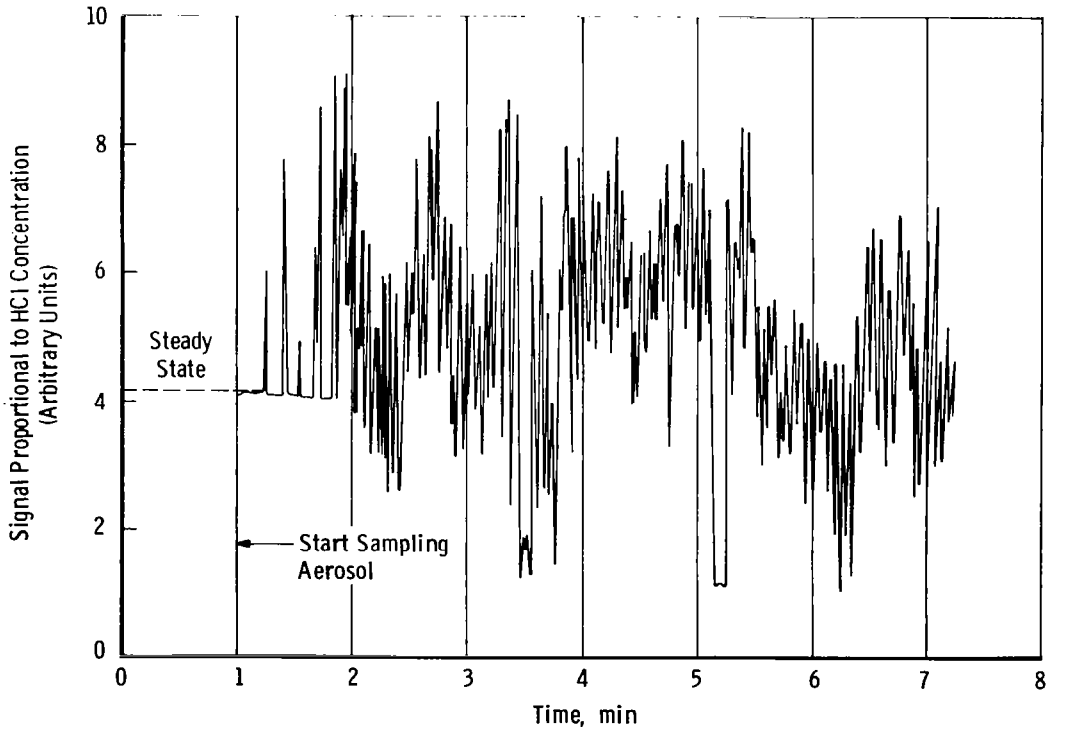

Figure 52. Geomet response with aerosol present.

7.7 EVALUATION OF MODIFIED CONDENSATION NUCLEI COUNTER

In order to calibrate this instrument and correlate a specific increase in particle count to a particular concentration of HCl gas in the sampled atmosphere it was found necessary to carefully control the rate at which the NH_3 was introduced into the sampling inlet. Since the required rates were very low, the first method used was to provide a relatively high pressure source (15 psig) of NH_3 and use a small orifice leak at the inlet (Fig. 53a). This required an additional valve and vacuum pumping system to purge the NH_3 from behind the leak and provide a positive shutoff of NH_3 after each pulse. This technique worked well during the development phase when the system was checked out with gas mixtures. It was determined during these calibration runs that while the HCl was adsorbed on the walls of long inlet tubes, the ammonium chloride particles were not significantly attenuated by sampling tube lengths up to 15 ft. Thus, by adding the ammonia at the inlet to the sampling tube, the basic instrument could be mounted outside the test volume and the inlet could be located with considerable freedom inside the chamber.

After use in the first two chamber firings the orifice in the calibrated leak became plugged. It was determined that this was due to Al_2O_3, evidently drawn into the orifice during the purge period in the cycle when, with a negative pressure behind the leak, there was a reverse flow and the sample gas was drawn into the orifice. In order to avoid this problem, the NH_3 addition system shown schematically in Fig. 53b was built. In this system there are two identical sample inlets, one with an ammonia addition and the other without. A specially constructed two-way valve connects these inlets to either the nuclei counter or a vacuum pump. The flow rate through the vacuum pump is adjusted to match that through the condensation nuclei counter. The pulse sampling is accomplished by operating the two-way valve.

This system worked well with tests made at low relative humidities, and a sample data trace is presented in Fig. 54a. However, at the higher relative humidities the instrument exhibited some strange behavior which was at first attributed to instrument malfunction but later was determined to be a real effect evidently associated with an acid aerosol formed by the exhaust products in the test chamber.

A sample of this anomalous data is presented in Fig. 54b. As can be seen, the particle count with NH_3 addition has dropped below the normal count. Subsequent tests have been conducted which indicate that when NH_3 is added to the sample gas which contains a mixture of water vapor and aerosol droplets, some of the NH_3 is adsorbed

by the droplets. This lowers the H_2O vapor pressure of the droplet and results in the droplets' starting to grow. These droplets, which would normally be small enough to pass through the tubulation and humidification section of the condensation counter, are now effectively filtered by impact on the interior surfaces of the system and are thus lost. This loss of aerosol results in a net decrease in particle count in the expansion section of the instrument.

Because of the uncertainties involved in reproducing equivalent aerosol droplets, it is not deemed feasible to calibrate the counter as an HCl detector for use under these conditions. However, the system does provide an indication of the presence of an acid aerosol, and as such it was used in the 12V chamber test. It is of interest to note that in the 12V tests the CNC data would indicate that the acid aerosol persisted for approximately 5 min.

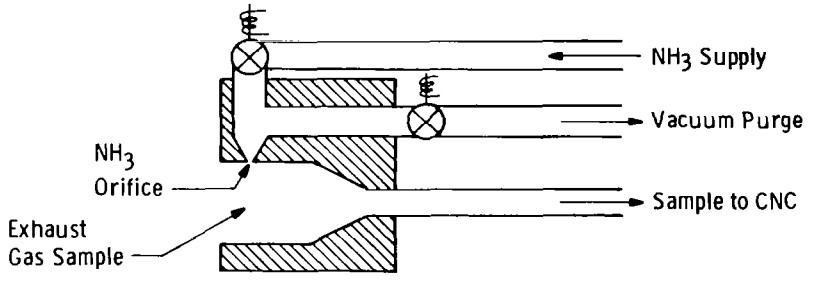

a. Initial NH_3 system

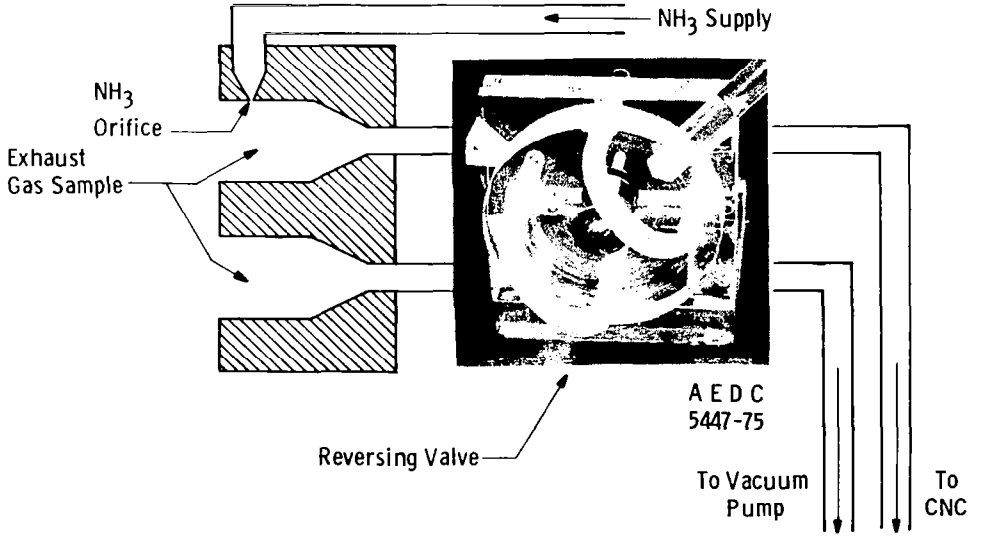

b. Second NH_3 system

Figure 53. Inlet systems to modified CNC.

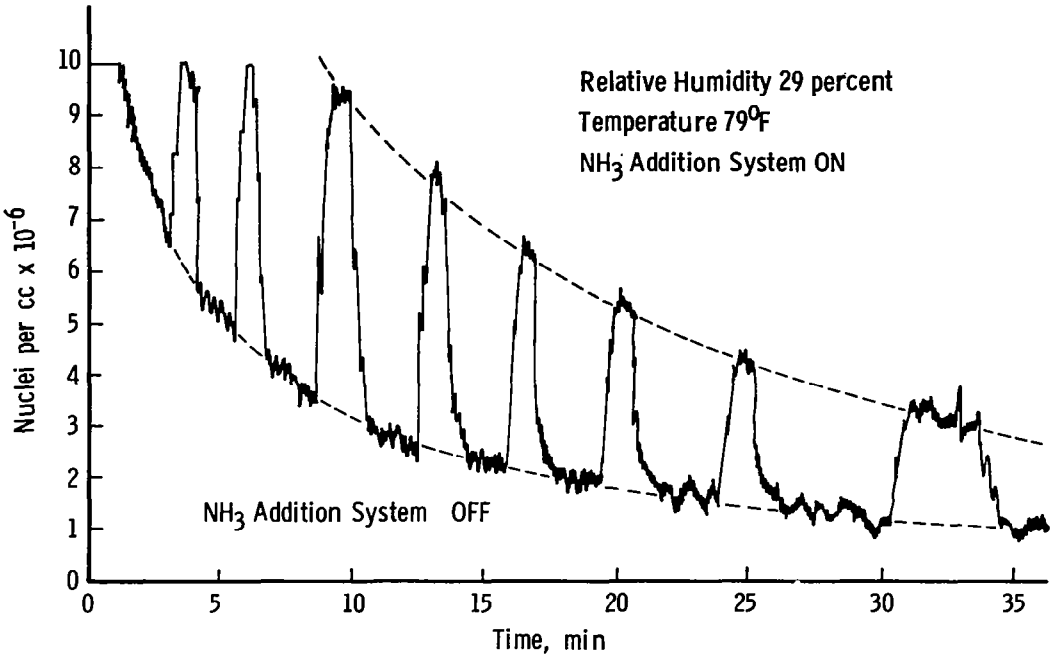

a. Raw signal from gaseous HCl detector

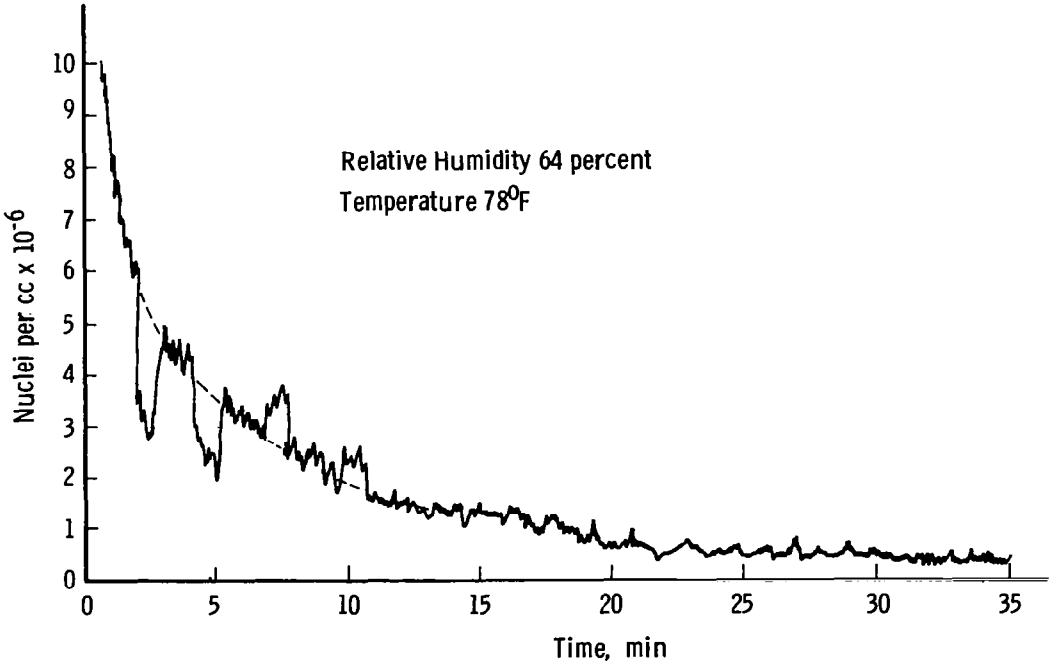

b. Anomalous signal at high humidity

Figure 54. Sample data traces.

7.8 EVALUATION OF CASCADE IMPACTOR

In sampling solid particles it is desirable to have each plate coated with a sticky film to prevent the larger particles from being blown from plate to plate. Nondrying films of a stiff grease are recommended. Several techniques were evaluated during these tests. They included glass slides coated with silicon grease, double-sided adhesive tape, and thin aluminum foil.

The grease and adhesive coatings proved equally effective in collecting the samples; however, they both presented a problem when the samples were transferred to a scanning electron microscope (SEM) for detailed analysis. For observation under the SEM the particles must first be coated with an electrically conductive film. In the case of the grease film it was found that the sample had to be washed in a freon solvent and then returned to a sample disk. In this processing many of the particles were lost, and many coagulated to form large lumps. Attempts to separate these lumps using an ultrasonic bath to vibrate the sample while the freon solvent was evaporating were not successful.

Samples collected on the adhesive tape were successfully coated with a metallizing film; however, under the combined environment of the high vacuum and the heat from the scanning electron beam, the adhesive shriveled and distorted, making the particle field hard to distinguish and analyze.

The uncoated aluminum foil did have some carryover of the larger particles but was better suited for SEM analysis. It was also noted that on one set of the sample disks the first stage displayed the characteristic etched stain produced by acid droplets, which had been previously noted on the copper-plated fallout disks.

Since this technique was developed during the later period of rocket firings, there are no comparative data taken over a variety of test conditions. However, it is suggested that in future tests this instrument loaded with copper-plated glass disks in each stage can serve to detect not only the Al_2O_3 particulates but also the acid droplets which might be present in a particular exhaust cloud sample.

7.9 EVALUATION OF ROTATING VANES

In general it might be stated that this system was too effective in collecting particles. Even with short operating periods of 10 to 15 sec, the Al_2O_3 particles completely coated the collector tape, making it very difficult to separate the individual particle sizes. Thus, while this simple approach can provide bulk samples, it would be necessary to provide a sample collector with some remotely operable cover to provide a shorter sampling period. It is felt, however, that in view of the present state of the art in remote control of model aircraft this would present no problem.

7.10 EVALUATION OF COPPER-COATED FALLOUT PLATES

These plates proved to be extremely useful in both confined and free atmospheric tests. Besides collecting a representative sample of the particles settling out, they also recorded the occurrence of acid droplets. Several methods of preparing the disks have been tried, including copper electroplate on polished aluminum stubs, copper foil, all copper stubs, sputter-coated glass slides, and vacuum-evaporated copper on glass. The latter method has proven to be the most effective. The 0.013-cm-thick glass cover slips were cemented to aluminum SEM sample buttons and then vacuum coated with approximately 500 Å of copper. After coating, the disks were stored for several days in dust-free sample boxes. During this storage period the copper coating developed the characteristic copper color indicative of a thin oxide coating. This oxide coating provides the reactive surface for both the acid and the gaseous HCl, the acid producing the stain and the gas reacting with the remaining surface so that with subsequent exposure to sunlight it turns a dark blue.

Besides producing a record of an acid aerosol droplet, the stain does provide some information about the size and the acidity of the droplet. In an attempt to quantify this information dilute solutions of HCl were prepared and sprayed through an atomizer, and the drops were allowed to impinge on two sampling disks. One of the disks was coated with silicon oil, and the other was not. The size of the droplets caught in the oil film were compared to the size of the stains. It was noted that the stain size is a function of both the acidity of the droplet and the droplet size. For a general approximation however, the liquid droplet diameter is close to the diameter of the inner circle in the stains. The pH of the dilute acids required to produce stains comparable to those recorded from the rocket motor tests ranged from

pH 1 to pH -1. Figure 55 presents the equilibrium concentration of gaseous HCl in ppm that would exist over various HCl acid dilutions. As can be noted, acid droplets in equilibrium with an exhaust cloud containing 100 ppm of HCl and having a temperature of 25°C can be expected to have a pH as low as -0.68.

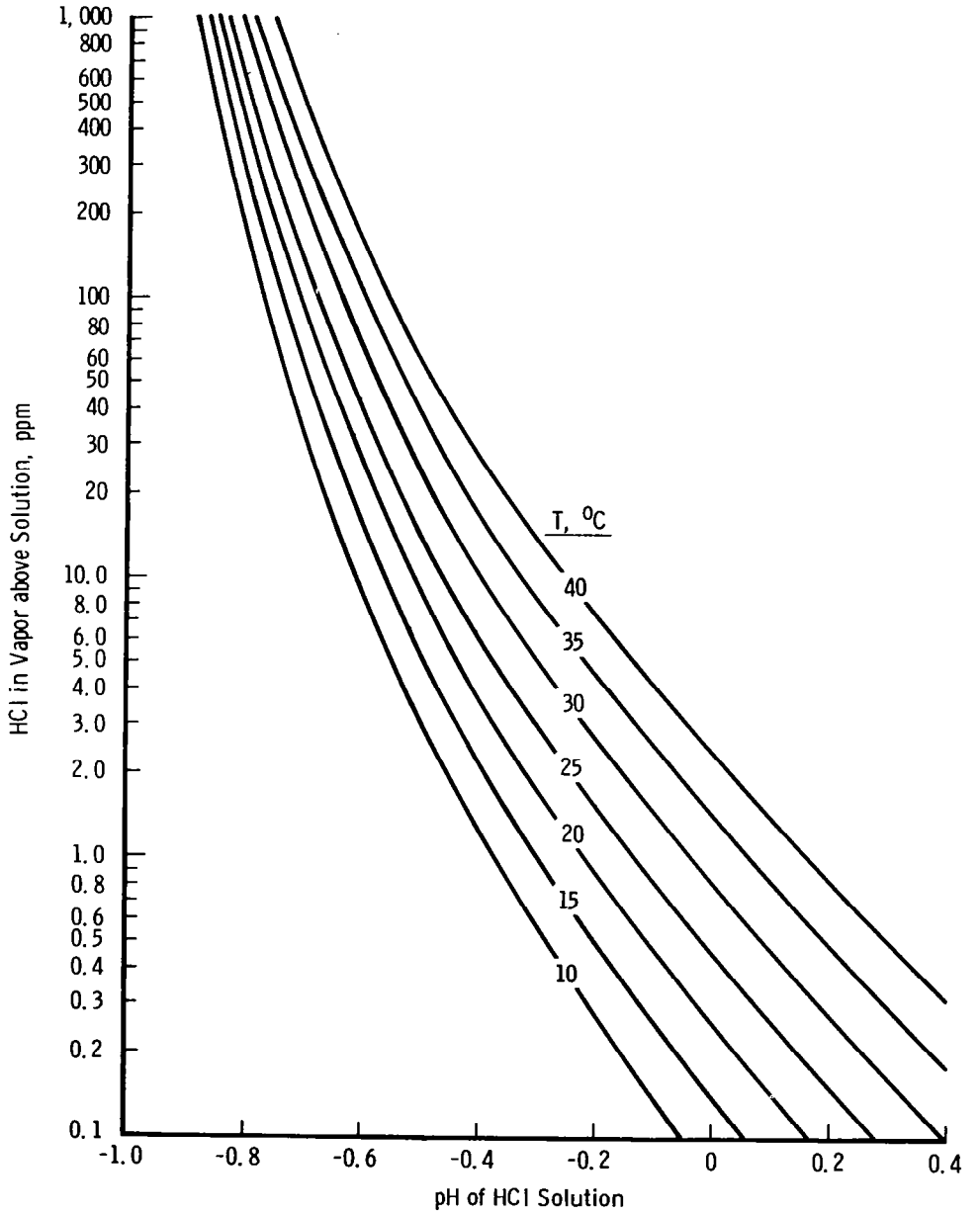

Figure 55. HCl gas in equilibrium with dilute acid, ppm.

Besides visual comparisons of the types of etched stains produced by various concentrations of acids, several of the SEM photos showing well-defined cuprous chloride crystals were used to estimate the acidity of the droplet which caused them. The technique used was to estimate the size of the droplet from the size of the inner stain. Then an enlarged print of the sample was used to estimate the total volume of cuprous chloride. Estimates of the crystal thickness were made by comparison to the diameter of the spherical aluminum oxide nucleus. The sample shown in Fig. 56 was analyzed using this method with the following results. The total quantity of cuprous chloride was determined as 3.3×10^{-11} gm and the volume of the acid droplet as 1.16×10^{-10} cm^3. Assuming complete reaction, then an estimate of the acidity of the droplet which landed on the sampling disk is a pH of -0.4. This sample was taken from test No. 14 in the AEDC environmental chamber and was collected between t = 1 min and t = 3 min. It can be noted from Fig. 21 that the concentration of HCl in the chamber during this period was approximately 6 ppm. This would indicate that droplets produced in the exhaust cloud are in equilibrium with the maximum concentration of HCl gas to which they are exposed. Estimates of the acidity of some droplets have been as high as pH = -0.6.

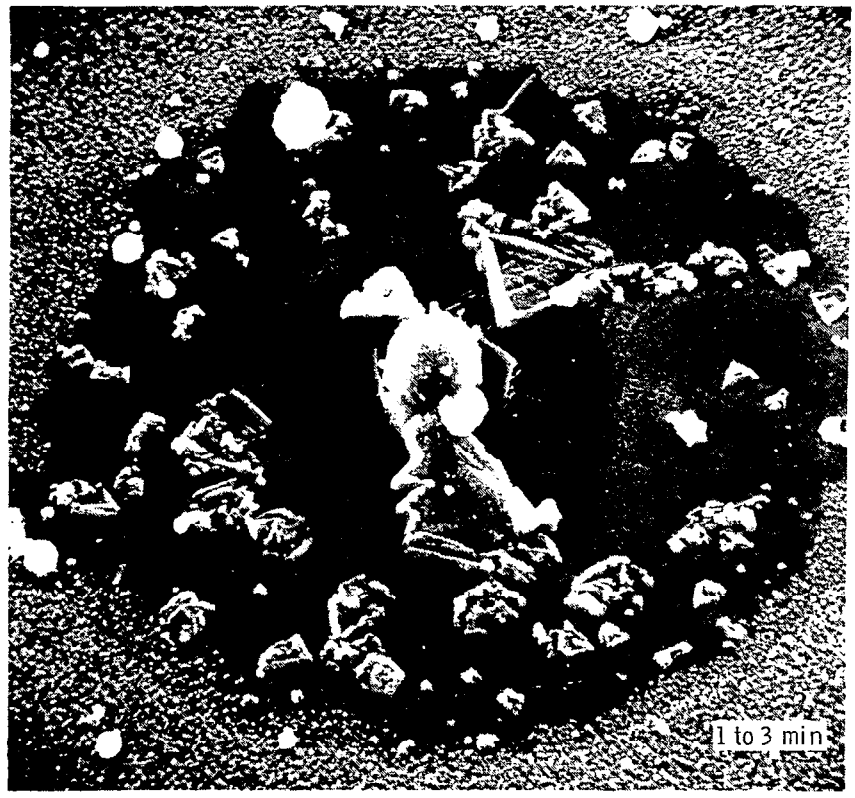

Figure 56. Acid droplet stain (AEDC Test No. 14).

This technique is only applicable to those cases where the cuprous chloride crystals are reasonably distinct. In many cases an addition of aluminum chloride in the droplet completely masks the cuprous chloride.

8.0 PARTICULATES IN THE EXHAUST CLOUD

8.1 ALUMINUM OXIDE PARTICLES

The Al_2O_3 particles collected and examined during these tests cover a wide size range and include a variety of types.

The dust particles from <0.01 to 0.1 μ are irregularly shaped and in many cases have agglomerated into clusters. The delicate, lace-like nature of these clusters would suggest that this agglomeration occurs under relatively quiescent conditions well outside of the turbulent exhaust plume. Those particles in the size range from 1 to 100 μ are spherical. It is quite common to find some of the smaller spheres attached to the larger ones. Figure 57 would indicate that this agglomeration occurred while the larger sphere was still molten, since the smaller ones are imbedded in its surface. However, other groups such as that shown in Fig. 58 indicate that the attachment occurred well after solidification. Clusters of the larger spheres (20 to 100 μ) are rare, and it is felt that those which have been observed are a result of the collection process.

When examined under the optical microscope the Al_2O_3 spheres can be divided into three types, according to their physical appearance. The first can be compared to a loosely compacted snowball (Fig. 59a). It can be broken open easily with a micropick and in many cases reveals a metallic aluminum core. This type of sphere is produced almost exclusively, when solid propellant fuel is burned at low pressure in an inert atmosphere of nitrogen or argon. It is typical of the type of particle produced in tests which are conducted in closed environmental chambers where the quantity of fuel burned is large compared to the available oxygen in the test chamber, thus resulting in a premature quenching of the burning aluminum droplet. This type of particle was not observed in the samples from the rocket motors used in the tests either at AEDC or MSFC, but was produced by burning small samples of fuel in a combustion bomb (150 psia maximum pressure).

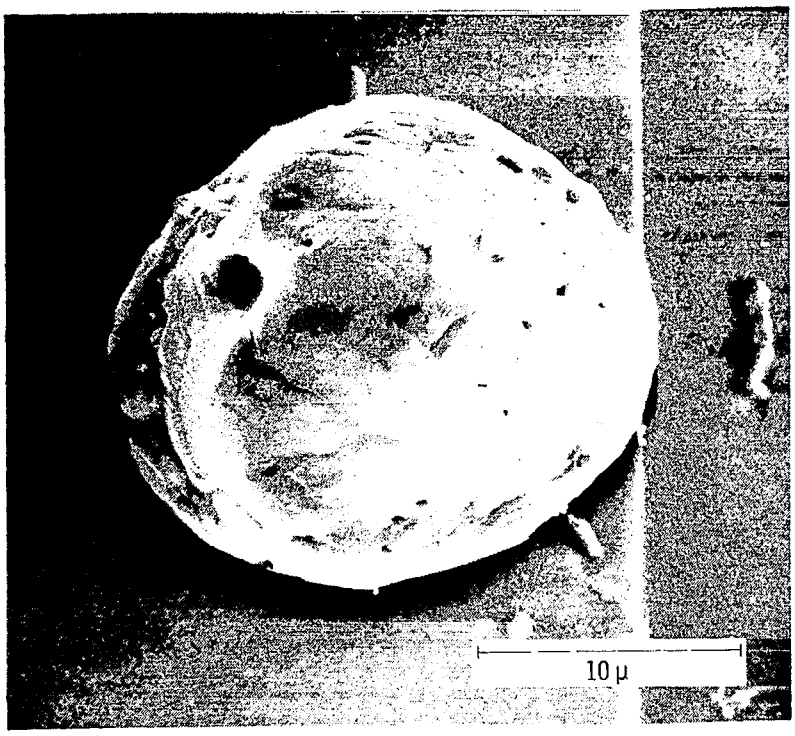

Figure 57. Fused Al_2O_3 spheres.

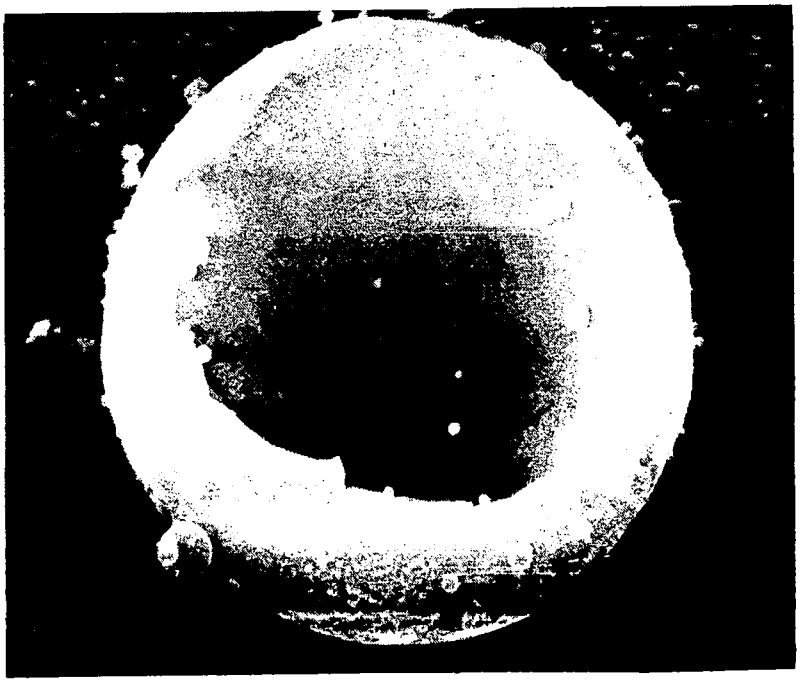

Figure 58. Al_2O_3 spheres loosely attached.

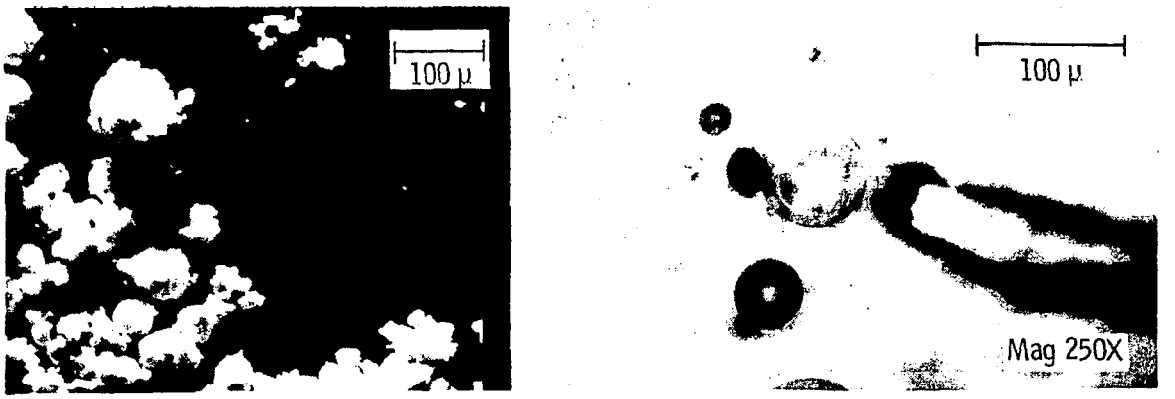

a. Snowlike

b. Solid and hollow

Figure 59. Varieties of Al_2O_3 spheres.

The other two types are shown in Fig. 59b. One is transparent, and the other is opaque. The opaque spheres appear smooth, with the coloration of small pearls. In this photograph a polarized light source was used to better define the transparent sphere, with the result that the white opaque spheres appear grey.

8.1.1 Transparent Spheres

The transparent spheres range in size from 10 to > 100 μ. In a more detailed examination with the scanning electron microscope they are found to be hollow (Fig. 60) and have a shell thickness on the order of 0.1 μ (Fig. 61). An enlarged view of the surface structure of these particles is shown in Fig. 62. The dendritic growth of the crystals as the melt solidified can be quite easily seen. The satellite particles attached to the surface are the opaque type and obviously became attached after solidification.

These hollow spheres have appeared in varied numbers in all of the tests. It has been found, however, that they can be produced in copious quantities by free-burning the fuel in air with a relative humidity greater than 80 percent.

Several suggestions have been made as to the mechanism by which these spheres are produced. Bartlett et al. (Ref. 3) propose a burning model in which the aluminum oxide forms on the surface of the molten aluminum, which is then inflated by the aluminum vapor. This vapor diffuses through the shell and burns on its outer surface.

Brzustowski (Ref. 13) takes issue with this model, which requires a stable liquid shell surrounding a liquid core at the same time subjected to external aerodynamic forces. He refers to his own work, in which he also observed hollow spheres produced from burning aluminum wires. No coating of metallic aluminum was observed inside these spheres, and thus he suggests that they are not blown up by aluminum vapor. His suggestion is that they are probably inflated by hydrogen which was dissolved in the aluminum sample. Drew et al. (Ref. 14), using high speed photography to observe burning aluminum droplets, observed that the oxide forms a molten lenslike cap on one side of the aluminum sphere and suggest that the hollow oxide spheres are most likely formed by gases blowing bubbles out from this cap.

Figure 60. Broken Al_2O_3 sphere.

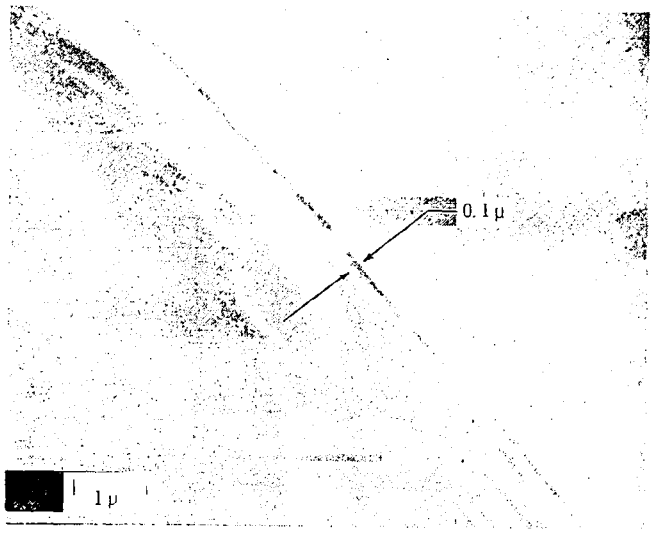

Figure 61. Edge view of shell.

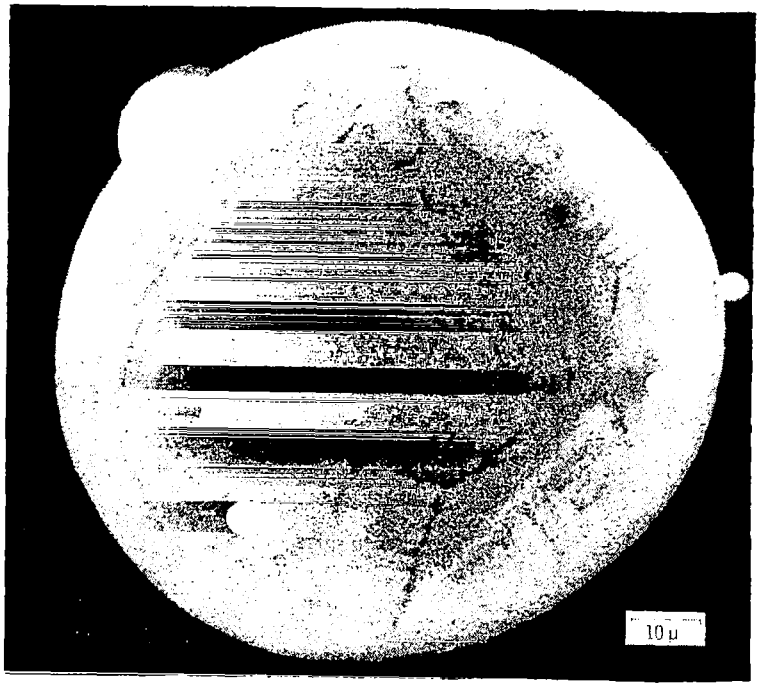

Figure 62. Surface structure of shell.

Prentice (Ref. 5) reports that the formation of hollow spheres is associated with the environment in which the aluminum is burned. Aluminum spheres burning in a wet atmosphere were observed to explode, resulting in a shower of aluminum oxide balloons and solid spheres. Addition of CO_2 to the gas mixture resulted in an even more violent explosion of the aluminum droplet. Prentice suggests that the solid spheres are α-alumina and that the balloons formed in the presence of CO_2 are a non-stoichiometric A 1-0-C species. The authors' observations would confirm Prentice's results for conditions of high humidity. Since the solid rocket propellant also produces CO_2, then the oxycarbides that he proposes are also a possible product of combustion.

It would appear that these hollow spheres are produced from aluminum burning outside the rocket combustion chamber, and thus would account for only a small precentage of the total aluminum oxide produced by a rocket motor. They would be most likely to occur shortly after ignition when fuel close to the nozzle could be ejected unburned. Evidence of these tracers from burning fuel has been observed in both the environmental chamber tests and the MSFC tests.

Even though these particles may account for only a small percentage of the total Al_2O_3, they can play an important role in the atmospheric condensation processes, and with apparent densities as low as 0.024 gm/cc, they can remain in the atmosphere for long periods of time.

8.1.2 Opaque Spheres of Aluminum Oxide

Upon closer examination the opaque spheres of aluminum oxide are far from the simple, smooth spheres observed under the optical microscope. Figures 63a, b, and c present SEM photographs of spheres with a plate-like structure. Sample (a) was taken from the exhaust of a scaled Minuteman series monitor with 7,000 lb of propellant, sample (b) from the small motor used in the AEDC tests with 0.25 lb of propellant, and sample (c) from the Tomahawk TEM-416 motors (400 lb of propellant) fired in the MSFC tests. The similarity of these samples, obtained from such a wide range of motor sizes, confirms the original premise that small motors can be used to produce a representative spectrum of particles.

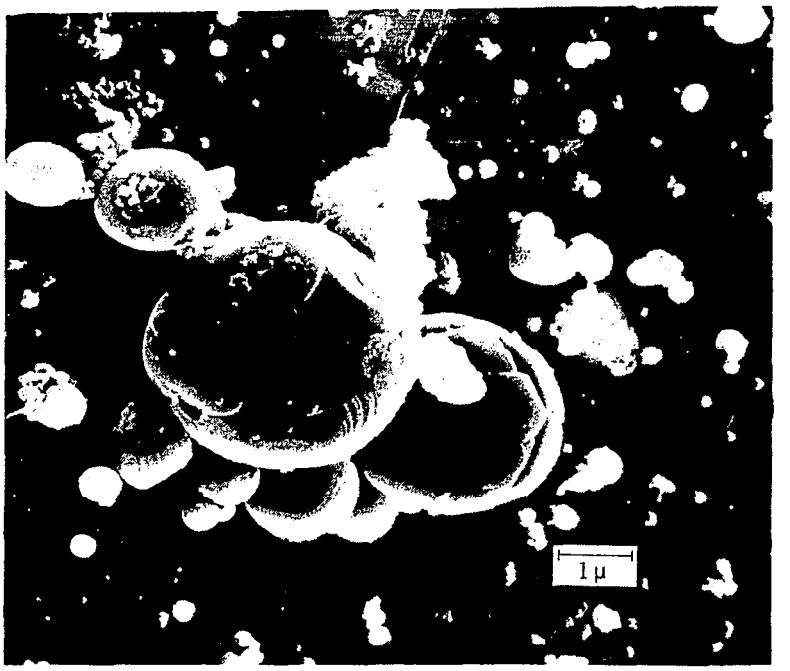

a. 7,000-lb scale minuteman motor

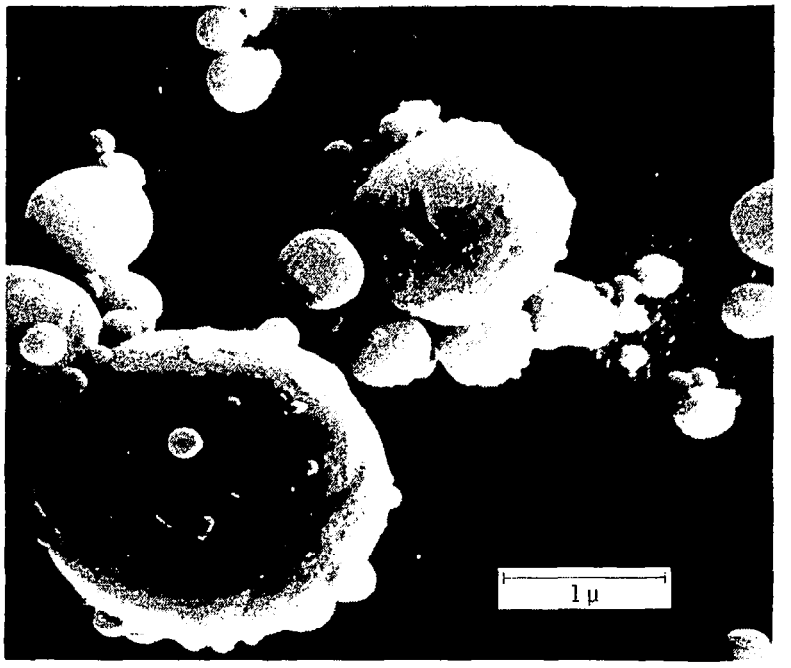

b. 0.25-lb AEDC variable load motor

Figure 63. Plate-like structure.

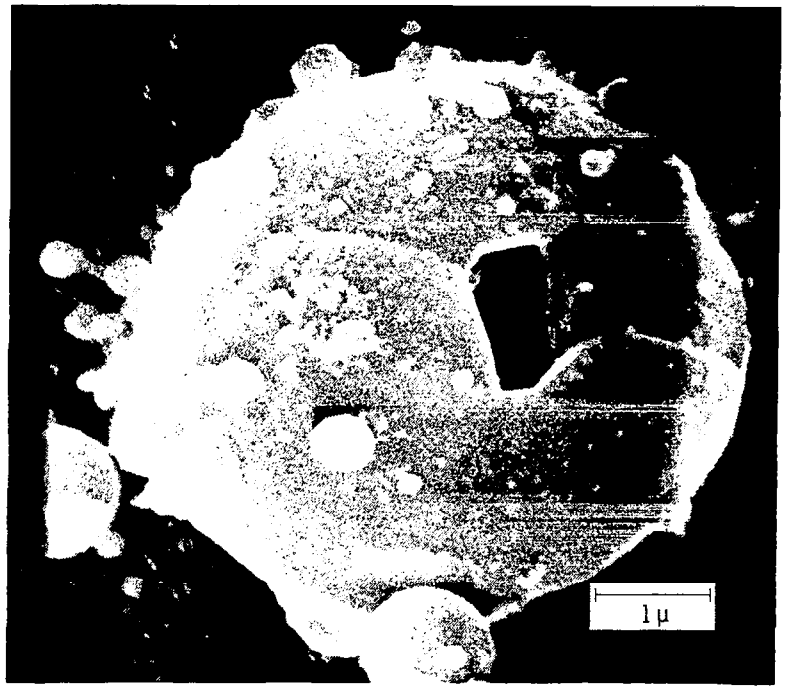

c. 400-lb Tomahawk (MSFC tests)
Figure 63. Concluded.

8.2 AEROSOL DROPLETS

The aerosol droplets collected on the fallout disks in both the environmental chamber and the open test site at MSFC are associated with large Al_2O_3 spheres (5 to 50 μ) which apparently serve as condensation nuclei. Two such droplet records are presented in Fig. 64, showing the similarity between the environmental chamber and the free atmospheric tests. Figures 65a, b, and c present a sequence of views of a typical droplet stain and its component parts. In the overall view, Fig. 65a, there are three particles which served as nuclei for droplets. The dark shadow areas around some of the other particles are caused by charging and are an artifact of the scanning electron microscope. The center stain enclosed by the dashed lines is enlarged in Fig. 65b. In this photo it is obvious that the large particle arrived in the droplet, whereas the smaller particles settled later. If they had been there first or had been in the droplet, then they would have served as focal points for the crystals as the droplet evaporated and thus would be encased in crystals. The crystals themselves (Fig. 65c) are of particular interest in that their basic triangular shape indicates a cubic lattice structure. This fact,

coupled with the x-ray scans, shows them to be cuprous chloride (Cu Cl). In the x-ray scan for chlorine and aluminum it was noted that while the stronger signals were coincident with the Al_2O_3 spheres and the cuprous chloride crystals, there was a slight background signal of both aluminum and chlorine over the complete stain area. Careful examination of Fig. 65b shows what appear to be cracks in a rather thin layer of material coating the surface surrounding the nucleus. This material does not have the crystalline structure of the cuprous chloride and has the appearance of dried mud. As will be explained, further tests have confirmed that this is aluminum chloride.

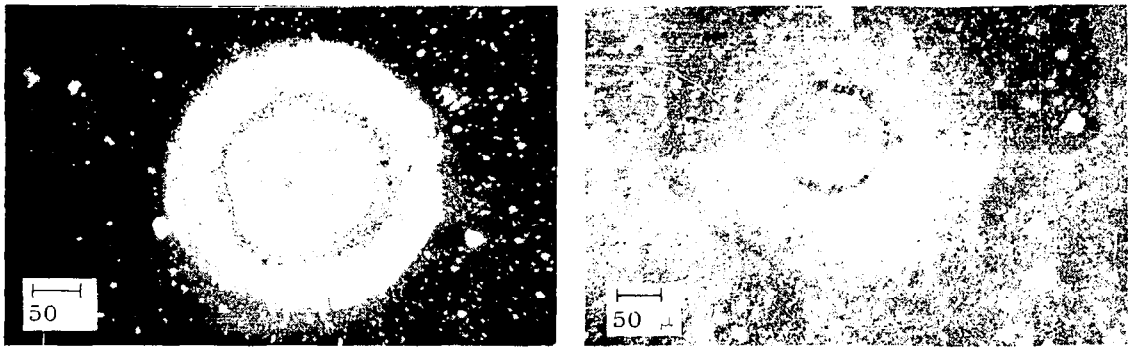

a. AEDC Test No. 13 (64-percent humidity)

b. MSFC Test No. 1 (74-percent humidity)

Figure 64. Comparison of acid droplet stains.

To confirm the fact that the triangular crystals are indeed a product of a hydrochloric acid droplet, a sample disk was sprayed with droplets of dilute acid with a pH of -0.68. The resulting stain is shown in Fig. 66a and a closeup of the crystals is in Fig. 66b.

Several grams of aluminum oxide collected from tests in the 12V chamber were mixed with 5 cm^3 of hydrochloric acid of pH -0.68. The mixture was then centrifuged and the clear liquid decanted. This liquid was then sprayed through a glass nebulizer and the droplets caught on a glass slide. The resulting deposit after the water had evaporated is shown in Fig. 67. Once again the mud-like nature of the deposit is quite evident. X-ray analysis again confirms the material as aluminum chloride. There are several Al_2O_3 spheres present which appear to be opaque in this photo taken under the SEM. However, when viewed under the optical microscope, these spheres are all the hollow, transparent type. Because of their apparent low density, these spheres remained on the top of the liquid during centrifuging and

thus were decanted with the liquid. A subsequent test in which a sample of the liquid was carefully removed, via a hypodermic syringe, from below the surface of the clear liquid left only the aluminum chloride deposit and no Al_2O_3 sphere.

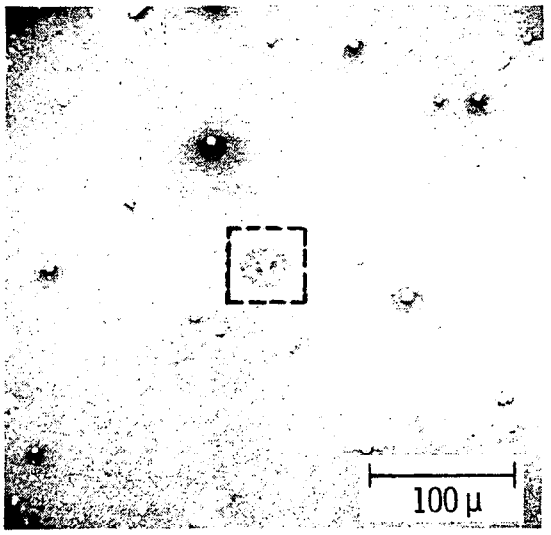

a. 100X

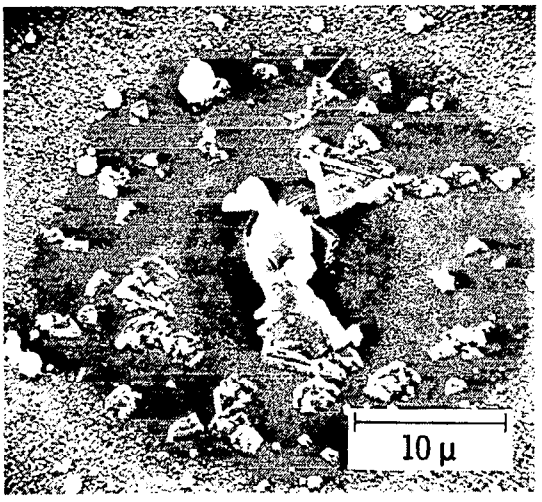

b. 1,000X

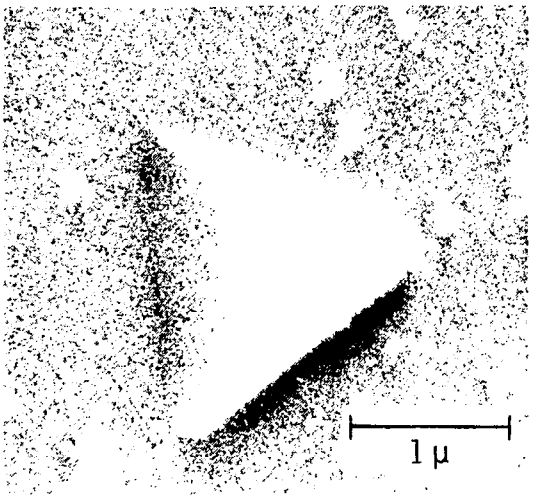

c. 10,000X

Figure 65. SEM photos of sample disk.

a. 100X b. 1,500X

Figure 66. Stain from hydrochloric acid droplet.

Figure 67. Aluminum chloride deposit.

8.3 ANALYSIS OF MSFC SAMPLE (TEST NO. 1, LOCATION J)

From the many samples of acid aerosol droplets observed at the MSFC tests we would like to present one example in some detail. An overall view of the stain has been presented in Fig. 64b. A series of closer views is shown in Figs. 68a, b, and c. The mud-like aluminum chloride is quite evident in Fig. 68b and has served to mask the typical triangular crystals of the cuprous chloride. However, x-ray scans of the material indicate the presence of chlorine, copper, and aluminum. The shape of the nucleus is suggestive of an aluminum oxide sphere as the core, but the photographs do not provide conclusive evidence. Figure 68c shows a fissure in the chloride coating (marked with a dot).

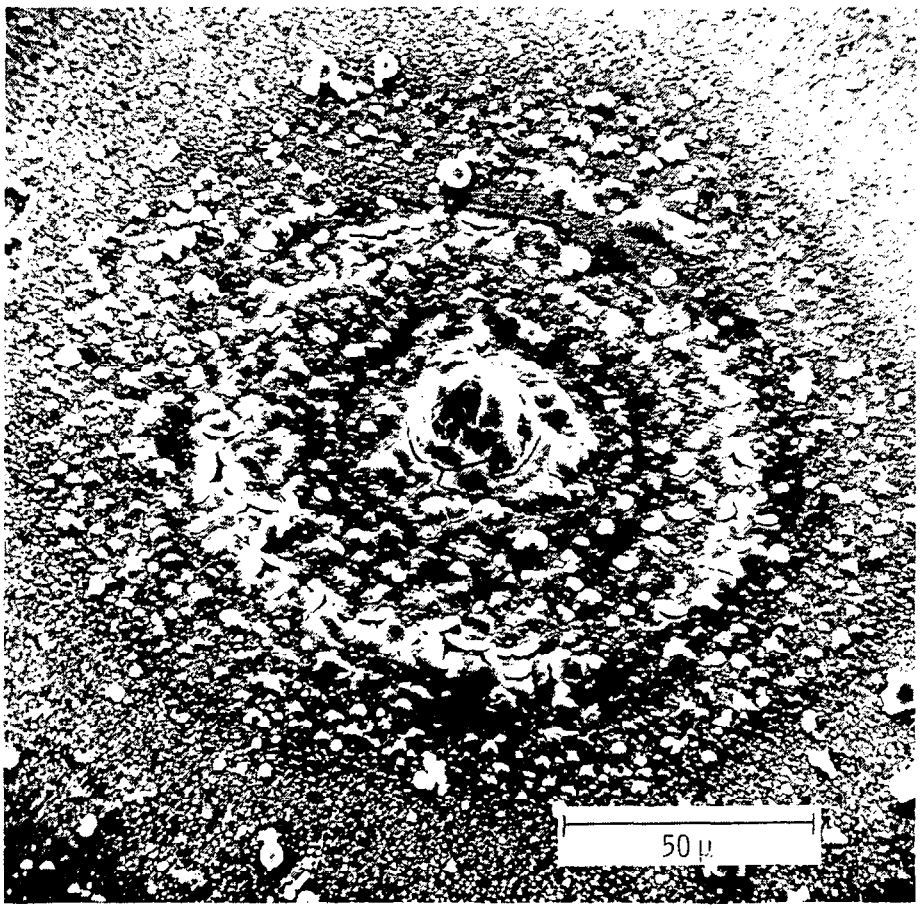

a. Center of sample

Figure 68. Sample from MSFC Test No. 1.

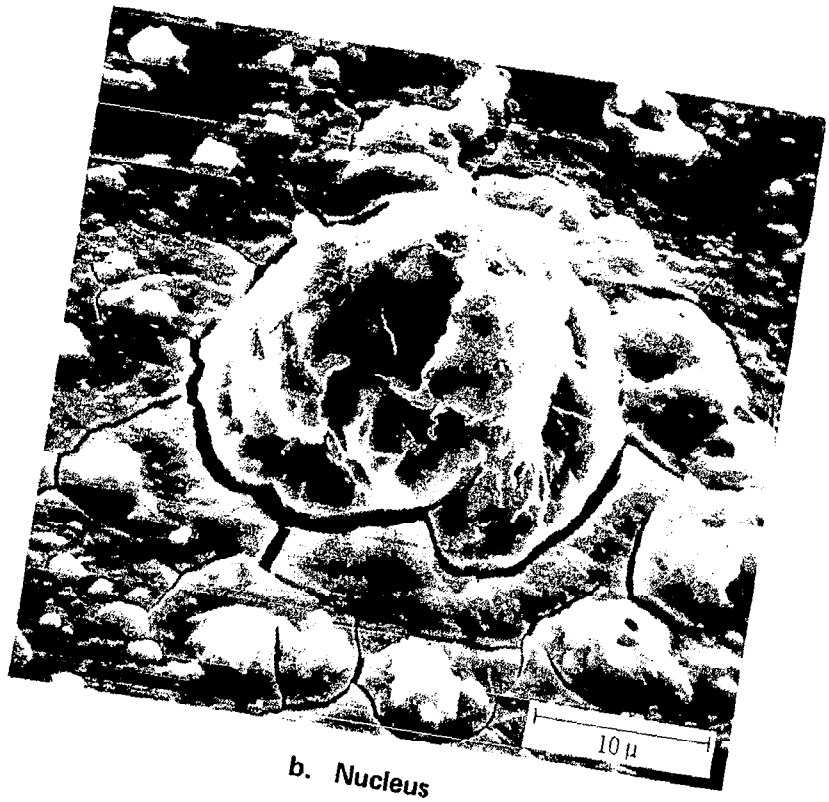

b. Nucleus

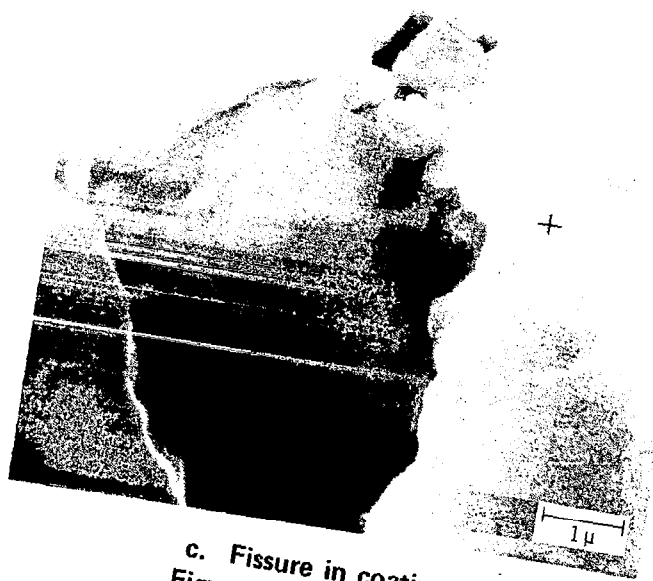

c. Fissure in coating

Figure 68. Concluded.

The electron probe was focused down this fissure and also, for comparison, on the surface at the point marked with an X. The resulting scans are presented in Figs. 69a and b. The Ca and Cr peaks are from the metal coating used to prepare the specimen for the SEM and are not a part of the sample. Similarly, the Fe peak is an artifact of the SEM system and is produced by stray electrons striking the pole pieces of the magnets. The peak heights can be considered semiquantitative in that comparison of the aluminum peaks in both Figs. 69 a and b show the heavy aluminum concentration in the core of the nucleus. Unfortunately, the instrument is not capable of detecting the elements below 10 in the periodic table and thus cannot confirm the oxygen peak associated with the aluminum. However, two factors indicate that the aluminum peak represents an Al_2O_3 sphere. The first is that no evidence of unburned aluminum has been found on any of the fallout plates from rocket motors sampled during these tests, and the second is that the particle arrived in a hydrochloric acid droplet which would have dissolved the nucleus had it been metallic aluminum. And if this were the case, then the core should have just as strong a chlorine peak from the resulting aluminum chloride as does the surface.

8.4 CONDENSATION NUCLEI

In examining the fallout sampling disks one can easily see that while the larger particles form nuclei for acid droplets not all of the large particles participate. There is nothing to suggest that there is a size perference among the larger spheres, nor a preference for hollow versus solid spheres. In view of the fact that there is some aluminum chloride associated with the residue on the disks, then one can suggest that those particles participating as condensation nuclei may consist of both α and γ phase alumina. Suggestions have been made that a rapidly quenched surface and a more slowly cooling interior could produce an α-core with a γ-surface shell. This would be an unusual occurrence in crystal growth since the driving mechanism for crystal definition is more strongly influenced by an existing structure than by the cooling rate. And secondly, since the γ-phase converts to α at temperatures of 1,100°C, it is hard to see how radiative and convective heat transfer at the surface of a 60-μm sphere can maintain surface temperatures in the shell below this value with a 2,045°C molten core.

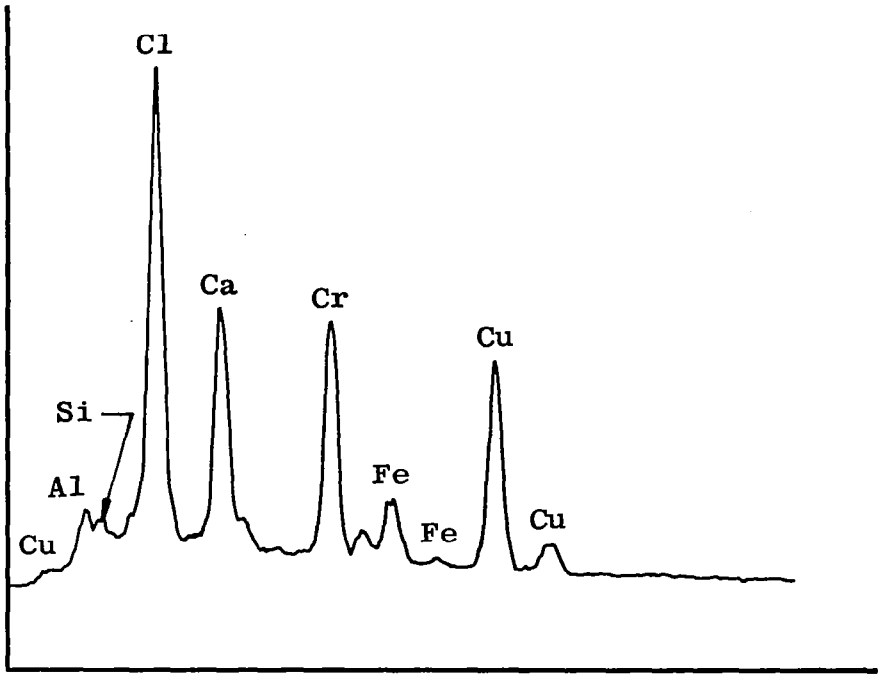

a. Surface

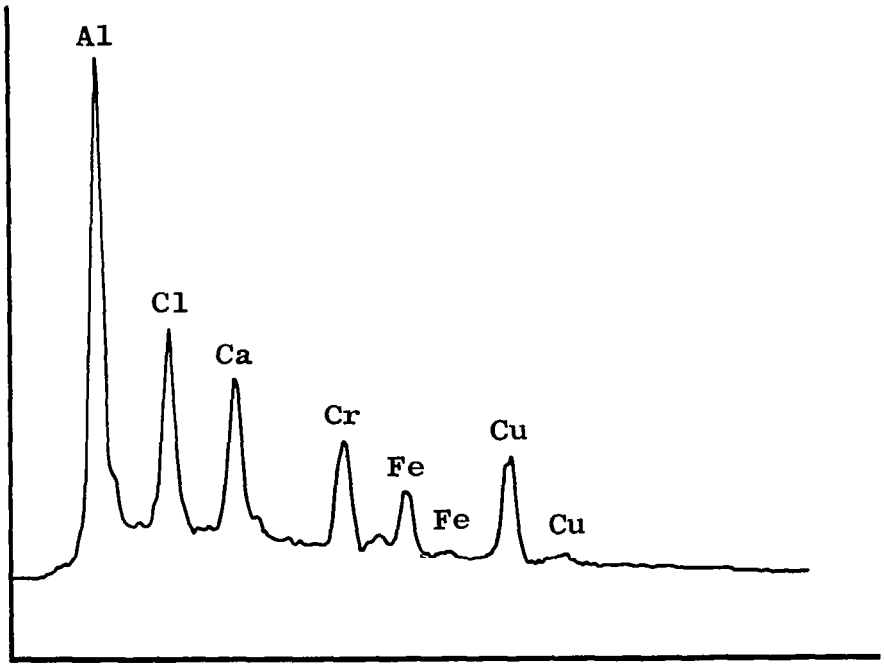

b. Down fissure

Figure 69. Elemental scan.

In a search for a more probable explanation, Fig. 70 is presented as an Al_2O_3 particle which is of possible interest as a condensation nucleus. This sample taken from a rocket motor firing in a 29-percent relative humidity environment has a coating of submicron particles. An enlarged view of the edge of this particle is shown in Fig. 71a along with an elemental scan for aluminum shown in Fig. 71b. This confirms the fact that these submicron particles are an aluminum compound. An elemental scan for chlorine showed no chlorine present and indicates that they are not aluminum chloride particles and are indeed submicron aluminum oxide particles.

Aluminum oxide can exist in several crystalline forms. The most commonly occurring are designated α-alumina and γ-alumina. The α-Al_2O_3 is the stable form; it melts at $\approx$2,045°C and boils at 2,980°C. It has a specific gravity of 3.99, is insoluble in water, and is very resistant to attack by all aqueous acids. Alumina slowly solidifying from the melt will form 100-percent α-phase. The γ-Al_2O_3 is designated as a metastable phase. It has a specific gravity of 3.42 to 3.64, is hygroscopic, and is soluble in acids. Upon heating to $\approx$1,100°C the γ-phase converts over to the more stable α-phase. The γ-phase can be produced by rapidly quenching the melt.

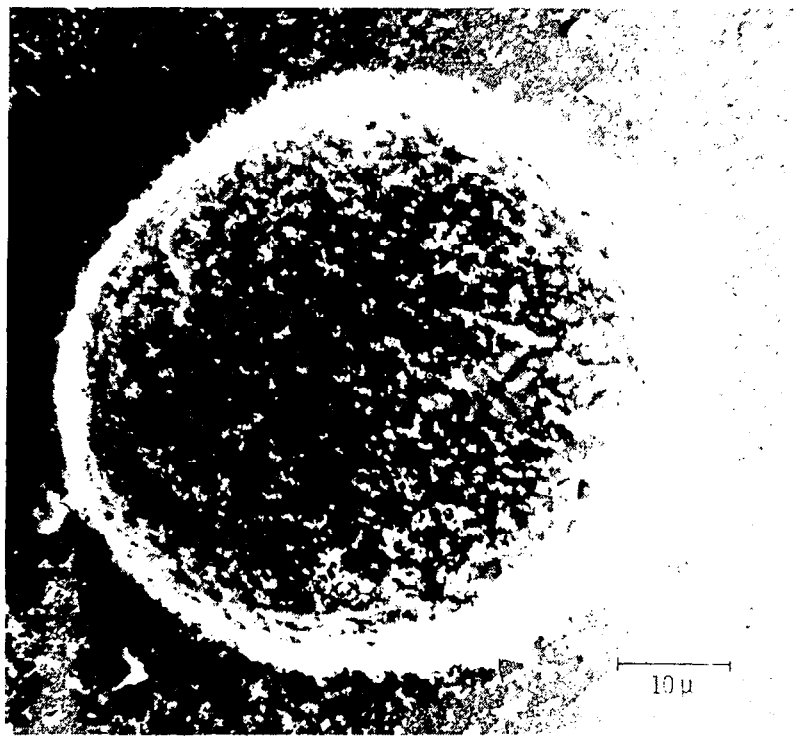

Figure 70. Al_2O_3 particle with surface deposit.

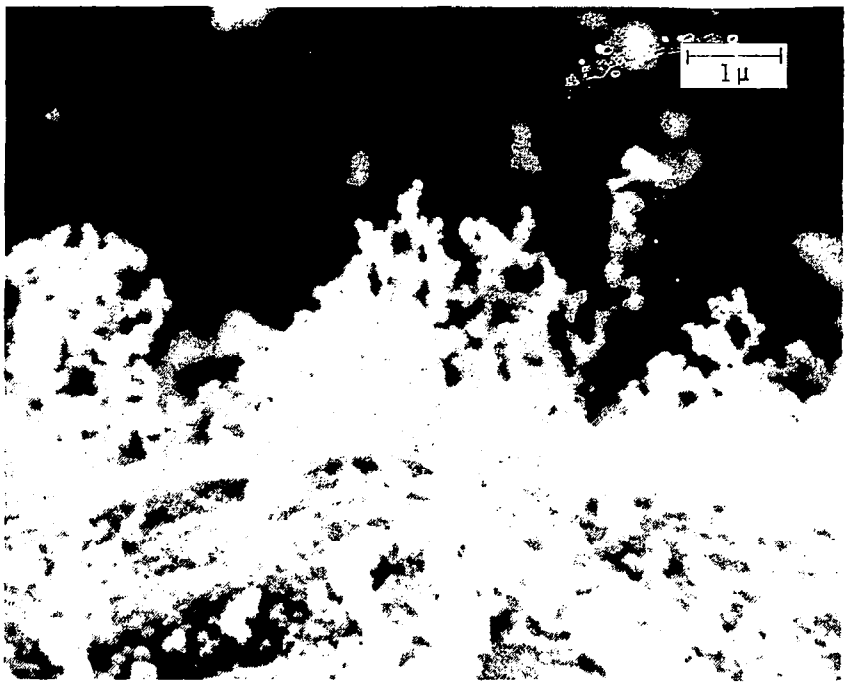

a. Visible photo

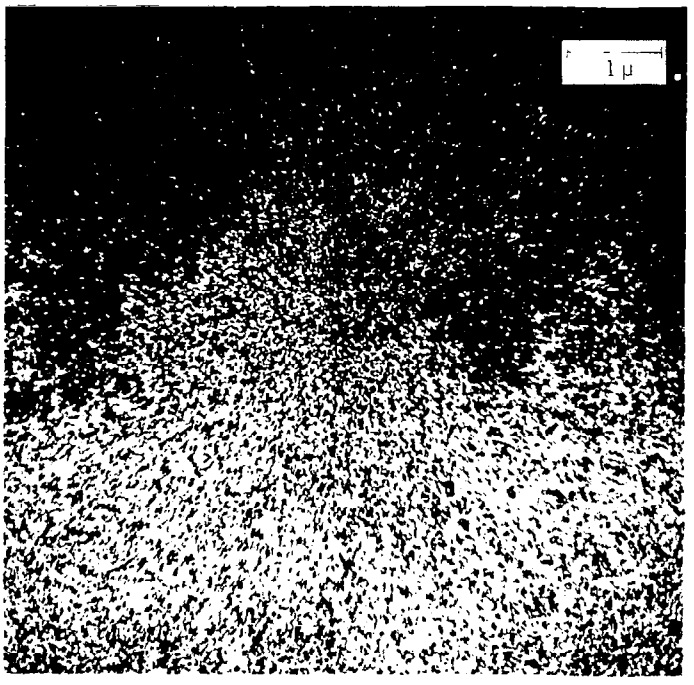

b. X-ray of aluminum compounds

Figure 71. Edge view of particle.

Both types of alumina are found in the samples of aluminum oxide from solid rocket motors. Two bulk samples of Al_2O_3 particles analyzed by M. P. Nadler, of the Naval Weapon Center, yielded the following results.

Sample	Alumina Content, percent				
	Particle Size			α-Phase	γ-Phase
	$<0.1\ \mu$	0.1 to $0.5\ \mu$	$>0.5\ \mu$		
1	94	6	0	<1	99
2	33	52	15	15	85

These data would indicate that the submicron particles are predominantly the γ-phase and that the larger spheres are the more stable α-phase. Further evidence to confirm this generalization is contained in the fact that bulk samples from the larger rocket motors show an increase in the presence of the α-phase but also show a corresponding increase in the percentage of larger particles.

The crystalline structure of the Al_2O_3 particles is of particular importance when one considers their behavior in the presence of water vapor and hydrogen chloride. The α-phase can be considered inert in the presence of the H_2O and HCl; however, the γ-phase is extremely active. Being hygroscopic, it will absorb water vapor, and the resultant wetted surface will adsorb HCl. The resulting hydrochloric acid will then dissolve the original aluminum oxide.

The Al_2O_3 sphere shown in Fig. 70 is possibly the ideal combination of the two types of oxide to act as a condensation nucleus. One can postulate that the 60-μ sphere (most probably α-phase) would serve as the large stable particle of sufficient radius to assure that the resulting condensed droplet would be above the critical size for continued growth. The smaller particles (γ-phase) provide the surface activation to initiate the condensation process at relative humidities much less than 100 percent. Since the γ-phase is soluble in the resulting HCl/H_2O droplet, then traces of the surface coating would not be evident when examining droplets and particles collected after the condensation event.

8.5 ALUMINUM OXIDE PARTICLE SIZES

The aluminum oxide particles produced by the solid rocket motors are not considered hazardous in terms of their toxicity. However, they could conceivably play a significant role in inadvertent weather modification by seeding clouds, especially if they should remain airborne for extended time periods. There are three mechanisms by which these particles can be removed from the atmosphere: they can slowly settle due to gravitational forces and eventually deposit on the ground; they can be washed out of the air by an overriding rainfall; or they can themselves initiate condensation and become the nuclei of raindrops, which then fall to the ground. The effectiveness of each of these mechanisms is a strong function of the particle size. Thus in order to predict the possible residence times in the atmosphere and the eventual disposition of the Al_2O_3 there is a need to know the size distribution of the particles.

The particles produced from a solid rocket motor range in size from 0.005 to 100 μm in diameter. In considering the terminal velocity, or settling rate, over this size range one must allow for the fact that the smaller particles have dimensions approaching the mean free path of the gas molecules and allow for slip correction. For the larger particles, the resistance varies as V^s where V is the velocity and s is a factor which steadily increases with Reynolds number. The calculation of terminal velocities can be divided into four flow regimes as indicated in Table 4 (derived from Ref. 15).

Table 4. Settling Velocities of Particles

Particle Size Range, μm	Flow Regime	Terminal Velocity
0.001 to 0.1	Molecular	$V_T = \frac{d\rho g\ \alpha\lambda}{9\ z}$
0.1 to 1.0	Cunningham	$V_T = \frac{d^2\rho g\ \left(1 + \frac{2\beta}{d}\right)}{18\ z}$
1.0 to 10.0	Stokes	$V_T = \frac{d^2\rho g}{18\ z}$
10.0 to 1,000.0	Klyachko	$V_T^2 = \frac{1/3\ d\rho g}{\rho_a\left(\frac{6}{Re} + \frac{1}{\sqrt[3]{Re}}\right)}$

where d = diameter of particle (cm)

ρ = density of particle (gm/cm^3)

ρ_a = density of air (gm/cm^3)

z = viscosity of air ($dyne\text{-}sec/cm^2$)

λ = mean free path of air molecules (cm)

α = coefficient determined by the degree of accommodation of the gas molecules to the particle surface:

for diffuse reflection with conservation of gas molecule velocities = 1.09
for specular reflection = 1.175
for diffuse reflection with gas molecules accommodating to particle surface temperature = 1.131

β = coefficient determined by the ratio of gas molecules which are reflected diffusely to those reflected specularly:

for glass spheres $\beta = 0.82 \times 10^{-5}$
for oil droplets $\beta = 0.813 \times 10^{-5}$
for brass cylinders $\beta = 0.66 \times 10^{-5}$

The predicted terminal velocities for Al_2O_3 spheres in a quiescent atmosphere are presented in Fig.72. For particles larger than 10 μm the settling rates are sufficiently high that, assuming no unusual atmospheric conditions causing large updrafts, they can be expected to fall out within 12 to 14 hours (assuuming a cloud stabilization height between 1 and 2 kilometers). The residence times for 10- to 0.5-μm particles range from 1 day to 6 months if they are removed solely by gravitational settling. However, overriding raindrops are quite effective in washing out particles in this range and thus would most probably prove to be the dominant mechanism for their removal. Particles smaller than 0.5 μ are not effectively captured by rainfall since they are sufficiently small that they can follow the airflow around the droplets. Their residence time can be estimated in terms of years, if gravitational settling is the only removal mechanism. This would indicate that these particles have the potential for direct involvement in rain-making processes in the atmosphere. That is, they may become condensation nuclei for ice crystals or water droplets.

There are experimental data available which report that by far the greater part of the mass of Al_2O_3 produced by big rocket motors lies in the 1-μm and larger size range (Refs.12 and13), thus suggesting that it would be rather quickly removed from the atmosphere. However, there are some data which indicate that 25 to 50 percent of the mass of Al_2O_3 might be contained in particles less than 1.0 μm in diameter (Refs.17 and 18). A considerable portion of this report is spent in reconciling these seemingly conflicting data.

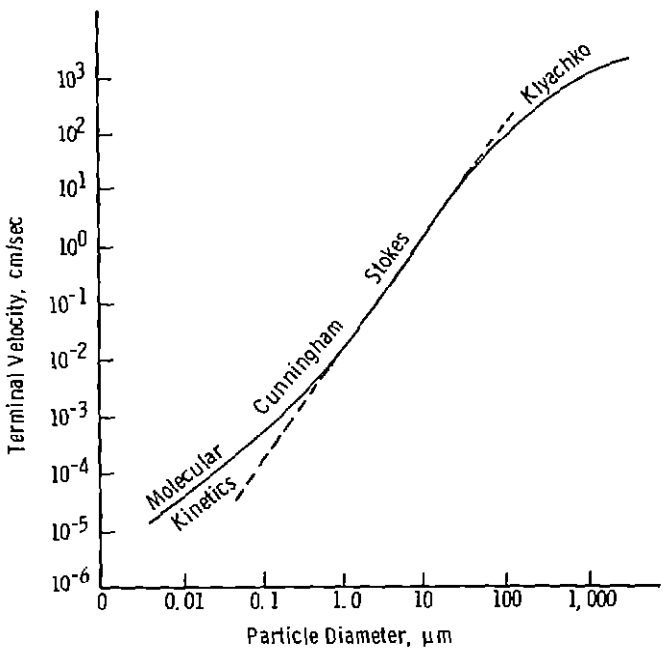

Figure72. Terminal velocity of Al_2O_3 spheres.

GENERAL COMMENTS

The candidate propellant for the Space Shuttle solid rocket motors contains approximately 16 percent aluminum powder. In this percentage range the aluminum can be considered a significant portion of the fuel. However, it serves a dual purpose in that it also tends to stabilize the burning process. It has long been recognized that combustion instabilities in solid rocket motors can be alleviated by adding powdered metals to the fuel mix. There is therefore a considerable body of literature and data concerning metal oxide particles produced by solid propellant rocket motors. However, before embracing these data and applying them to the environmental concerns posed by Shuttle operations, one should be fully aware of the prime interest which prompted these previous studies.

DAMPING COMBUSTION INSTABILITIES

The combustion rate of solid propellants is pressure sensitive. Therefore, acoustic waves which may be generated within the combustion cavity can cause accelerated burning at the antinodes. If this accelerated burning feeds pressure pulses back into the acoustic field in a resonant mode, then the resulting undamped system can lead to a violent failure of the rocket motor. It has been found that these instabilities can be damped by the inclusion of the metal oxide particles in the acoustic field in the combustion cavity. Figure 73 presents the curves showing attenuation α_D/C_m versus particle size for three frequencies as derived from the theory of Temkin and Dobbins and calculated by Dehority (Ref 19). As can be seen, the range of particle size of interest is from 0.5 to 50 μm, with the bulk of the attenuation for low frequencies being produced by particles in the 2- to 20-μm range. However, while some particles are beneficial inside the combustion cavity, they are detrimental to rocket performance (specific impulse) as they are ejected along with the gases through the nozzle. With a requirement for a sufficient number of large dampers to maintain combustion stability, and a need to limit the number of particles in the flow field to an absolute minimum, the processes involved in the formation of the oxide particles are of great interest. Many experiments have been conducted and attempts made to collect samples of these oxide particles to determine their number and size distribution. Since the particle sizes of interest for damping and specific impulse loss have been from 2 to 50 μm, the majority of the collection techniques as well as the counting and sizing methods have been oriented toward this size range. Thus in many cases the submicron particles have been ignored.

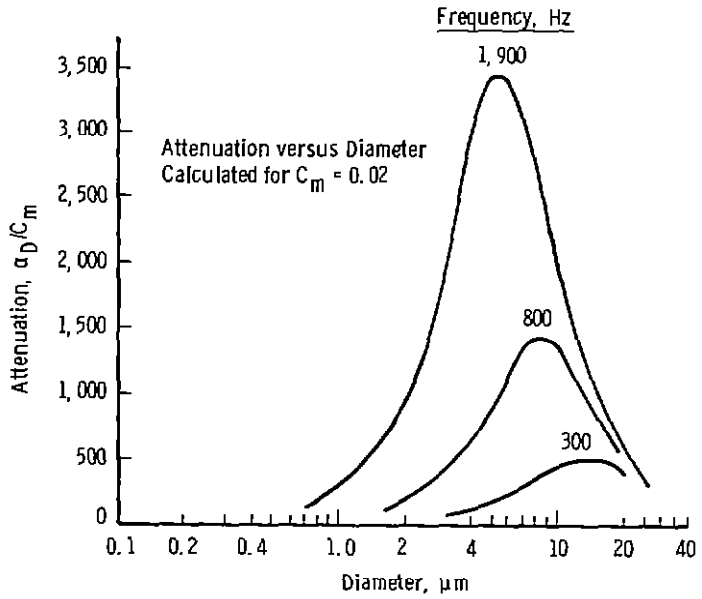

Figure 73 Attenuation versus particle size.

MEAN DIAMETERS

In some instances it is convenient to refer to a particular size distribution of particles in terms of a mean particle diameter. The most commonly understood mean diameter is the linear mean; i.e.,

$$\bar{d}_{10} = \frac{\Sigma d dn}{\Sigma\, dn}$$

However, other mean diameters are also calculated and used depending on the particular field of application. In general, the mean diameter can be of the form

$$\bar{d}_{qp}^{(q-p)} = \frac{\int_{d_o}^{d_{max}} d^q \frac{dn}{dx} dx}{\int_{d_o}^{d_{max}} d^p \frac{dn}{dx} dx}$$

where p and q can take integral values from 0 to 3 and 1 to 4, respectively. Each combination of p and q places a specific emphasis on a particular size range within the distribution. For example, the linear mean $\bar{d}_{10}$ heavily emphasizes a large number of small particles, whereas a $\bar{d}_{43}$ mean minimizes the contribution of the smaller particles. Since the larger particles are of prime concern in combustion stability and two-phase flow losses, then the $\bar{d}_{43}$ mean diameter is usually reported; i.e.,

$$d_{43} = \frac{\Sigma d^4\, dn}{\Sigma d^3\, dn}$$

This method of summarizing the experimental data has led to a misconception of the total range of particle sizes produced by solid rocket motors and has fostered a false impression that there is a general consistency in the data collected from the various test programs. Figure 74 presents raw data in the form of bar graphs of particle size distributions obtained from Al_2O_3 samples taken from Titan III-C firings. The samples were analyzed using the same methods but were collected using different techniques. As can be seen, the size distributions are radically different, whereas the calculated mean particle sizes from these two data sets are $\bar{d}_{43}$ = 11.4 and 12.6 μm, which would seem to be in reasonably good agreement.

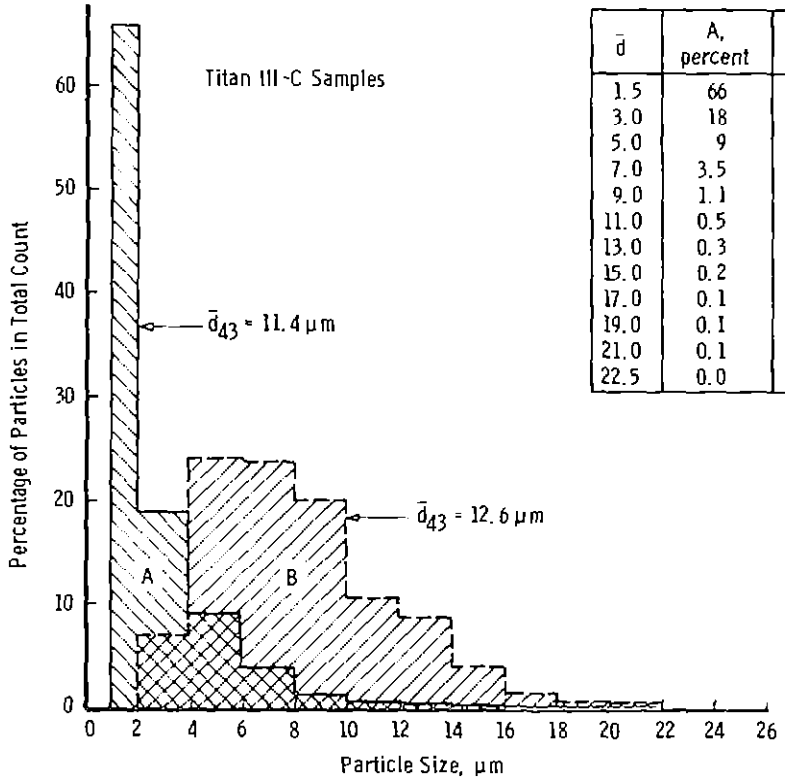

$\bar{d}$	A, percent	B, percent
1.5	66	0
3.0	18	7.1
5.0	9	23.5
7.0	3.5	23.4
9.0	1.1	20.3
11.0	0.5	11.7
13.0	0.3	8.5
15.0	0.2	3.3
17.0	0.1	1.4
19.0	0.1	0.5
21.0	0.1	0.2
22.5	0.0	0.1

Figure 74 Bar graph of Al_2O_3 particle sizes.

PARTICLE SIZE DISTRIBUTION FUNCTIONS

There are several ways of presenting particle size distributions. In addition to the histogram, there is a variety of distribution functions, and again one finds the format choice determined by the eventual use of the experimental data. In order to compare data from various sources, particle size information presented in this report has all been fitted to a distribution function.

There are several mathematical functions which have been used to provide a representation of particle size distributions. In many ways they are all variants of the expression

$$\frac{dN}{dD} = aD^p \exp(-bD^n)$$

In some cases an attempt is made to relate one or more of the constants (a,p, b, or n) to some physical parameter of the particle formation process. Nukiyama and Tanasawa (Ref. 20) obtained extensive data on drop sizes in sprays formed by air atomization and from data defined p = 2 and n = 1 for these sprays with b some undetermined function of the physical characteristics of the liquid, nozzle design, and the relative velocity of the liquid and air. Similarly, Worster et al. (Ref. 11), using available data on Al_2O_3 particle sizes, defined p = 3 and proposed a functional relationship between the constants a and b and the throat diameter of the rocket motor which produced the particles. Rosin et al. (Ref. 21) used a semiempirical technique to derive a functional relationship between the constants to fit the equation to data obtained from grinding coal dust. In this case p = n - 4 and $a = 6bn/\pi$, with b and n determined empirically.

It would appear that the possibility of defining the constants in terms of such fundamental physical properties as viscosity, surface tension, density, etc. of the particles and the force fields in which they are formed is very remote. However, the apparent universality of this function in its ability to fit the size distribution of particles formed by a variety of processes can be used to advantage in comparing data such as those obtained in collections of Al_2O_3 from rocket exhausts. It is particularly useful in that it predicts a finite number of small particles and defines a specific particle size where the distribution peaks. In many experimentally observed particle collections this peaking of the data is noted (Figs. 75 and 76). However, in some samples which are collected, due to the collection technique or the method of analysis, the data are truncated and the peak is missed. In the curves presented in this report the data were used to obtain the best-fitting distribution function, and the resulting peaking of the distribution function is thus in some cases an "extrapolation" of the distribution below the observed particle size. All distributions have been normalized to this maximum peak or mode for ease of comparison.

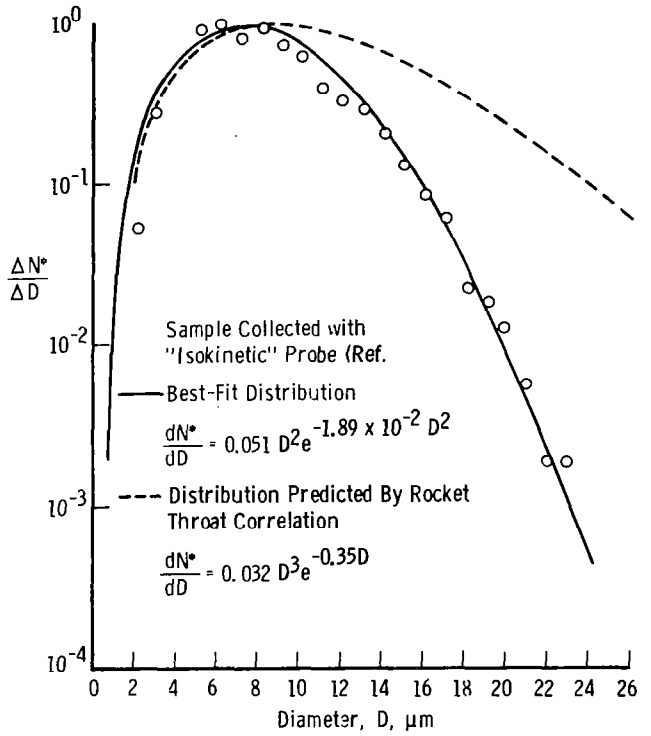

Figure 75 Size distribution from Titan III-C missile.

Fitting Data to Distribution Function

The following method was used to choose the appropriate values of the constants a, b, n, and p. The distribution function can be written as

$$\log\left(\frac{1}{D^p}\frac{dN}{dD}\right) = \log a - b\,D^n \log e$$

Thus, the data were plotted as $\log[(1/D^p)(dN/dD)]$ against D^n for various values of n and p. The values of n and p were adjusted for the best straight line fit. For the majority of the data examined, values of n = 0.3 and p = 2 were satisfactory. The total range of values was n = (0.3 to 1.0) and p = (1 to 3). From these data fits, values of a and b can be calculated from the slope and intercept. In order to obtain some uniformity in plotting the distribution functions, the functions were normalized at their mode. The mode was determined by setting

$$\frac{d}{dD}\left(\frac{dN}{dD}\right) = 0$$

and thus $D = n\sqrt{p/bn}$ for the maximum value of (dN/dD).

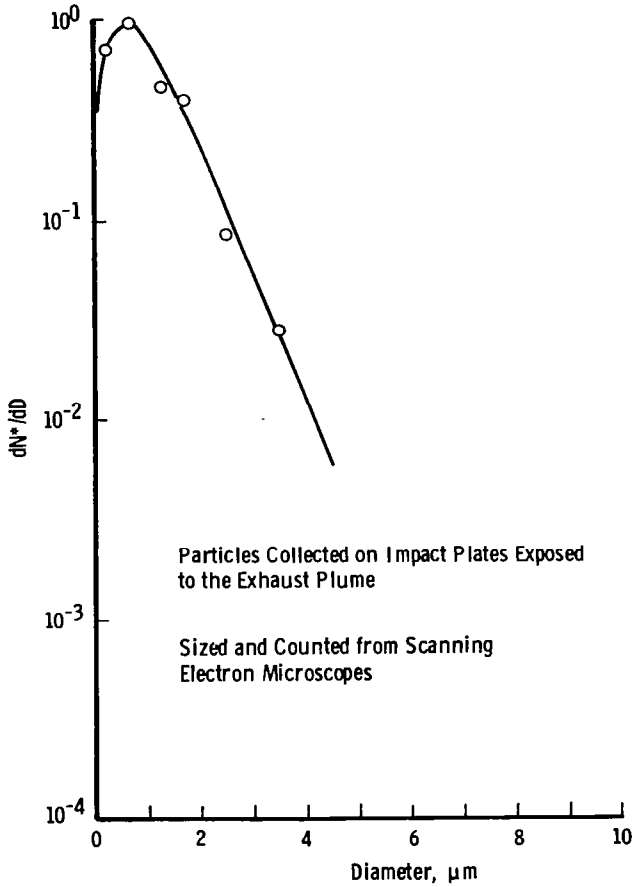

Figure 76 Particle data from a variety of fuel loads.

3.5 COMPARISON OF Al_2O_3 PARTICLE SIZE DATA

Data obtained from many rocket motor firings using a variety of collection techniques have been combined to support the hypothesis that the mean particle size produced by solid rocket motors is a function of the throat diameter of the rocket.

Samples of data used to obtain this correlation along with the empirical distribution function are presented in Figs.75 and 77. As can be seen, the correlation does a fair job of accomodating the data, especially when one considers the orders of magnitude difference in the size of rocket motors presented in these two examples. Confidence in such a correlation and particle size distribution function is greatly shaken however, when one compares data presented in Fig.78 . These data all represent size distributions of particles from Titan III-C rocket motors, taken using different collection techniques. As can be quite readily seen, the data indicate a wide variety of size distribution functions. It is also

of interest to note that the size distributions curves 3 and 4, determined by two separate laboratories analyzing the same sample, are not in agreement. Thus it would appear that although the same samples and similar sizing techniques may be used, the results, while close, will not be identical. However, when one examines the results where the same samples were analyzed using different techniques, one finds significant differences. Figures 79 and 80 present the particle size distribution curves for samples from two experimental motors with 5-cm (2-in.) diameter nozzle throats and different fuel mixes. One method of analysis was by optical microscope, and the other was by a scanning electron microscope (SEM). There are two points of interest in these curves. First, it is noted that there is a distinct shift to smaller particles when the SEM is used. It is possibly a trivial point, but these data emphasizes the fact that even if the submicron particles are collected, they cannot be counted if they cannot be seen. The SEM easily resolves particles well below the visibility of the optical microscope and thus shifts the observed size distribution toward smaller particles. Second, this same shift occurs for each of the fuel formulations. These data thus serve as a reminder that regardless of biases introduced by the particle sizing and counting technique, there is a difference due to the propellant mix.

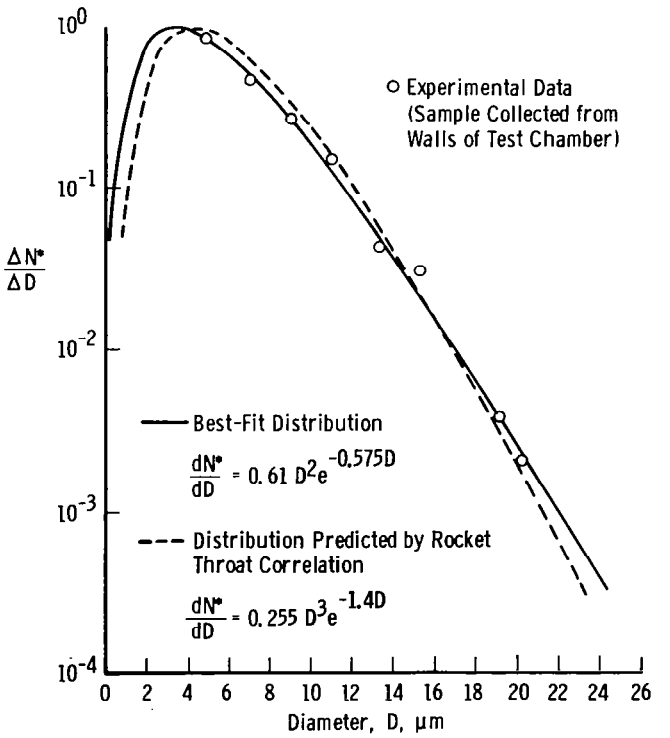

Figure 77 Size distribution from small motor (0.85-in. throat).

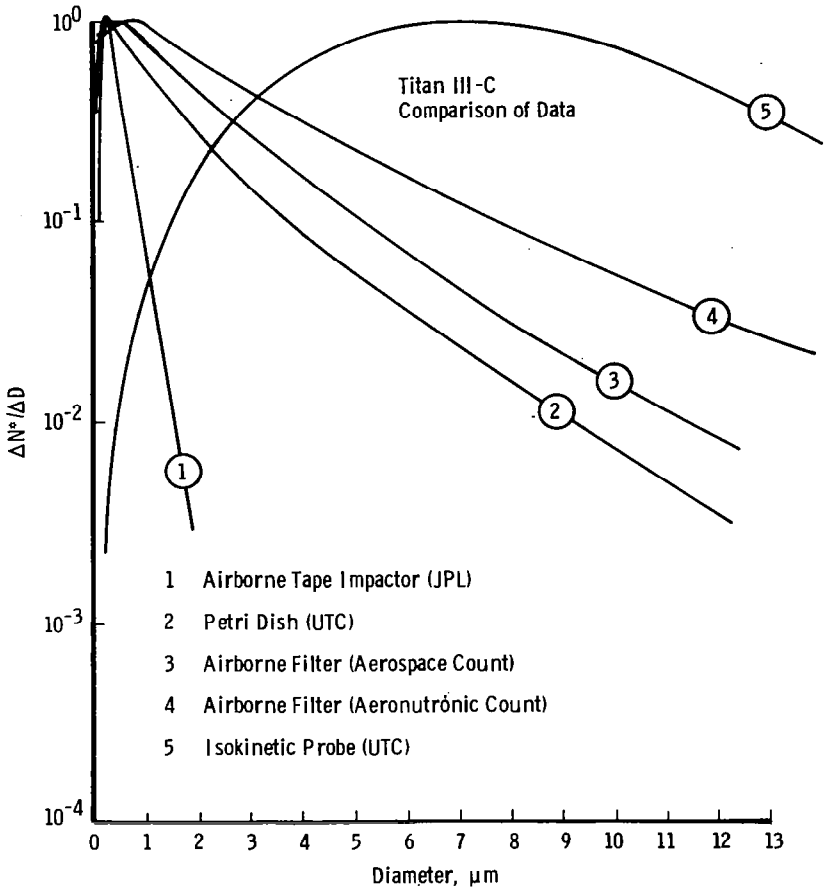

Figure 78 Size distribution of particles from several Titan III-C missiles.

Of particular interest are the distributions presented in Fig. 81. The samples were taken from the two extremes of rocket motors, a Titan III-C (95.75-cm throat) and a small experimental motor (5-cm throat). However, the collection technique, settled sample in petri dishes, was the same. The similarity of these data would confirm the suggestion that available data to date are more characteristic of the collection technique than of the rocket motor which produced the samples.

Brown et al. (Ref. 22) present Al_2O_3 particle size data taken from an experimental test motor in which they were able to vary the fuel formulation (percentage of Al and size of Al powder), combustion chamber pressure, combustion chamber size, and expansion ratio. They suggest that none of these parameters had significant influence on the particle size distribution which they observed (Fig. 76). However, one wonders if the collection and analysis technique which remained the same for all tests could possibly mask any subtle changes in the particle size distribution.

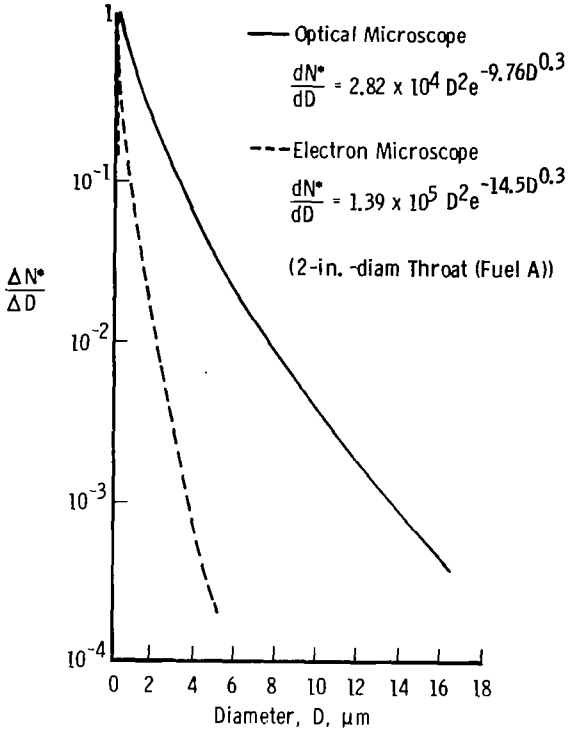

Figure 79 Particle size distribution from small motor (Fuel A).

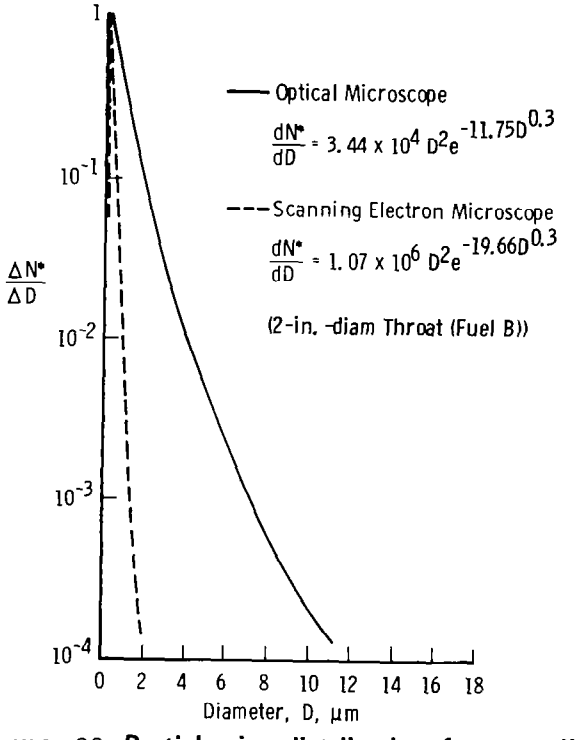

Figure 80 Particle size distribution from small motor (Fuel B).

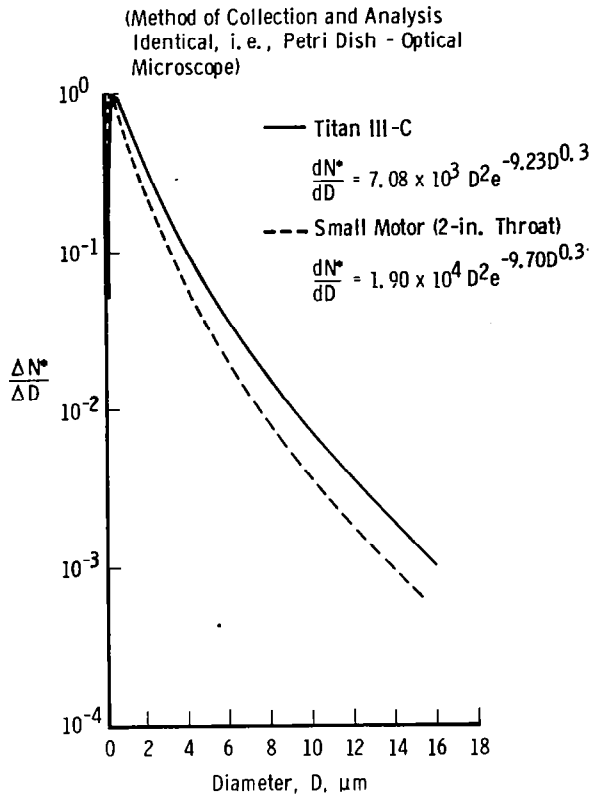

Figure 81 Size distributions of particles collected by Petri dish.

Al_2O_3 SAMPLING TECHNIQUES

The data presented thus far are representative of sampling techniques where the Al_2O_3 has been collected at a considerable distance from the rocket. Due to the obvious hostile environment close to the exhaust nozzle there are limits on where samples can be taken. A successful attempt to obtain Al_2O_3 particles on the launch platform of a Titan III-C was made by Willougby (Ref.12) using an "isokinetic probe". This probe was aligned with the flow field and was so constructed that the exhaust gases flowing around the probe produced a low pressure region at the base of the probe, thus drawing a sample of the rocket plume through the sampling section. Here the gases were allowed to decelerate and deposit the particles on a sampling surface.

Sampling methods may be classed as passive and active. The passive collectors include petri dishes, polyethelene sheets, sticky tapes, and in one case, even rainwater accumulated on the roof of an automobile. The active collectors, consisting of filters and

impactors (wire, flat disk, cascade, or tape) where cloud samples are drawn through the collector, have been used at stationary ground points and also aboard aircraft flown through exhaust plumes.

Samples have been processed by a variety of methods to produce particle size distribution data. Where the collection technique has produced a reasonably dispersed monolayer of particles, the usual method of analysis has been counting and sizing under an optical or scanning electron microscope. In those instances where the sample was too dispersed (collected on large polyethelene sheets) or too closely packed, the sample was washed from the collector and then redistributed on an appropriate microscope slide. It was assumed that all the sample was α-phase and thus was unaffected by the washing process. Usually this process involved using ultrasonic baths to try to avoid coagulation of the particles as the liquid carrier evaporated. Samples collected on filter papers have been analyzed in terms of mass loading by simply weighting the filter and also by ashing the filter and recovering the Al_2O_3 by repeated washing of the residue. An extremely complex preprocessing procedure has been described as follows:

> "The ground sampling panels were cut into 3-in.-wide strips and scrubbed in 600 cc of water. The solids were filtered and the filter dried and ashed at 600°C in a porcelain crucible. The residue was treated with aqua regia and heated to just under boiling for 1/2 hr. The resulting material was cooled, diluted with water, and filtered. The filter was dried and ashed at 600°C in a platinum crucible, and the remaining material was treated with 50 percent HF for 1/2 hour at a temperature just under boiling. The resulting material was filtered and ashed in a porcelain crucible. The Al_2O_3 particles were then sized and counted."

It can be quite easily seen from these comments on the general techniques used to collect and analyze samples (the latter technique in particular) that there are several biases against the submicron particles.

The samplers at ground level collecting the fallout from the exhaust have an extremely effective atmospheric filter to remove the submicron particles. The "isokinetic probe" which removes this filter suffers from the fact that its sampling surface is an impaction collector, and at the lower velocities in the probe the larger particles impact and the submicron particles flow around the surface. Devices flown through the exhaust cloud with some attempt to sample isokinetically would be expected to produce a more representative sample. Unfortunately, in most cases what is gained in the sampling is lost in the processing for the filters, and the sticky tapes employed are either burned or washed to extract the sample from the collector.

RESULTS FROM THE MSFC SAMPLING TESTS

These tests were conducted in order to compare the various sampling techniques that have been used in previous field tests. The particle size distributions obtained from the MSFC scaled shuttle tests are presented in Figs. 82 and 83. As can be seen in Fig. 82, the various collection techniques do bias the size distribution. It is interesting to note that the "isokinetic" probe data from these tests are quite similar to those from the UTC Titan samples (Ref. 12). The distributions presented in Fig. 83 compare the Tomahawk data to other rocket motors where the sample has been collected by fallout into petri dishes.

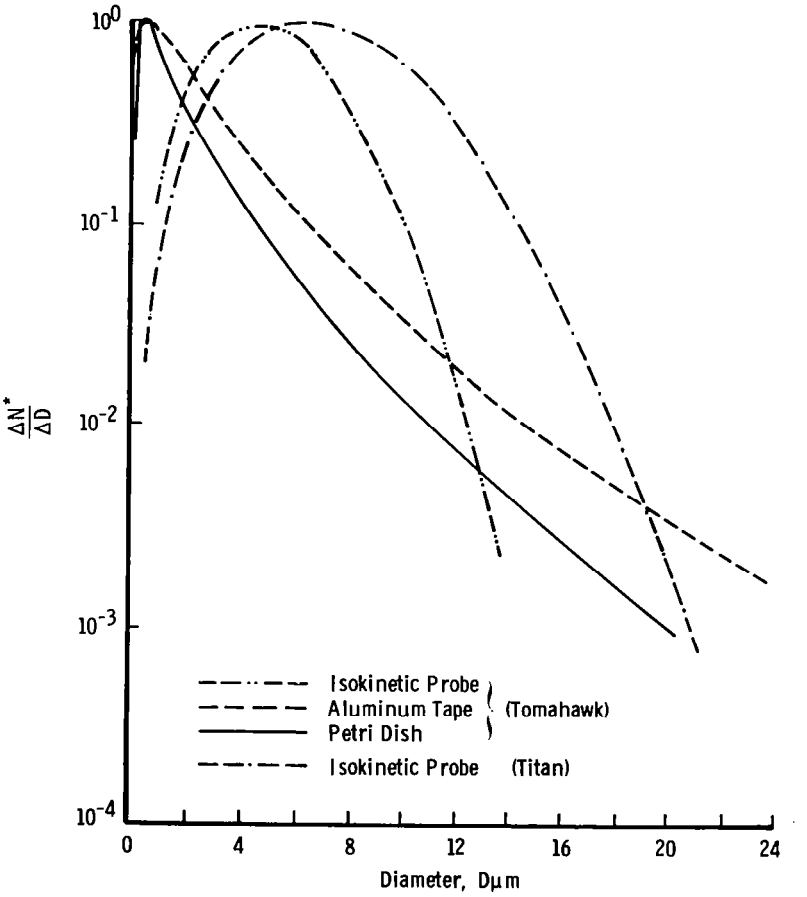

Figure 82 Particle size distributions (Tomahawk MSFC).

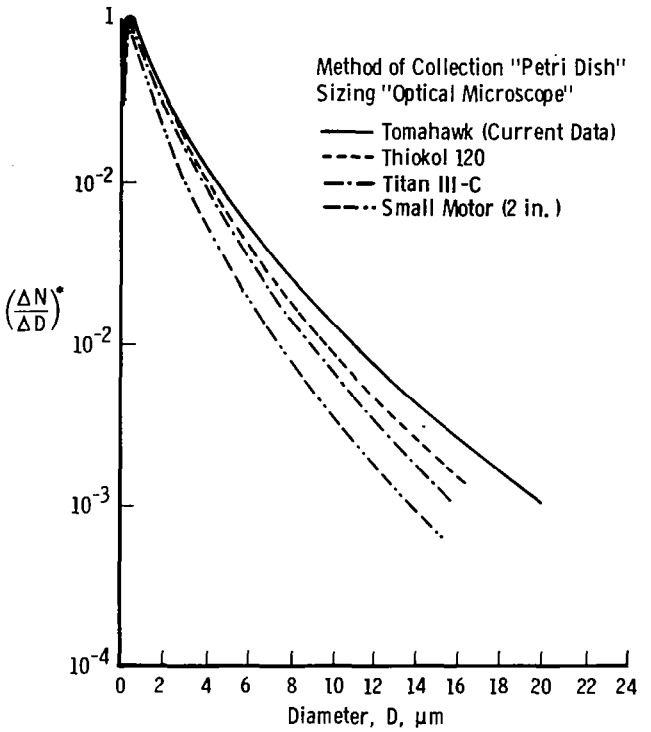

Figure 83 Comparison of Petri dish data.

TITAN III-D PLUME SAMPLING

These particular data have been singled out for emphasis, in that they would appear to be the least biased by sampling and counting techniques. The data were taken by JPL under the direction of Dr. J. Varsi at the Eastern Test Range on June 20, 1975 (Ref17). The rocket plume was produced by a Titan III-D and was sampled at an altitude of 20 km approximately 10 min after launch. The sampling aircraft flew through the plume and collected the Al_2O_3 isokinetically. Submicron-sized particles were analyzed using an electric mobility analyzer, and micron-sized particles were collected on a moving tape impactor. An additional measurement of the total particle concentration was made using a condensation nuclei counter.

Electric Mobility Analyzer

The electric mobility analyzer sizes particles by drawing a sample of the aerosol through an ionization section where the particles are charged. The sample stream is then surrounded with a sheath of clean air, and the flow passes between two electrodes. A known high voltage is impressed between these electrodes, thus applying an attractive sideways force on the particles. If each particle has the same charge, then for a particular

voltage only particles of a specific size or smaller will be able to migrate through the clean air sheath to the attracting electrode. Thus by programming the high voltage applied and by measuring the current flow which results from particles migrating to the electrode, one can calculate a size distribution of the particles in the sample. The instrument has a reported capability of sizing particles from 0.005 to 1.0 μm (Ref. 3). For particles larger than 1.0 μm, wall losses and ambiguities caused by multiple charging of the particles render the data questionable. Indeed, the multiple charging problem can render the data questionable when the particle species are unknown since a mixture of particles can have a variety of charging properties (i.e., oil droplets, soot, clays, acid aerosols, etc.). The particle sample obtained with the mobility analyzer can be used to provide an absolute particle concentration in that the device operates with measured flow rates and thus yields particle counts per volume of sampled air.

Tape Impactor

The tape impactor collects particles on the sticky surface of a tape which is slowly moving past the sampling orifice. The particle-laden air is drawn into the sampler and accelerated through a nozzle which faces the tape. Because of their momentum, large particles ($>$ 1.0 μm) impact on the surface and are captured. Some of the smaller particles can follow the airstream as it turns and flows around the tape, and thus there is a gradual decrease in the collection efficiency for smaller particles. Correction factors are applied to the data to account for these losses. Since the tape is constantly moving, it produces a well-spaced collection of particles which can later be sized and counted. The size distribution measured by the tape impactor can, however, be distorted by loss of larger particles in the inlet and nozzle section; in addition, it does require extreme care in the sizing and counting since the particles are not randomly distributed over the tape surface (i.e., due to the shape of the nozzle and the direction of tape travel the particles will tend to distribute themselves according to size).

Aiken Nuclei Counter

An Aiken nuclei counter does not yield a size distribution but can give an approximate value for the number density of particles. It operates by drawing a known volume of the air into a chamber saturated with water vapor. A piston or diaphragm is then released which results in an adiabatic expansion of the vapor mixture. In this supersaturated environment water vapor condenses on all the particles present, and the resulting cloud of droplets is detected by an optical sensor. The optical measurement is a simple extinction measurement and is successfully converted to a number density because of two factors. First, the water droplets observed are much larger than the original particles, and therefore the unknown indices of refraction of the particles are not

important. Second, the growth process of the water drops is such that the smaller drop radii will increase at a much faster rate than the larger ones. Thus, the final cloud of droplets will all be close to the same size at the time of the extinction measurements. The instrument can therefore be calibrated with a known aerosol number density generated in the laboratory and can be expected to hold this calibration for an unknown aerosol sample where the particle composition and size may be quite different.

Data Fitted to a Distribution Function

The particle counts per size interval from the mobility data were fitted to a distribution function as previously described. The curve was normalized to the mode and is presented in Fig. 84 The data from the tape impactor provide a second particle size distribution, which partially overlaps the mobility data. However, the overlap is in a regime where the tape impactor data have large correction factors applied to allow for small particle losses. Thus a distribution function was fitted to the tape impactor data for particle sizes greater than 0.5 μm. Both sets of data indicate an inflection point around the 0.35-μm particle size, and the tape impactor data were therefore scaled to match the mobility distribution at this point.

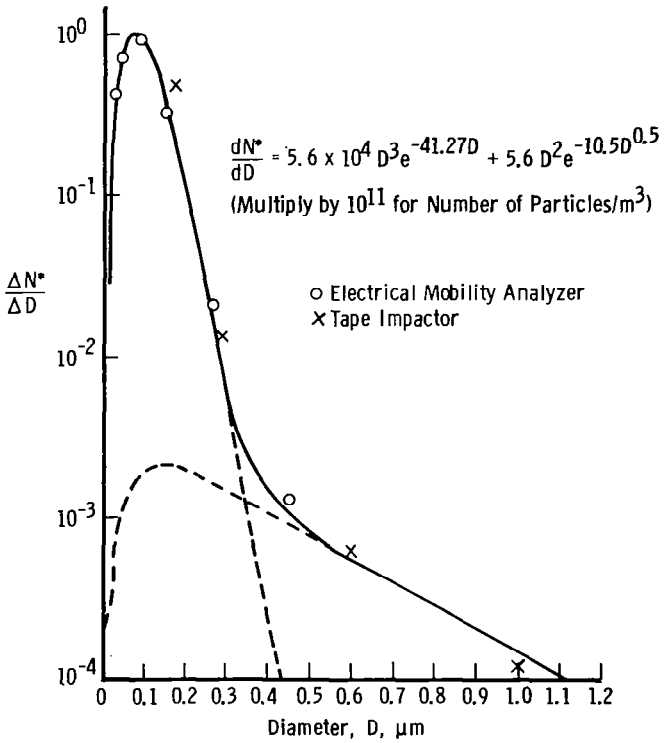

Figure 84. Titan III-C data reported by Varsi (JPL) (Ref. 17)

The resulting distribution is shown in Fig. 84 with data points from both instruments. The poor fit of the 0.1-μm data from the tape impactor can be accepted since in this range the instrument count has been corrected by a large and somewhat questionable loss factor. It is immediately obvious that this distribution is quite different from those presented previously. The most striking point is that its mode is in the submicron range. Since there is a delay between plume formation and sampling (T_o + 10 minutes), the first impulse is to suspect that the larger particles have settled out. However, calculating the settling rate of a 10-μm Al_2O_3 particle and considering the 10-minute interval, the total distance fallen would be approximately 9 m. It would thus seem that this settling would be insignificant insofar as skewing the size distribution, at least up to the 10-μm particle sizes. Similar calculations for 100-μm particles suggest that they could be depleted due to gravitational settling.

The closure condition based on calculated emissions from the solid motors at 20 km altitude of 930 gm of Al_2O_3 per meter of altitude and an estimated plume diameter of 2 km (Ref17) yields an average mass loading in the atmosphere of 2.9×10^{-4} gm/m^3.

Using the particle size distribution in Fig. 84 and adjusting the particle number density to match the value measured by the Aiken nuclei counter (i.e., 3×10^{10} particles/m^3), one can integrate the equations to yield an atmospheric mass loading. These calculations indicate values of 5.24×10^{-5} gm/m^3 for particles sized from 0.025 to 0.525 μm and 4.78×10^{-5} gm/m^3 for particles from 0.525 to 6.0 μm, or a total of 1.0×10^{-4} gm/m^3. Considering the possible uncertainties of such values as the plume diameter and the aluminum oxide deposition rate, as well as the possible biases which might be included in the particle measurement techniques, these values are in remarkably good agreement.

A second point of interest in these data is that the size distribution is bimodal. Kraeutle et al. (Ref. 18) have observed this bimodal nature of the Al_2O_3 particle distribution in samples taken from smaller rocket motors. A size distribution from their data is shown in Fig. 85 . When this is compared to the Titan III data, one notes that the distribution of the small particles is similar; however, the larger particles ($>$ 1 μm) are an order of magnitude more numerous. Using this distribution function and assuming a number density of 3×10^{10} particles/m^3 for the Titan plume, one calculates a mass loading of 2.3×10^{-2} gm/m^3 with 10 percent of the mass in the submicron-sized particles.

Repeating this exercise with the distribution function derived from data collected by petri dish technique (curve 2, Fig. 78) yields a mass loading of 1.1 gm/m^3, obviously orders of magnitude too high. The Kraeutle distribution is seemingly high but certainly within reason. It is unfortunate that the relatively easily obtained measurement of total

particulate mass loading was not made on the Titan cloud fly-through. This information would be of great value in evaluating the validity of various distribution functions.

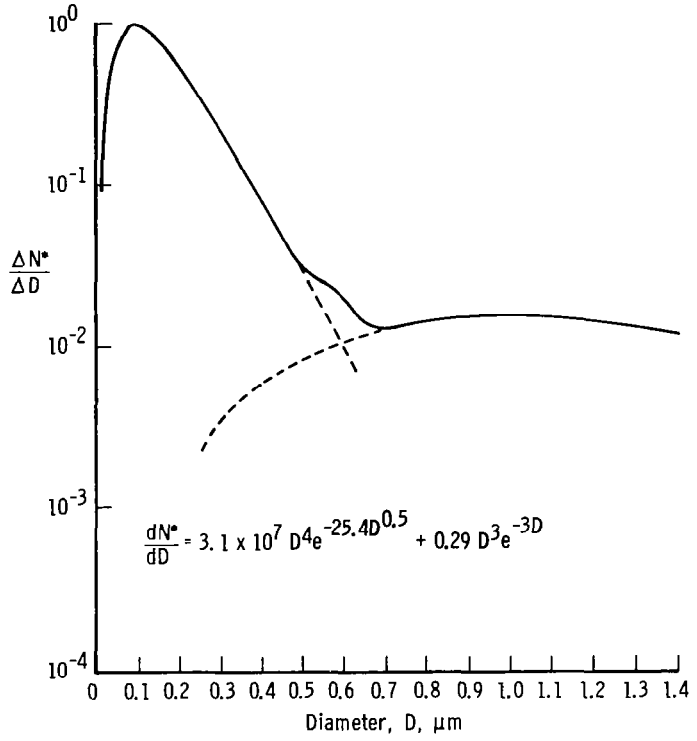

Figure 85 Al_2O_3 particle distribution reported by Kraeutle (Ref. 18).

ALUMINUM COMBUSTION

The problem of aluminum combustion and its oxide formation has received a great deal of attention and has been extensively reported in the literature. However, due to the extremely hostile environment in the combustion chamber and nozzle expansions of the exhaust gases from solid rocket motors, the physical and chemical processes which result in the eventual aluminum oxide particles observed downstream are not well known. A good review of the many facets of the problem is presented by Pokhil et al. (Ref. 24). More specific studies of the problems associated with aluminum combustion both in the rocket environment and under controlled laboratory conditions are presented in work such as that by Crump et al. (Ref. 25) and Prentice (Ref. 26). From these and similar studies the following observations can be made.

1. The molten aluminum droplets in the combustion chamber are, in general, considerably larger than the particles of aluminum included in the fuel. It is noted that as the fuel surface recedes, the aluminum particles are exposed and tend to cluster. Rather than leave the surface immediately, they melt and form a liquid Al and solid Al_2O_3 matrix before being swept into the gas stream. This process of agglomeration thus suggests that the final Al_2O_3 particle size cannot be directly related to the original size of metallic aluminum particles in the fuel. The degree of agglomeration is influenced by several factors which include initial particle sizes of both fuel and oxidizer, uniformity of mixture, type of binder, rate of burning, pressure in combustion chamber, and thickness of oxide coating on the metallic auminum particles used in the fuel (Ref. 27).

2. During the melting and agglomeration process, the oxide coatings from the original aluminum particles crack open and accumulate on the surface of the droplets. As the heating process continues, these shell fragments melt and form a visible lens cap-like structure on the surface of the spherical molten aluminum.

3. Ignition appears to occur as the molten Al-Al_2O_3 droplet leaves the surface and enters the high temperature combustion zone. From high-speed photographs it is seen that the flame stands off from the surface of the droplet, thus indicating a gas phase reaction. Due to the continuum radiation produced from all the Al_2O_3 in the combustion chamber it is impossible to distinguish any spectra indicating the occurrence of the suboxides AlO and Al_2O. However, supplementary evidence from the ignition of aluminum-filled flash bulbs does show emission lines of AlO (Refs. 24 and 28).

Porter et al. (Ref. 29) studied the species vaporizing from an Al-Al_2O_3 mixture using a mass spectrometer. Their system was limited to temperatures of 1,800°K; however, they identified Al and Al_2O as the prime gaseous constitutents with a trace signal of AlO. Brewar et al. (Ref. 30) conducted similar vaporization experiments and concluded that in the Al-Al_2O_3 mixture the basic sub-oxide is Al_2O, whereas in the vaporization of Al_2O_3 alone, AlO is the dominant gas species. It was also observed that when molten aluminum was in contact with the Al_2O_3 the evaporation rate of the Al_2O_3 was increased by two orders of magnitude.

Considering these comments and then returning to the observations of molten aluminum droplets with molten lens caps of Al_2O_3 surrounded by a reactive flame zone,

one can see that the production of aluminum oxide particles in a rocket motor is a complex process. The sub-oxides are obviously formed in the reaction zone surrounding the burning droplet, with possible additions from the evaporation of Al_2O_3 at the $Al\text{-}Al_2O_3$ interface on the droplet. Adding to this complexity is the fact that the droplets and gases are swept from the surface of the burning propellant and are rapidly accelerated through the nozzle and into the expanding plume. From these observed processes one can speculate that there are at least two possible sources of Al_2O_3 particles, the liquid Al_2O_3 lens caps which remain as residue after the Al has evaporated, and Al_2O_3 formed from the condensation of the gaseous sub-oxides.

CONDENSATION OF GASEOUS OXIDES

There is no experimental evidence that either of the sub-oxides can exist in the solid or liquid phase. Material identified by Hock et al. (Ref. 31) as solid Al_2O and AlO was later shown to be Al_4C_3 and $AlTaO_4$ by Yanagida (Ref. 32). Thus condensation of gaseous $AlO\text{-}Al_2O$ to Al_2O_3 is both a chemical and physical process. Hermsen (Ref. 33) has applied the classical homogeneous nucleation theory as presented by Frenkle (Ref. 34) to predict nucleation rates. To circumvent the problem of not being able to define a supersaturation of the $AlO\text{-}Al_2O$ gas, Hermsen uses the ratio of the partial pressure of the Al gas to the equilibrium vapor pressure of Al gas in Al_2O_3 vaporization products. Regardless of the confidence one might have in this treatment of the problem, the predicted nucleation rates are of questionable value since they vary by a factor of 10^{16} over the temperature range of interest (i.e., from 2,000 to 3,000°K). It would thus seem that until the condensation process can be identified, it is premature to try to adapt existing condensation theories to predict nucleation rates. While the actual process involved in the condensation of the sub-oxides is not yet known, it is not unreasonable to suggest that condensation is the major source of the submicron particles observed in the rocket exhaust plume.

DISPERSION OF LIQUID Al_2O_3

It has been noted that due to an agglomeration process at the burning surface of the fuel relatively large droplets of molten aluminum with attached Al_2O_3 lens caps enter the gas flow field. A typical histogram of these agglomerated droplet sizes as measured by Boggs et al. (Ref. 27) is presented in Fig. 86. From the scaled photographs of burning droplets as shown in Ref. 27, one can estimate that the volume of liquid Al_2O_3 in the lens cap is approximately 0.8 percent that of the molten aluminum droplet. The order of magnitude of this value is confirmed by the observation that the original aluminum powder (approx. 15-μm diameter) has on the average a 75-Å-thick coating of Al_2O_3 (Ref. 35). Assuming negligible evaporation or condensation of the liquid Al_2O_3, one can

predict a range of residual alumina droplets from 4 to 40 μm in diameter based on the agglomerated particle sizes shown in Fig. 86.

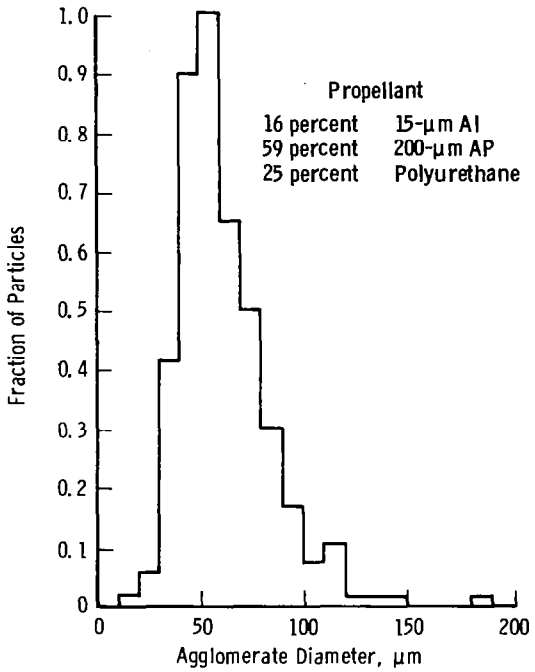

Figure 86. Histogram of agglomerated Al droplet sizes.

It is also observed that a considerable quantity of liquid Al_2O_3 accumulates on the nozzle walls and is shed due to the high velocity gases. Bartlett et al. (Ref.3 6) have used the droplet stability criteria of a critical Bond number to calculate the maximum size of a molten aluminum oxide droplet which could survive the aerodynamic forces in the rocket flow field. In a similar manner one can postulate the maximum aerodynamic drag forces which might be encountered and, equating these forces to the surface tension of liquid Al_2O_3, calculate that the minimum droplet size produced by this mechanism would be on the order of 1 μm. It would thus appear that the agglomeration process at the burning surface and aerodynamic dispersal of liquid Al_2O_3 provide particles in the micron size range.

9.0 SUMMARY

9.1 AEDC ENVIRONMENTAL TESTS

Comparison of data obtained both in the 12V chamber and in the free atmosphere indicates that tests made in an environmental chamber can provide a realistic method of investigating the condensation processes which might occur in rocket exhausts. The absolute quantities of the species, as expected, were compromised by losses to the chamber walls. However, since the absolute quantities of specific species expected from a scaled motor are also questionable, it is not considered worthwhile to pursue the approach of trying to inventory all the species and balance a mass budget. While these chamber tests cannot provide quantitative data which might be extrapolated and used to predict the inventory of species in the ground cloud produced by the shuttle, they have provided information on some of the condensation processes which might be expected. These tests suggest that acid aerosols will be produced in the ground cloud whenever the relative humidity at the launch site is greater than 65 percent. The acidity of these droplets is determined by the maximum concentration of HCl gas to which it is exposed after it was formed. In the environmental chamber test droplets were collected with acidities estimated at pH = -0.6. These droplets contained a relatively large Al_2O_3 nucleus (5 to 50 μ) and traces of aluminum chloride as well as the hydrochloric acid.

The size range and type of aluminum oxide particles collected during the chamber tests were comparable to those collected from a 7,000-lb scaled Minuteman, also fired at AEDC, and the 400-lb Tomahawk rockets fired at MSFC. In general, it has been observed that the submicron particles are predominantly γ-phase alumina and the large particles the α-phase. There is evidence reported in the literature which suggests that some of the large, hollow spheres observed among the Al_2O_3 particles may be aluminum oxicarbide, although this has not been confirmed.

Al_2O_3 PARTICLE SIZE DISTRIBUTIONS

From the observations cited, there is ample evidence to support a multimodal distribution function for the Al_2O_3 particle sizes. If, as has been suggested, the larger

particles are produced by an agglomeration and dispersal process and the smaller ones by condensation, then an argument can be made in favor of the strong submicron particle mode of the Varsi and Kraeutle distributions. In the large motors such as Titan, Super Hippo, and Shuttle, the agglomerated droplets are confined in the combustion zone (≈3,500°K) for a much longer period than in small motors. In this environment the liquid Al_2O_3 droplets from the agglomeration process are in a reducing atmosphere of Al gas and thus are evaporating. If this evaporation yelds Al_2O, then it is not rate controlled by the partial pressure of aluminum oxide produced by the combustion of the aluminum directly in the oxidizer. The net result would be a depletion in the number and size of liquid Al_2O_3 droplets and an increase in the sub-oxides which would participate in a chemical/physical condensation process producing submicron particles. This argument does not consider the additional processes of particle growth, coagulation, and remelting which might occur in the exhaust flow field. It does, however, question the accepted viewpoint that bigger motors produce bigger particles, and in fact suggests that the reverse may be true.

These factors plus the noted bias in previous data thus argue in favor of the bimodal particle size distribution functions as derived from data by Varsi and Kraeutle with significant quantities of Al_2O_3 contained in the submicron particles. These size distributions are recommended at this time as the best estimates for particles produced by shuttle operations.

Unfortunately, in spite of all the previous efforts to determine the particle size distribution of Al_2O_3 in rocket plumes, it appears that further measurements, preferably made within the exhaust cloud, are still needed. In order that the data can be checked for consistency, three types of measurements should be made. The first and possibly the easiest measurement is total mass loading in the cloud. This measurement can be made using absolute filters for average values or possibly Quartz Crystal Microbalances (QCMs) in conjunction with a precipitator (electrostatic or inertial) for determining cloud profiles. The second measurement needed is a count of the total number of particles per unit volume. A condensation nuclei counter would yield this data. The third measurement is the particle size distribution. No one instrument can cover the size range of interest (0.005 to 50μm). The electric mobility analyzer would appear to be the most promising for the 0.005- to 0.5-μm size range. Inertial impactors can operate effectively over a range from 0.1 to 10 μm. A Cascade impactor with QCM readout at each stage could give near real time readout and thus indicate the homogeneity of the cloud section sampled. The particles ranging from 0.5 to 50 μm can be detected by optical scattering, and there are a variety of instruments available for this measurement range.

It should be noted that all of these measurements, including the simple total mass determined from weighing collections on filters, will be compromised if there are significant numbers of condensed water or acid droplets in the cloud. Therefore, the rocket cloud must be formed in a relatively dry atmosphere, a condition which adds another constraint to the problem of cloud sampling.

Additional studies of the basic mechanism of Al_2O_3 particle formation would be worthwhile, since if the condensation and coagulation process is occurring to a significant extent outside the combustion chamber, then the Al_2O_3 particles deposited in the stratosphere can be quite different from those observed from the same engine at low altitude. This would be of concern, for example, in the operation of the solid rocket motor for the interim upper stage (IUS) of the space shuttle operations.

9.3 ACID DROPLETS

It is apparent that the acid droplets which can occur as a result of launches involving solid rocket motors can be traced to at least four possible sources. The first is sprays and deluge water at the launch pad. Droplets from this source include a variety of solid material washed out of the plume. They can be expected to fall out in the immediate vicinity of the launch pad and can cause cosmetic damage to plants. A second source is acid aerosols formed due to condensation of H_2O and HCl on Al_2O_3 nuclei. This occurs in the rising portion of the plume and would be expected close to the launch site. The formation and growth of droplets from this source will be determined by the local atmospheric conditions (i.e., temperature and relative humidity) as ambient air mixes with the cooling plume gases. These droplets will be in equilibrium with the local HCl concentration in the plume and thus may be very acidic. The observation that many of these droplets contain significant quantities of aluminum chloride suggests that they may be an effective sink for some of the HCl, thus reducing the total burden of HCl to be dissipated in the remaining cloud. A third possible source is an overriding rainfall, which would wash HCl from the cloud. These droplets would be mildly acidic. Cosmetic spotting of vegetation would depend on whether the rainfall continued after the exhaust cloud passed, since further rainfall would effectively wash away the acid droplets. A fourth source of acid droplets occurs when plants have been covered with water droplets either by a preceding rain shower or by irrigation sprays and are then subjected to exposure to low concentrations of HCl. These droplets can result in cosmetic spotting of vegetation. Further studies of the susceptibility of specific plant species to this type of damage is recommended.

REFERENCES

1. Solid Propellant Engineering Staff. "Nozzle Exit Exhaust Products from Space Shuttle Boost Vehicle (November 1973 Design)." J. P. L. TM33-712, February 1975.

2. Kaufman, J. W., Susko, M., and Hill, C. K. "Prediction of Engine Exhaust Concentrations Downwind from the Delta-Thor Telsat-A Launch of November 9, 1972." NASA TM X-2939, November 1973.

3. Bartlett, R. W., Ong, J. N., Jr., Fassell, W. M., Jr., and Papp, C. A. "Estimating Aluminum Particle Combustion Kinetics." Combustion and Flame, Vol. 7, September 1963, pp. 227-234.

4. Hermsen, R. W. and Dunlap, R. "Nucleation and Growth of Oxide Particles in Metal Vapour Flames." Combustion and Flame, Vol. 13, June 1969, pp. 253-261.

5. Prentice, J. L. "Aluminum Droplet Combustion: Rates and Mechanisms in Wet and Dry Oxidizers." NWC TP 5569, April 1974.

6. Sehgal, R. "Experimental Investigation of a Gas-Particle System." Research Summary, JPL Tech. Rept. No. 36-13, March 1962.

7. Crowe, C. T. and Willoughby, P. G. "A Study of Particle Growth in a Rocket Nozzle." AIAA Journal, Vol. 5, No. 7, July 1967, pp. 1300-1304.

8. Dobbins, R. A. and Strand, L. D. "A Comparison of Two Methods of Measuring Particle Size of Al_2O_3 Produced by a Small Rocket Motor." AIAA Journal, Vol. 8, No. 9, September 1970, pp. 1544-1550.

9. Eisel, J. L., Price, E. W., and Brown, B. G. "Al_2O_3 Particles Produced During Solid Propellant Combustion." AIAA Paper No. 74-197, presented at the AIAA 12th Aerospace Sciences Meeting, Washington, D. C., Jan.-Feb. 1974.

10. Radke, H. H., Delaney, L. T., and Smith, P. "Exhaust Particle Size Data from Small and Large Solid Rocket Motors." Aerospace Corp., San Bernadius Operations Division, Report No. TOR-1001 (S2951-18)-3, July 1967.

11. Worster, B. W. and Kadomiya, R. H. "Rocket Exhaust Aluminum Oxide Particle Properties." ARI RR-30, August 1973.

12. Willoughby, P. G. "Sampling and Size Determination of Particulates from the Titan III-C Exhaust Plume." United Technology, TR-33-74-U1, February 1974.

13. Brzustowski, T. A. "Comments on the Paper 'Estimating Aluminum Particle Combustion Kinetics' by Bartlett, et al." Combustion and Flame, Vol. 8, December 1964, pp. 339-340.

14. Drew, C. M., Gordon, A. S., and Knipe, R. H. "Study of Quenched Aluminum Particle Combustion." AIAA Preprint 64-487, 1963.

15 Fuchs, N. A. The Mechanics of Aerosols. Pergamon Press, New York, 1964.

16. Pearce, B. E. "Radiant Heat Transfer within a Solid-Propellant Rocket Motor." Journal of Spacecraft and Rockets, Vol. 15, No. 2, March-April 1978, pp. 125-128.

17. Varsi, G. "Proceedings of the NASA Atmospheric Effects Working Group Meeting." Vandenburg Air Force Base, October 27-28, 1976.

18. Victor, A. C. and Breil, S. H. "A Simple Method for Predicting Rocket Exhaust Smoke Visibility." Journal of Spacecraft and Rockets, Vol. 14, No. 9, September 1977, pp. 526-533.

19. Dehority, G. L. "A Parametric Study of Particulate Damping Based on the Model of Temkin and Dobbins." NWC-TP-5002, September 1970.

20. Nukiyama, S. and Tanasawa, Y. "An Experiment on the Atomization of Liquid by Means of an Air Stream." Transactions of the Society of Mechanical Engineers (Japan), Vol. 4, No. 14, February 1938.

21. Rosin, P. and Rammler, E. "The Laws Governing the Fineness of Powdered Coal." Journal of the Institute of Fuel, Vol. 7, 1933.

22. Brown, B. and McArty, K. P. "Particle Size of Condensed Oxides from Combustion of Metalized Solid Propellants." Eighth Symposium (International) on Combustion, California Institute of Technology, Pasadena, California, August-September 1960, pp. 814-823.

23. Liu, B. Y., Editor. Fine Particles: Aerosol Generation, Measurement, Sampling, and Analysis. Academic Press, Inc., New York, 1976.

24 Pokhil, P. F., Belyayev, A. F., Frolov, Yu. V., Logachev, V. S., and Korotkov, A. I. "Comubstion of Powdered Metals in Active Media." FTD-MT-24-551-73, 1972.

25 Crump, J. E., Prentice, J. L., and Kraeutle, K. J. "Role of the Scanning Electron Microscope in the Study of Solid Propellant Combustion: II. Behavior of Metal Additives." Combustion Science and Technology, 1969, Vol. 1, pp. 205-223.

26. Prentice, J. L. "Aluminum Droplet Combustion: Rates and Mechanisms in Wet and Dry Oxidizers." NWC-TP-5569, April 1974.

27. Crump, J. E., Editor. "Combustion of Solid Propellants and Low Frequency Combustion Instability." NOTS-TP-4244, June 1967.

28. Herzberg, G. Molecular Spectra and Molecular Structure: Spectra of Diatomic Molecules. D. Van Nostrand Co., Inc., New York, 1950.

29. Porter, R. F., Schissel, P., and Inghram, M. G. "A Mass Spectrometric Study of Gaseous Species in the Al-Al_2O_3 System." Journal of Chemical Physics, Vol. 23, No. 2, February 1955, pp. 339-343.

30. Brewer, L. and Searcy, A. W. "The Gaseous Species of the Aluminum-Alumina System." Journal of the American Chemical Society, Vol. 73, 1951, pp. 5308-5314.

31. Hoch, M. and Johnston, H. L. "Formation, Stability, and Crystal Structure of the Solid Aluminum Sub-Oxides Al_2O and AlO." Journal of the American Chemical Society, Vol. 76, 1954, pp. 2560-2561.

32. Yanagida, H. and Kroger, F. A. "Condensed Phases in the System Al_2O_3-Al." American Ceramic Society Bulletin, Vol. 47, No. 4, 1968, p. 366.

33. Hermsen, R. W. and Dunlap, R. "Nucleation and Growth of Oxide Particles in Metal Vapour Flames." Combustion and Flame, Vol. 13, No. 3, June 1969, pp. 253-261.

34. Frenkel, J. Kinetic Theory of Liquids. Oxford University Press, London, 1946, p. 397.

35. Price, E. W. "Summary Report of JANNAF Worshop on 'Behavior of Aluminum in Solid Propellant Combustion'." Proceedings of the 13th JANNAF Combustion Meeting, March 1976, Vol. II, pp. 453-458.

36. Bartlett, R. W. and Delaney, L. J. "Effect of Liquid Surface Tension on Maximum Particle Size in Two-Phase Nozzle Flow." Pyrodynamics, Vol. 4, 1966, pp. 337-341.

1. REPORT NO.	2. GOVERNMENT ACCESSION NO.	3. RECIPIENT'S CATALOG NO.
NASA CR-3136		

4. TITLE AND SUBTITLE	5. REPORT DATE
Analysis of the Measured Effects of the Principal Exhaust Effluents from Solid Rocket Motors	January 1980
	6. PERFORMING ORGANIZATION CODE
7. AUTHOR(S)	8. PERFORMING ORGANIZATION REPORT #
R. Dawbarn, M. Kinslow, and D. J. Watson	
9. PERFORMING ORGANIZATION NAME AND ADDRESS	10. WORK UNIT NO.
Arnold Engineering Development Center Arnold Air Force Station, Tennessee 37389	M-282
	11. CONTRACT OR GRANT NO.
	PO H-19386B
	13. TYPE OF REPORT & PERIOD COVERED
12. SPONSORING AGENCY NAME AND ADDRESS	Contractor
National Aeronautics and Space Administration Washington, D. C. 20546	14. SPONSORING AGENCY CODE

15. SUPPLEMENTARY NOTES

Prepared under the sponsorship of the Environmental Effects Technical Task Team (Dr. J. B. Stephens and H. C. Euler), Atmospheric Sciences Division, Space Sciences Laboratory, NASA Marshall Space Flight Center

16. ABSTRACT

The purpose of this study was to determine the feasibility of conducting environmental chamber tests using a small rocket motor to study the physical processes which occur when the exhaust products from solid rocket motors mix with the ambient atmosphere, particularly the interaction between hydrogen chloride, aluminum oxide, and water vapor.

Several types of instruments proposed for measuring HCl concentrations were evaluated during this test series. Under some conditions it was noted that acid aerosols were formed in the ground cloud. These droplets condensed on Al_2O_3 nuclei and were associated with the rocket exhaust cooling during the period of plume rise to stabilization.

The environmental chamber study was followed by a test series which consisted of monitoring outdoor firings of the solid rocket motors of a 6.4 percent scaled model of the Space Shuttle at the Marshall Space Flight Center. This effort included experiments with the interaction of the exhaust effluents with vegetation downwind of the test site.

The final phase consisted of an evaluation of the available data concerning aluminum oxide particles produced by solid rocket motors. These studies include a review of the aluminum combustion process and a justification for the particle size distribution suggested as being the most representative for the Shuttle boosters.

17. KEY WORDS	18. DISTRIBUTION STATEMENT
Rocket Exhaust Particulates Rocket Motor Exhaust Diffusion Rocket Exhaust Cloud Rise Atmospheric Diffusion	Category 45

19. SECURITY CLASSIF. (of this report)	20. SECURITY CLASSIF. (of this page)	21. NO. OF PAGES	22. PRICE
Unclassified	Unclassified	148	$7.25

* For sale by the National Technical Information Service, Springfield, Virginia 22161

NASA-Langley, 1980